Microchimica Acta (2021) 188: 411
https://doi.org/10.1007/s00604-021-05003-9

REVIEW ARTICLE

Nano optical and electrochemical sensors and biosensors for detection of narrow therapeutic index drugs

Omid Heydari Shayesteh[1,2,3] · Reza Mahjub[4] · Akram Ranjbar[3,5] · Katayoun Derakhshandeh[4] · Mahdi Jamshidi[5]

Received: 26 April 2021 / Accepted: 24 August 2021 / Published online: 6 November 2021

Abstract

For the first time, a comprehensive review is presented on the quantitative determination of narrow therapeutic index drugs (NTIDs) by nano optical and electrochemical sensors and biosensors. NTIDs have a narrow index between their effective doses and those at which they produce adverse toxic effects. Therefore, accurate determination of these drugs is very important for clinicians to provide a clear judgment about drug therapy for patients. Routine analytical techniques have limitations such as being expensive, laborious, and time-consuming, and need a skilled user and therefore the nano/(bio)sensing technology leads to high interest.

Keywords Nanotechnology · Biosensor · Narrow therapeutic index drugs · Nano optical and electrochemical sensor

Introduction

Many deaths annually occur due to drug-related problems (DRPs) worldwide, which impose various costs on the health care system of governments [1–3]. Therefore, reducing of DRPs can benefit the health of both patients and society. The therapeutic index (TI) is the range of therapeutically effective dose to the toxic dose of a pharmaceutical agent. One of the major candidates to create DRPs are drugs with a narrow TI (NTIDs) that have a narrow window between their therapeutic and toxic doses [4, 5]. The US Food and Drug Administration (FDA) has identified approximately 25 NTI drugs (Table 1). Some of them are utilized in critical therapies such as heart failure, thromboembolic and seizure disorders, asthma, depression, and thyroid dysfunction [28–30].

Common side effects of NTI drugs such as bleeding (dabigatran) [31], osteoporosis (warfarin) [32], nephrotoxicity and ototoxicity (vancomycin) [33], coma, seizures, memory problem (lithium carbonate) [34], abnormal heart rhythms, headaches and dizziness (theophylline) [35], and arrhythmia cerebellar syndrome (phenytoin) [36], increased risks of suicide, and nausea (carbamazepine) [37, 38] have been reported. For detection of trace levels of NTI drugs, various analytical methods such as high-performance liquid chromatography [39, 40], gas chromatography [41], gas and liquid chromatography-mass spectrometry, [42–44] and immunoassay [45] are already being used. Although these methods have high sensitivity and are routinely used in laboratories and research works, they have disadvantages (e.g., complexity and long time of analysis and need for a skilled user, high cost, and complex instrumentation). Researchers are now shifting to low cost and rapid sensing strategies [46].

In analytical approaches, by generating an optical and electrochemical signal, (bio) sensing technology is applied for detecting analyte concentrations. Generally, a (bio) sensor contains two essentially functional components: a diagnostic element whose role is to identify analytes in a matrix and a signal converter (transducer) to generate an analytical signal. Biosensors use a biological component for the recognition of targets. This biological element can be a microorganisms, cells, enzymes antibodies, nucleic acids, etc. that recognizes

✉ Omid Heydari Shayesteh
Shayesteh_777@yahoo.com

1 Department of Medicinal Chemistry, School of Pharmacy, Hamadan University of Medical Sciences, Hamadan, Iran

2 Research Center for Molecular Medicine, Hamadan University of Medical Sciences, Hamadan, Iran

3 Nutrition Health Research Center, Hamadan University of Medical Sciences, Hamadan, Iran

4 Department of Pharmaceutics, School of Pharmacy, Hamadan University of Medical Sciences, Hamadan, Iran

5 Department of Toxicology and Pharmacology, School of Pharmacy, Hamadan University of Medical Sciences, Hamadan, Iran

Table 1 Sample list of narrow therapeutic index (NTI) drugs published by the FDA

Drug	Chemical structure	Therapeutic class	Therapeutic index	Adverse effects and toxicity	Ref.
Aminophylline	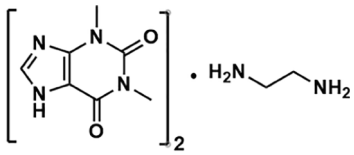	Bronchodilator	10- 20 µg/ml	Nausea, Headache, Insomnia, Restlessness, Seizures, Cardiac arrhythmias, Death	[6]
Carbamazepine	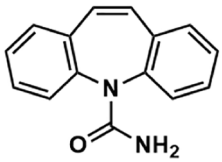	Anticonvulsants, analgesic	4–12 µg/mL	Somnolence,dizziness , gastrointestinal disturbance,hematolo gic abnormalities	[7]
Clindamycin	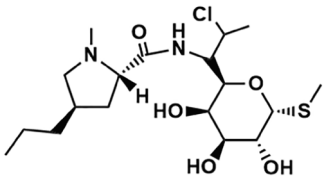	Lincosamide antibiotic	----------	Nausea, stomach pain, vomiting, joint pain, heartburn, white vaginal discharge and white patches in the mouth	[8]
Clonidine	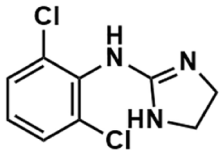	Antihypertensive	0.2-2.0 ng/mL	Dry mouth, dizziness, headaches, sleepiness	[9]
Cyclosporine	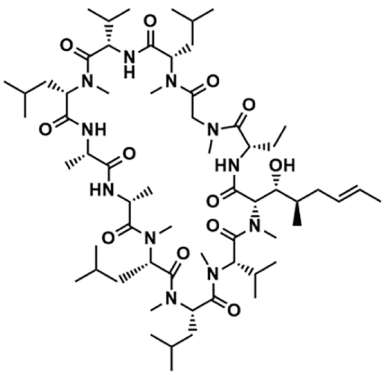	Immunosuppressa-nt	100-400 ng/mL	Gum enlargement, increased hair growth, convulsions, pepticulcers, pancreati tis, diarrhea, confusion, in creased cholesterol	[10]

Digoxin	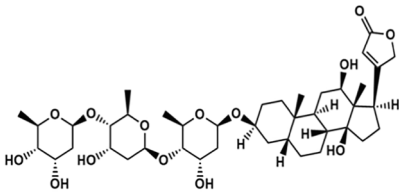	Cardiac glycosd-es	0.8-2.0 ng/ml	Dizziness, Diarrhea, Mental disturbances, Vomiting, nausea	[11]
Disopyramide	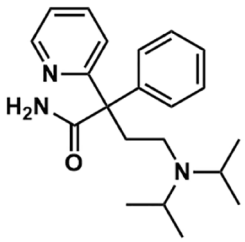	Antiarrhythmic	2-4 µg/ml	Xerostomia (dry mouth, nose or eyes), abdominal discomfort, nausea, constipation and, most importantly, urinary hesitancy	[12]
Gentamycin	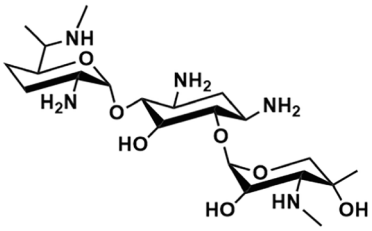	Aminoglycoside antibiotics	5-10 µg/ml	Ototoxicity, neurotoxicity nephrotoxicity	[13]
Guanethidine	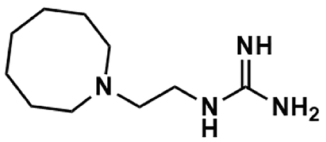	Antihypertensive	----------	Diarrhea or increase in bowel movements, sexual problems in males, slow heartbeat, stuffy nose	[14]
Isoetharine mesylate	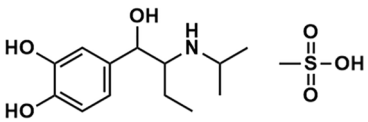	Bronchodilator, adrenergic (Inhalation-Local)	----------	Tremor, headache	[15]
Isoproterenol	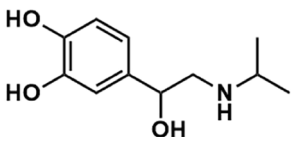	Bronchodilator, cardiac stimulant	----------	Nervousness, headache, dizziness, nausea, visual blurring, tachycardia	[16]

Levothyroxine	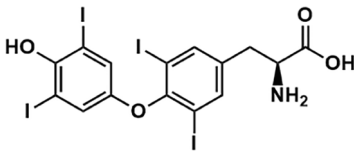	Thyroid hormone replacement	0.4-4.5 mU/L	Weight loss, increased appetite, palpitations, nervousness, diarrhea, abdominal cramps, sweating, tachycardia,	[17]
Lithium Carbonate	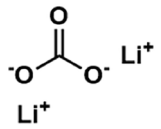	Antimanic, antipsychotic	0.6 -1.2 mM	Shaking, dizziness, drowsiness, vomiting, diarrhoea	[18]
Metaproterenol	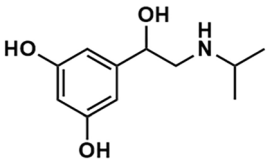	Bronchodilator, antiasthmatic	----------	Tremor, nervousness, dizziness, weakness, headache, nausea	[19]
Minoxidil	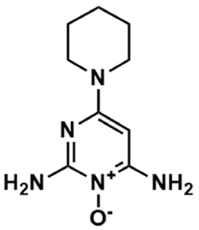	Antihypertensiv-e	----------	Sodium and fluid retention, cardiovascular effects	[20]
Oxtriphylline (choline theophyllinate)	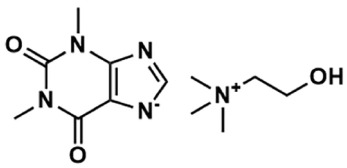	Bronchodilator	----------	Abdominal pain, confusion or change in behavior, convulsions, dark or bloody vomit	[21]
Phenytoin	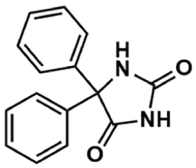	Anticonvulsants, antiepileptic	10-20 µg/mL	Headache, nausea, vo miting, constipation, d izziness, feeling of spinning	[7]
Prazosin	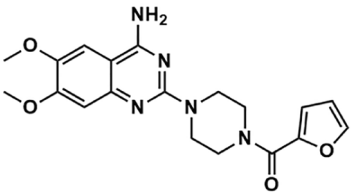	Antihypertensiv-e	----------	Dizziness, headache, drowsiness, lack of energy, weakness, palpitations , nausea	[22]
Primidone	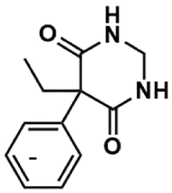	Anticonvulsants	5- 10 µg/ml	Drowsiness,	[23]

				listlessness, visual disturbances, headache, dizziness	
Quinidine	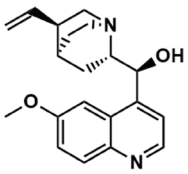	Antiarrhythmic	2-5 µg/mL	Decreased Appetite, diarrhea, nausea, stomach cramps, taste impairment, cardiac arrhythmia	[24]
Tacrolimus	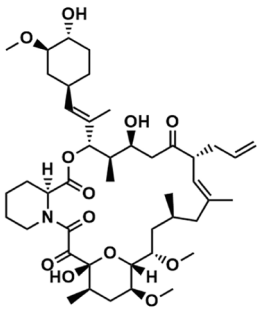	Immunosuppressant	5-15 ng/mL	Cardiac damage, hypertension, blurred vision, liver and kidney problems (tacrolimus nephrotox icity)	[10]
Theophylline	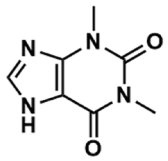	Bronchodilator	10-20 µg/mL	Loss of appetite, nausea, vomiting, abdominal pain	[25]
Valproic Acid	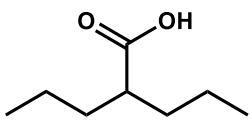	Anticonvulsants, antiepileptic	50–100 µg/mL	Congenital anomalies, infection, abdominal pain, asthenia, drowsiness, nausea, tremo	[7]
Vancomycin	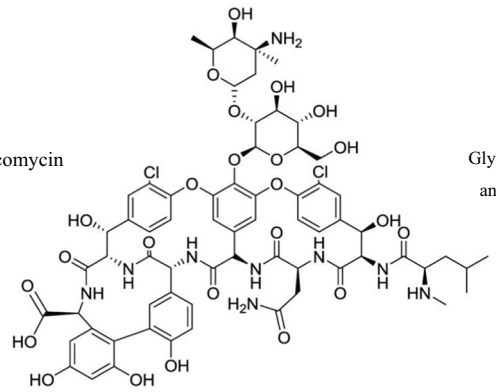	Glycopeptide antibiotics	15-20 µg/mL	Neutropenia, leukope nia, tinnitus, dizziness ototoxicity, neurotoxicity	[26]
Warfarin	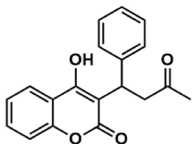	Anticoagulant	0.6-2.6 µg/mL	Severe bleeding, Red or brown urine, Severe headache or stomach pain, Dizziness or weakness	[27]

the target in complex matrices [47, 48]. The biosensors made with aptamer are called "aptasensor." Based on our knowledge, construction of biosensors for NTI drugs with known aptamer sequences has been investigated recently.

Nowadays, nanotechnology is playing a decisive role in the fabrication of (bio) sensors. New efficient transducers can be developed using various nanomaterials which improves sensitivity and performance of (bio) sensors [49]. On the other hand, the combination of nano and biomaterials can create powerful analysis platforms for diagnosis and detection a variety of analytes such as NTIDs (Scheme 1). In each subdivision of this review, NTIDs with greater frequency in terms of (bio)sensing technology are discussed in more detail. Other NTIDs are listed in the relevant tables. In the final section of this review, the major challenges and promising development in this domain are discussed. For writing this review, a literature search was performed in the period of 2000–2021.

Optical NTIDs nano sensors and biosensors

Due to their simple and straightforward use, quick response, and high sensitivity, optical techniques have been widely used for construction of nano sensors and biosensors [50]. In recent years, conventional optical methods including colorimetry, fluorescence, and chemiluminescence (CL) methods, due to their simplicity and device availability, have been used more widely in (bio) sensors.

Colorimetric-based techniques

A wide range of analytes are detected by colorimetric methods. These methods have some advantages over other methods including simplicity, low cost, and the ability to detect target concentration using the naked eye [51]. The application of nanotechnology leads to better analytical characters of (bio)sensors such as limit of detection, linear range, assays reproducibility, and ability to be miniaturized. Nanomaterials can be used as immobilization platform of detection element, interface, and signal amplifier in the fabrication of (bio)sensors [52]. Gold and silver nanoparticles have size/distance-dependent optical properties that are widely used to make (bio)sensors [53, 54]. Moreover, gold nanoparticles (AuNPs) show unique optical properties that are due to a phenomenon called surface plasmon resonance (SPR). At specific wavelengths, the collective oscillation of electrons on the surface of the particle results in strong absorption (and scattering) which means that the signal color generated by the particle can be seen at very low concentrations. For this reason, gold nanoparticles are widely used for the development of colorimetric sensors. In order to ensure maximum

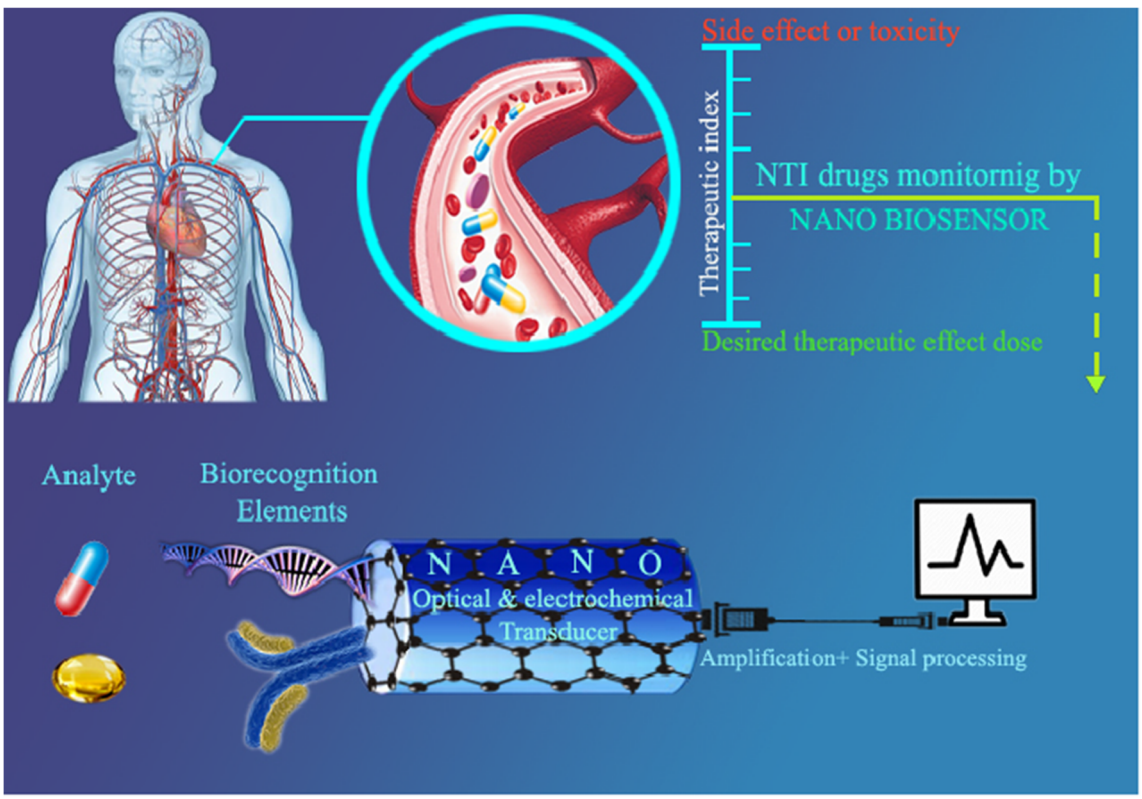

Scheme 1 Schematic representation of detection of NTIDs in blood matrix by nano optical and electrochemical sensor and biosensor

sensitivity in colorimetric detection, it is important to use gold nanoparticles with high molar extinction coefficients [55].

Detection and determination of theophylline

Katiyar et al. using stable RNA aptamer and gold nanoparticles (AuNPs) fabricated a fast and straightforward colorimetric aptasensor to detect theophylline in pharmaceutical samples with detection limit of 50 ng mL^{-1}. Results obtained by aptasensing method were compared with the HPLC method (Fig. 1). In this aptasensor, aptamer electrostatically binds to gold nanoparticles, thereby preventing salt-induced aggregation of AuNPs. However, by introducing theophylline into the assay solution, it reacts with aptamer and as a result, AuNPs are aggregated which leads to the color change from red to purple [56]. In the other study, a fast method for the detecting of theophylline using non-crosslinking AuNPs aggregation was developed. In this approach, compared with typical crosslinking AuNPs aggregation, the reaction is much faster. Inhere, firstly theophylline RNA-aptamer splits into two RNA segments which then interact with bare AuNPs. These RNA probes, which are circled on the surface of gold nanoparticles, cause the increase of the salt tolerance of AuNPs. With introduction of theophylline to assay solution, the RNA fragments are transformed into their three-dimensional form and complex with theophylline, therefore fewer RNA segments are available to uphold the AuNPs from salt-induced aggregation (Fig. 2). Aggregation of gold nanoparticles induced by theophylline can be assessed by changing the color of the assay solution from red to blue. The linear range of this aptasensor was in the range of 0.1 to 20 μM and the limit of detection was reported as 67 nM [57].

Detection and determination of digoxin

A colorimetric aptamer-based biosensor for sensitive detection of digoxin was developed by Emrani et al. [58]. Gold nanoparticles coated with aptamer, in the absence of digoxin, remain stable against salt-induced aggregation. Whereas, in the presence of digoxin in bio-assay solution, the aptamer binds to it. Under such conditions, the aptamer changes to its three-dimensional shape and as a result, AuNPs become aggregated and subsequently the color of assay solution changes from red to blue. The results of their experiments showed that the designed aptasensor with a limit of detection of 571 pM can determine the concentration of digoxin. It can also successfully detect digoxin in the complex serum matrix with high selectivity [58]. For fabrication of monoclonal antibody-based nanobiosensors (immunosensor), Nikfarjam et al. used the localized surface plasmon resonance (LSPR) properties of gold nanoparticles. Firstly, the gold nanoparticles using the citrate reduction

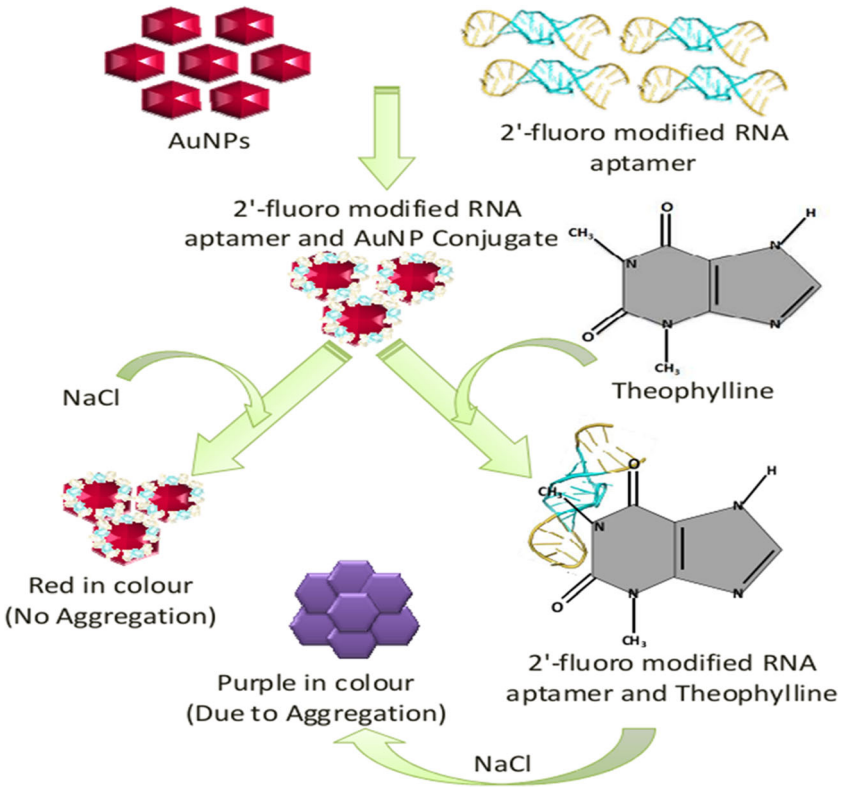

Fig. 1 Colorimetric method for detection of theophylline based on AuNPs and aptamer [56]

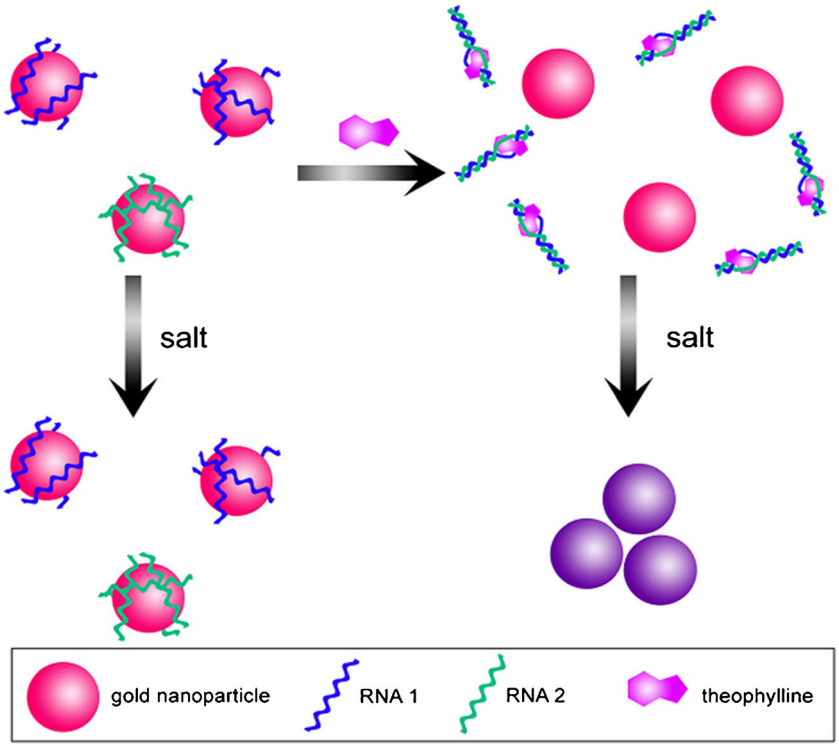

Fig. 2 Illustration of colorimetric detection of theophylline based on RNA aptamers recognition and non-crosslinking AuNPs aggregation [57]

method were synthesized, then the synthesized AuNPs were functionalized using 11-mercaptoundecanoic acid (11-MUA) ligand through thiol groups (Au-S-). The AuNPs were decorated by carboxyl group using EDC/NHS method, reacted with a monoclonal antibody (Fig. 3). Presence of digoxin molecules in the bio-assay solution and consequently their specific binding to the antibody cause an incredible increase in the optical absorption (in λmax = 520 nm). The observed rise in the optical absorption is used as the analytical signal to quantify digoxin. The limit of detection (LOD) of this colorimetric aptasensor was 2 ng/ml [59].

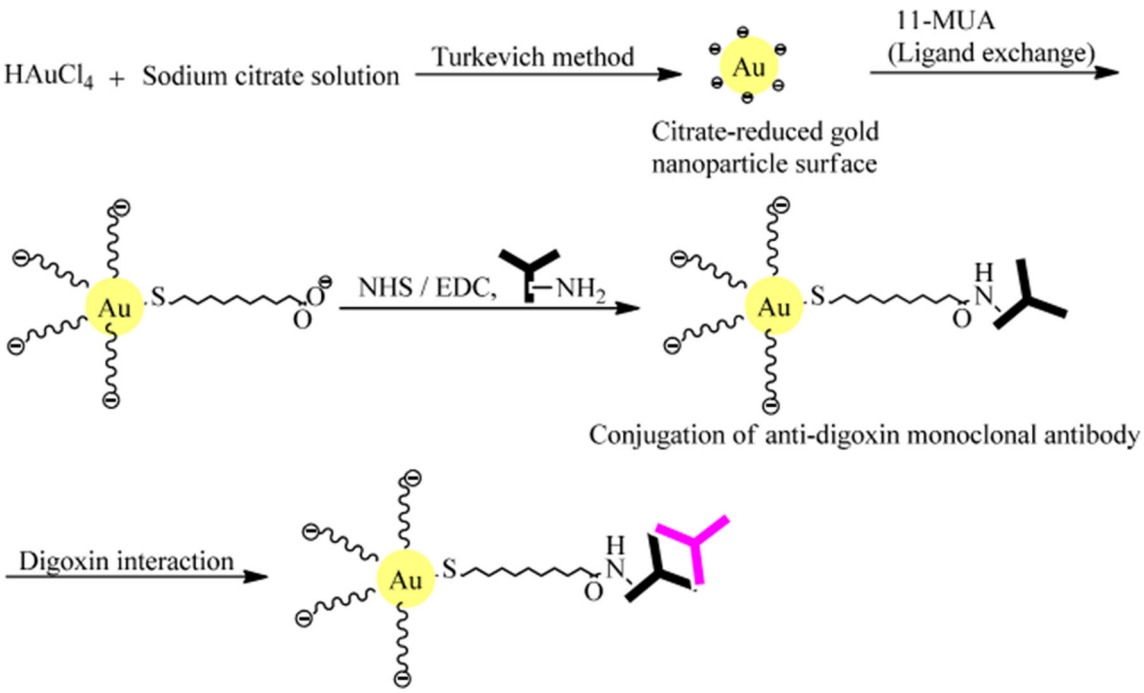

Fig. 3 LSPR nanobiosensor, schematic synthesis process of the antibody-conjugated11-MUA-GNPs and the analysis of digoxin [59]

Detection and determination of gentamicin

Yan et al. developed a simple colorimetric sensor that was based on two single-stranded DNA (ssDNA) oligonucleotides and AuNPs. They used chemometric techniques to discriminate of the five aminoglycoside antibiotics (AAs) including tobramycin, streptomycin, gentamicin, ribostamycin, and kanamycin. In this study, it was shown that the addition of gentamicin could trigger the detachment of DNA from AuNPs and consequently resulted in salt-induced AuNPs aggregation (Fig. 4). The spectral changes of AuNPs in the presence of variuos aminoglycoside antibiotics were analyzed with pattern recognition techniques, Fisher's linear discriminant (FLD) analysis, and hierarchical cluster analysis (HCA) [60]. This sensor quantified gentamicin in a concentration range of 120–280 nM and with a detection limit of 120 nM. Also, by this sensor, five AAs could be successfully distinguished from 20 interferences, in the actual sample of milk.

Miranda-Andrades and colleagues described a colorimetrical sensor using spherical AuNPs and gold nanorods (AuNRs) to detect gentamicin [61]. In order to determine the concentration of gentamaicin, the optical analytical signal of AuNPs and AuNRs towards gentamycin was assessed. Based on their result, high sensitivity was obtained by gold nanoparticles with signal monitoring of the rising plasmon coupling band. The results showed that this sensor is able to detect the gentamycin with a detection limit of 0.4 ng mL^{-1}.

Other colorimetric-based NTIDs nano sensors and biosensors

Jahed and coworkers used dopamine-capped silver nanoparticles for the determination of cyclosporine, based on the mechanism shown in Fig. 5.

The mechanism of this sensor is as follows; dopamine could protect AgNPs against aggregation; therefore, dopamine-capped silver nanoparticles remain dispersed in the absence of cyclosporine. The SPR peak of assay solution (bright yellow color) was obtained at 410 nm. However, upon the addition of cyclosporine, the characteristic peak will have a red shift (at 600 nm) due to the aggregation of silver nanoparticles. Therefore, optical absorption ratios ($A_{600/410}$) were used as the analytical signal to measure cyclosporine. It was shown that, in the concentration range of 0.17–0.85 μM, the detection signals were linearly correlated to the concentrations of the cyclosporine [62].

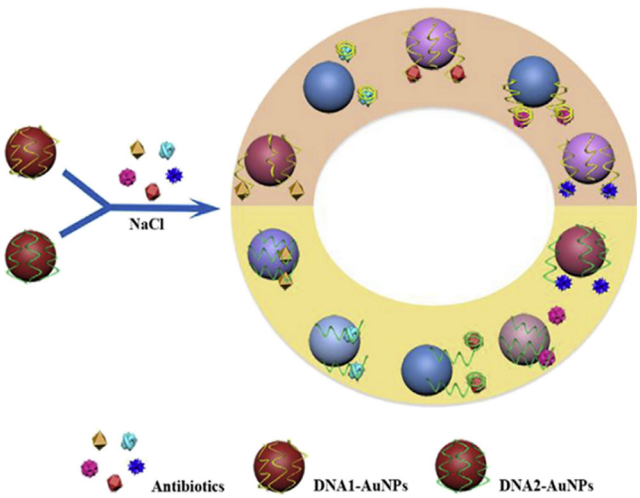

Fig. 4 Detection of AAs based on ssDNA-AuNPs conjugate [60]

For increasing the selectivity of unmodified AgNPs, several capping ligands including alkanethiols, amino acids, amines, and polymers can be used to decorate silver nanoparticles [63]. Based on this approach, Khoubnasabjafari and coworkers fabricated a nanosensor based on the aggregation of indoxyl sulfate capped silver nanoparticles (InS-AgNPs) for specific determination of phenytoin (PHT). Upon introducing PHT to assay solution, the intensity of the InS-AgNP SPR peak at 396 nm is reduced. With the peak disappearing at 360 nm, a new peak around 530 nm appeared and, meanwhile the color of assays solution changes from yellow to pink. The calibration graph of the assay was linear in the range of 25–450 mgL^{-1}, with a detection limit of 10 mgL^{-1} [64]. The list of fabricated colorimetric sensors and biosensors for the determination of NTIDs is summarized in the Table 2.

Fluorescence-based techniques

Fluorescence sensing is one of the most common optical techniques for the construction of sensors and biosensors. This approach has unique features including high sensitivity, simplicity, high signal production, reproducibility, and non-destructiveness [80]. Fluorescence intensity, quenching efficiency, fluorescence anisotropy, decay time, energy transfer (radiative or non-radiative), and quantum yield as an analytical signal can be explored in fluorescence sensing [81].

Over the years, organic dyes were used in fluorescence assays and many efficient fluorescent probes constructed with them were able to detect low concentrations of analytes in different matrices in environmental and clinical chemistry [82–85]. However, with the development of nanotechnology, in recent years, highly sensitive chemical and biological fluorescence nano sensors have been successfully fabricated for various applications. These nanomaterials include carbon nanostructures, quantum dots, noble metals, and upconversion nanoparticles [86]. For high sensitivity and reliable monitoring of NTIDs, various fluorescence-based sensors and biosensors have been developed and are reviewed briefly in this study.

Detection and determination of theophylline

DNA or RNA aptamer? Which is the better choice for the fabrication of an aptasensor? In recent years, many

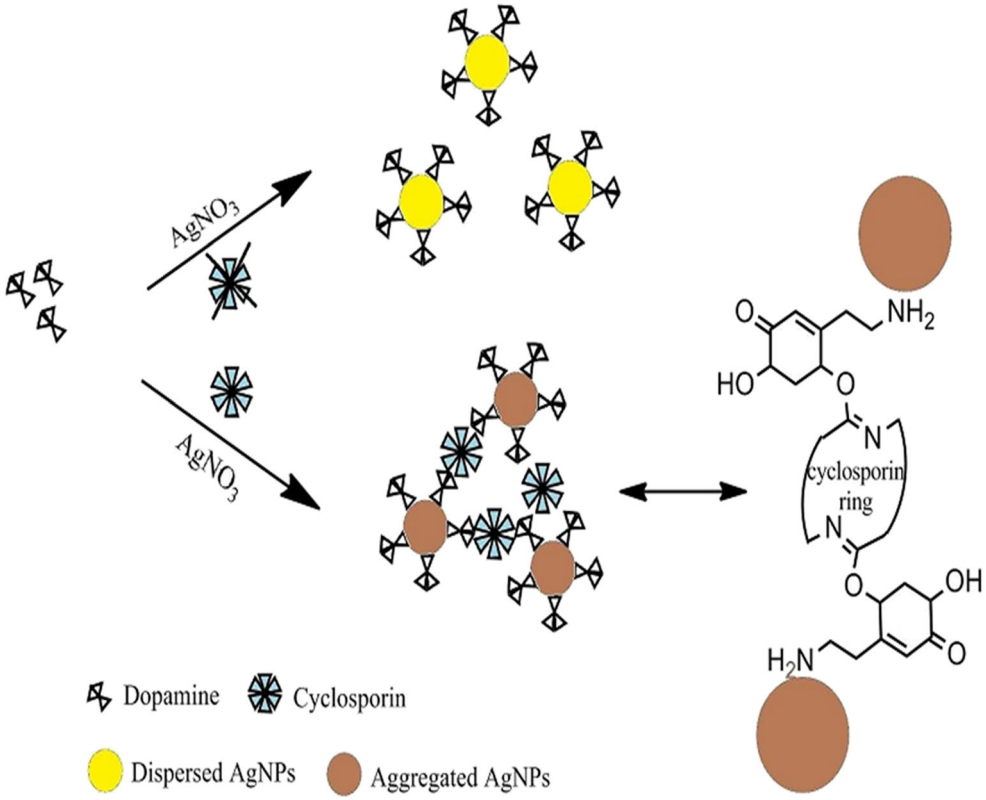

Fig. 5 The assay for colorimetric detection of cyclosporine with the dopamine-capped AgNPs system [62]

constructed aptasensors have used DNA aptamers due to their higher chemical stability and lower price than RNA aptamers [87]. Due to the inherently vulnerable property of RNA aptamer, few aptasensors have been fabricated using them. However, RNA aptamers have significant advantages over DNA aptamers as biorecognition element. For example, in comparison to DNA aptamers, more small molecules can specifically react with RNA aptamers [88]. Moreover, most

Table 2 NTIDs nano colorimetric sensors and biosensors

Strategy (recognition element)	Drug	Matrices	Linear range (nM)	LOD (nM)	Ref.
Water-compatible molecularly imprinted film/AuNPs	Theophylline	Aqueous solution	0.1–1000	0.1	[65]
Aptamer based nano probe sensor	Theophylline	Plant extrtacts and serum	–	50	[66]
Epicatechin coated silver nanoparticles	Gentamicin	Human blood plasma and serum	$0–100 \times 10^3$	1280	[67]
Cysteamine-modified gold nanoparticles	Gentamicin	Skim milk	0–200	12.45	[68]
Gold nanoparticles	Lithium	Aqueous solution	$10–100 \times 10^6$	–	[69]
Polyamidoamine dendrimer	Lithium	Alkali media	$1 \times 10^3–3 \times 10^4$	1000	[70]
Optically fingerprinted of Li_2CO_3	Lithium	Distillated water	100–600	50	[71]
Branched gold nanoparticles	Phenytoin	Human plasma	265.4–2654.1	83.2	[72]
Amphotericin B stabilized gold nanoparticles	Clindamycin	Human blood plasma and tap water	$0–100 \times 10^3$	20×10^3	[73]
Nanogold-labeled monoclonal antibody probe	Digoxin	Human serum	–	2.56	[74]
Gold nanoparticle lateral flow assay	Digoxin	Human serum	0–100	31.3	[75]
Monoclonal antibodies	Warfarin	Human plasma	12.9–806.2	–	[76]
Charge transfer complexation	Sodium valproate	Tablet and oral solution formulation	$69.3 \times 10^2–554.7 \times 10^2$	17.3×10^2	[77]
Nano MIP	Vancomycin	Milk	11.4–1140	2.8	[78]
Optical absorbtion/nanoMIPs	Vancomycin	Porcine plasma	–	10	[79]

(70%) reported aptamers are RNA sequences [89]. Also, RNA molecules are more versatile than DNA molecules and they are by nature single-stranded, which makes them more favorable as a binder. The stability of RNA molecules can be greatly improved through various modifications [90–93].

Jiang and his colleagues designed an RNA aptasensor using AuNP and theophylline RNA aptamer. High affinity and selectivity of RNA aptamer toward theophylline and fluorescence quenching of AuNPs led to the development of an efficient nano-bio-analytical platform for the detection of theophylline in serum. When theophylline is not present in the assay solution, the two individual segments are dissociated in solution. However, in the presence of the theophylline, the fragments form an aptamer–theophylline complex on the surface of AuNPs by an innate change in the secondary structure of aptamer fragments. Subsequently, the fluorescence of Cy3-labeled FR2 due to the occurrence of fluorescence resonance energy transfer (FRET) is quenched by AuNPs (Fig. 6). It is found that the detection limit of aptasensor was 0.05 μM, with a linear dynamic range from 0.1 to 10 μM in serum [94].

Lately, the combination of fluorescence detection methods with different nucleic acid amplification reactions can lead to development of a series of novel analytical platforms, which have developed outstanding sensitive and selective detection methods in bioanalysis [95]. These fluorescence approaches are based on nucleic acid amplification including fluorescent dyes aggression [96], fluorescence resonance energy transfer (FRET) [97], photo-induced electron transfer strategy [98], chemical conjugation of flurophores to DNA [99], a label-free fluorescent strategy [100], real-time [101], multiplex nucleic acid amplification strategies [102], and digital nucleic acid amplification methods [103]. Using various nuclease-assisted signal amplification techniques and nucleic acid molecular probes, ultra-sensitive biosensors have been developed. The prepared biosensors were used for determination of different analytes with a picomolar/femtomolar and even single molecule detection [104].

Lou et al. developed a fluorescence aptasensor, based on signal amplification by cryonase, for detection of theophylline in serum matrix. In their aptasensor, graphene oxide acted as a quenching agent which can decrease the fluorescence of labeled nucleic acid probes. The mechanism of the fluorometric method is as follows; FAM-tagged aptamer is absorbed on the graphene oxide (GO) and quenched by FRET, the aptamer/GO complex interacted with the theophylline. As a result, the aptamer deforms in its three-dimensional form and pairs with theophylline. Then, cryonase digestion occurs on the released complex, subsequently analyte can bind to another aptamer for another consequential split reaction. To amplify the fluorescence signal, cyclic reactions are done repeatedly till all fluorophores turn on (Fig. 7). By this fluorescence aptasensor, theophylline was quantitatively detected in a linear range of 50 nM–5 μM, and the detection limit was 47 nM [105].

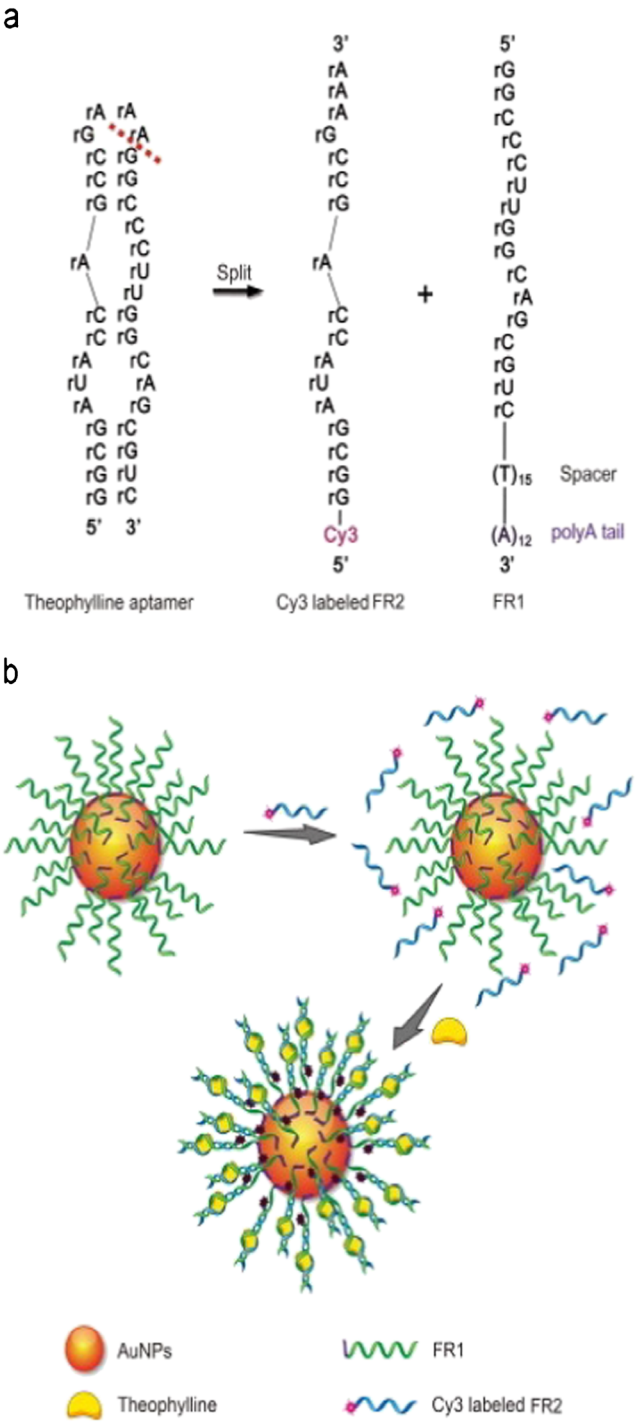

Fig. 6 Schematic representation of the design principle (a) and the sensing mechanism (b) of the self-assembling RNA aptamer-based gold nanoparticle sensor for theophylline detection in serum [94]

Detection and determination of digoxin

To achieve the higher sensitivity and lower detection limit, as the two important factors for performance of fluorescence-based sensor and biosensor, there is a need for powerful fluorophores [106]. Silica nanomaterials, due to their tunable size,

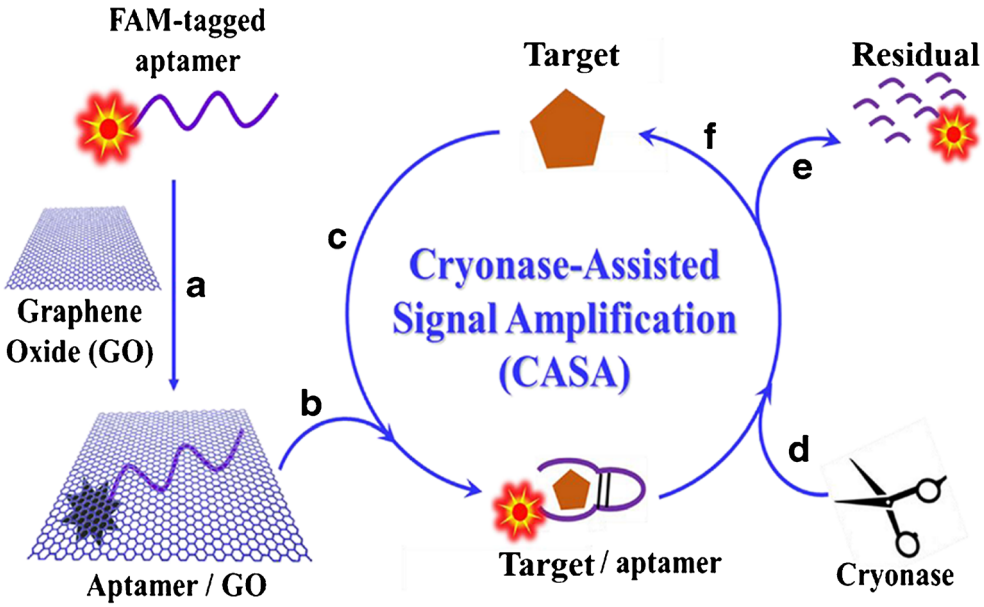

Fig. 7 The working mechanism of the cryonase-assisted signal amplification (CASA) for target assay [105]

optical transparency, high hydrophilicity, facilaited surface modification, biocompatibility, low cytotoxicity, and control over particle interactions, are considered as qualified candidates for making fluorescence based (bio)sensor [107][108].

Emrani et al. used streptavidin-coated silica nanoparticles (SNP) for construction of fluorescence-based biosensor. The SNP–double stranded DNA (dsDNA) complex will have an intense fluorescence signal in the absence of digoxin. With introducing digoxin into the assay solution, the aptamer transforms to its 3D-dimensional structure and binds to digoxin, as a result the labeled-complementary strand separates from dsDNA-SNPs, and decreases the fluorescence intensity (Fig. 8). This fluorescence-based aptasensor can detect digoxin with high selectivity, and a limit of detection was 566 pM [109].

Quality of immobilization of aptamer on the surface of transducer affected the stability, affinity, and specificity of the aptamer toward the analyte. There are various immobilization methods such as covalent binding, physical adsorption, self-assembly, avidin–biotin immobilization, and hybridization [110]. Elmizadeh and coworkers used two designs for immobilization of aptamer for construction of ultrasensitive fluorescent nano aptasensor for detection of digoxin (DX). In the first method, the fluorescence intensity of reduced

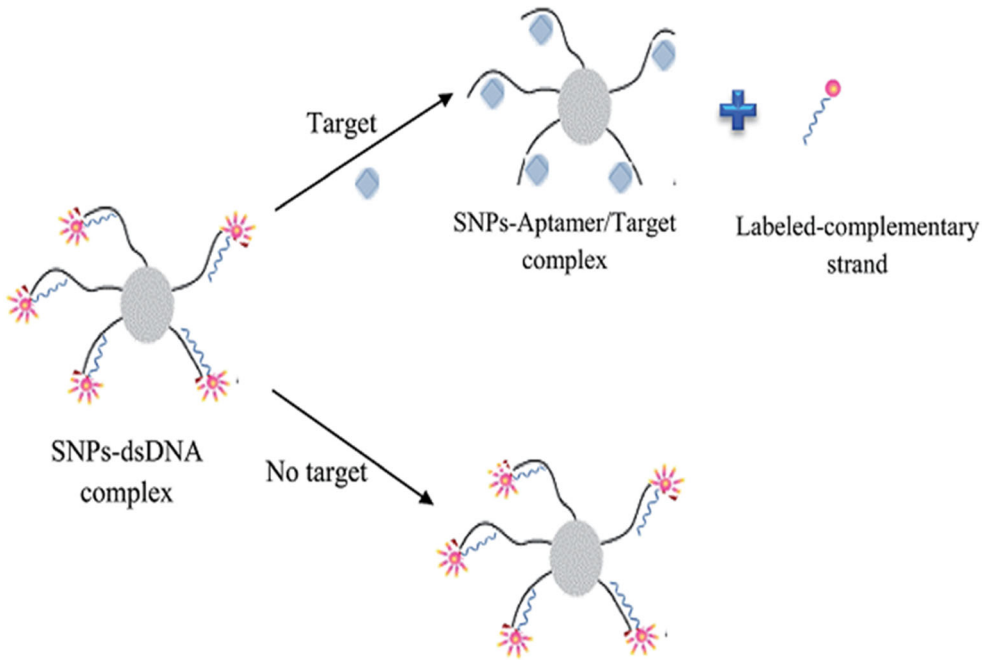

Fig. 8 Presentation of digoxin detection based on fluorescence property of silica nanoparticles and aptamer [109]

graphene quantum dots (rGQDs) increased by a label-free aptamer that directly interacted with rGQDs. Upon introducing DX to assay solution and formation of the aptamer-DX complex, the fluorescence intensity was reduced. In the second approach, an amine-modified aptamer was used. Amine modified aptamer-rGQDs fluorescence induced turn-off using oxidized carbon nanotubes (CNTs) via fluorescence resonance energy transfer (FRET) mechanism. In the following, addition of DX causes interaction with aptamer, and as a result inhibition of the connection between CNTs and amine-modified aptamer-rGQDs, and therefore the recovery of the rGODs fluorescence can be observed. Limit of detection was obtained as 29×10^{-12} mol L^{-1} and . 7×10^{-12} mol L^{-1} by label-free and labeled aptamer designs, respectively [111].

Detection and determination of vancomycin

Colloidal nanocrystalline semiconductors, known as quantum dots (QDs), are preferred to other luminescent materials due to higher quantum yield, flexible surface chemistry, better stability, great brightness, trivial photobleaching, and broad excitation spectrum as well as sharp and size-tunable emission spectrum [95]. These features have led to the emergence of QDs as a powerful candidate for construction of biosensors, especially for the development of fluorescence-based sensors and biosensors [112–116].

For sensitive detection of vancomycin in pharmaceutical formulation, environmental water samples, and spiked human serum, Liang and et al. developed an electron transfer and fluorescence "turn-off " based CdTe quantum dots [117]. The working mechanism of this sensor is as follows; glutathione capped-CdTe(GSH-CdTe) QDs were excited, leading to an electron transfer from its valence band to the conduction band and therefore a positively charged hole was formed in its valence band with a free electron in the conduction band. In the absence of vancomycin, recombination of the electron in the hole of the GSH-CdTe QDs occurs that consequently leads to fluorescent emission. However, in the presence of vancomycin, as an electron acceptor, the hindrance of the electron-hole recombination at the interfaces of GSH-CdTe QDs can occur (Fig. 9) and leads to fluorescence quenching. Fluorescence quenching was proportional to the increase in the concentration of vancomycin in the range of 1.53 ng mL^{-1} to 20.0 μg mL^{-1}, with a corresponding LOD of 0.460 ng mL^{-1}.

In a single wavelength fluorescence probe, the fluorescence intensity, as an analytical signal, depends on the concentration of the target analyte, whereas two or more fluorescence signals at different wavelengths are measured in the ratiometric fluorescent approach. Their intensity ratio which varied with the concentration of the target analyte in the assay solution is considered as an analytical signal. Indeed, an internal standardization was performed using this analytical fluorescence signal ratio that may affect the fluorescence signal and sensor performance [118]. To have a reliable and sensitive fluorescence sensor for measuring different analytes and overcome the mentioned obstacles, the ratiometric fluorescence technique can be used in the design of fluorescence-based sensors and biosensors [119–121].

For quantitative detection of vancomycin (VAN), Deng and coworkers developed a sensitive ratiometric fluorescent probe with the combination of coumarin and fluorescein as dual fluorescence reporters and a VAN binding peptide (i.e., D-Ala-D-Ala). Due to the stacking and self-quenching effects, the fluorophore pair which consisted of coumarin and fluorescein gave no significant fluorescent radiation (I_{446}), in the absence of VAN. However, by introducing VAN-(D-Ala-D-Ala) to assay solution, the fluorescence turned on (I_{519}), probably due to the disaggregation of fluorophores (Fig. 10). The intensity ratio of the dual emission bands I_{519}/I_{446} exhibited an excellent linear relationship with the concentration of VAN increasing from 0 to 20 μM in synthetic urine. The lowest detection limit was calculated to be 92.8 nM in urine [122].

Other fluorescence-based NTIDs nano sensors and biosensors

In the inner filter effect (IFE) based on sensor, electromagnetic radiation is absorbed either at the excitation or at the emission wavelength range of the fluorophore, then the chromophores act as a filter. Fluorescent carbon dots (CDs) have gained widespread attention as an analytical probe due to concentration-dependent luminescent properties [123]. In some of fluorescence based assay, considering the IFE, CDs as fluorophore were used for detection of various analytes such as acetamiprid (absorber: AuNPs) [124], paraoxon (absorber: p-nitrophenol)[125], Quercetin (absorber: Quercetin) [126] and hemoglobin (absorber: hemoglobin) [127].

Ma and coworkers used IFE technique for development of a simple and sensitive fluorescence sensor for recognition and determination of carbamazepine (CBZ). In their IFE system, blue-emitting carbon dots (CDs) act as a fluorophore and CBZ was an authoritative absorber that can competitively absorb the excitation light of quantum dot. Due to this quenching effect of CBZ, based on the IFE, it can decrease the fluorescence intensity of the CDs.

As a result, the fluorescence extinction of CDs depends on the concentration of CBZ. In this IFE-based fluorescence nano-sensor, the correlation between fluorescence quenching efficiency and concentration of CBZ is linear in the concentration range 10.0–90.0 μg mL^{-1}. Also, the limit of detection was 1.93 μg mL^{-1} [128].

For sensitive detection of warfarin, a fluorescence sensor was developed by quenching the fluorescence of l-tryptophan due to the interaction between warfarin and l-tryptophan(Fig. 11). The fluorescence quenching rate is proportional to the warfarin concentration. By this sensor, concentration of warfarin was obtained with a linear range and detection limit (3σ/

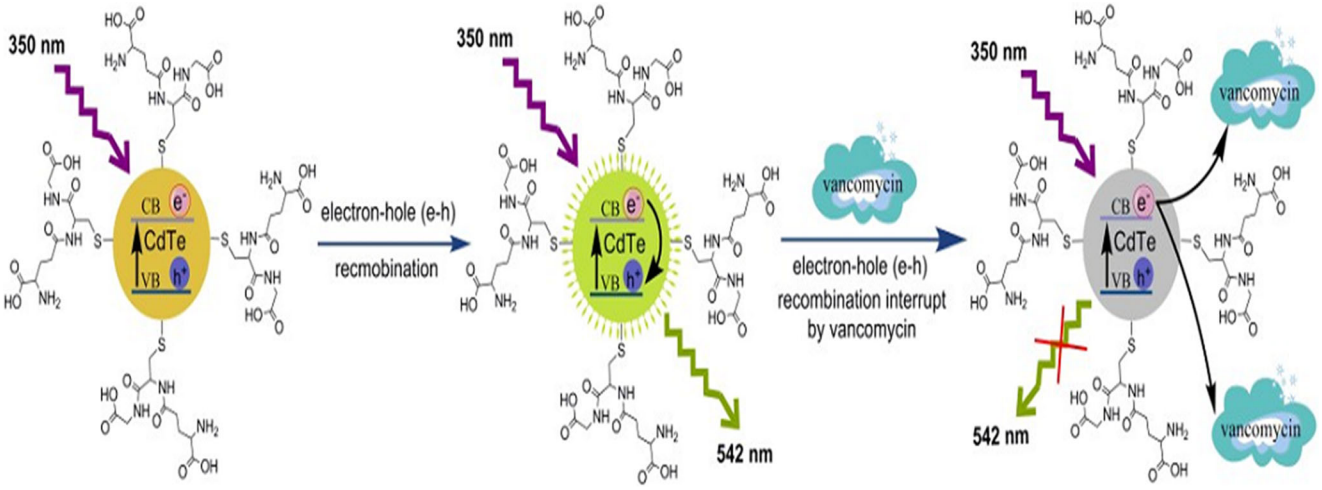

Fig. 9 Mechanism of the fluorescence quenching process for detection of vancomycin [117]

k) of 0.04–12.0 μmol L^{-1} (R^2 = 0.994) and 0.01 μmol L^{-1}, respectively [129]. In summary, selected fluorescence-based sensors and biosensors fabricated for NTIDs are presented in Table 3.

Chemiluminescence-based techniques

CL (Chemiluminescence) techniques are rapid and selective, thus CL-based sensors are superior to other optical methods, such as absorbance and fluorescence detection [151]. Prominent features such as high sensitivity, simple instrumentation, wide calibration ranges, suitability for miniaturization in analytical chemistry, and controllable emission rate have made CL a powerful analytical method for the detection of various analytes including drugs [152], biomarkers [153], pesticides [154], heavy metal [155], and others. Despite these advantages, only few CL-based sensors have been fabricated for the detection of NTIDs. Short lifetime and signal drift due to the irreversible consumption of CL reagents as well as poor reproducibility have limited the application of CL sensors in practice for routine analysis. However, for reduction in the consumption of the luminescent reagents, various CL-based sensors have been developed on the rolling circle amplification strategy and isothermal exponential amplification. Despite low sensitivity of CL sensors, as an important challenge, they are still suitable for practical applications [156]. In

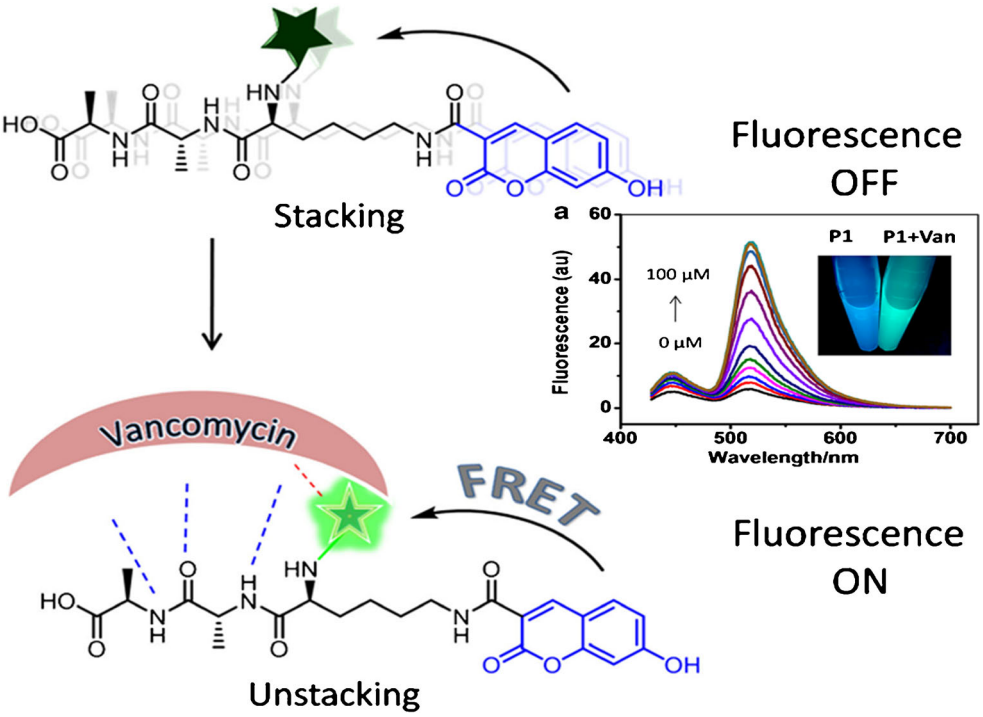

Fig. 10 Working principle of vancomycin detection by rational fluorescence strategy [122]

Table 3 NTIDs nano fluorescence-based sensors and biosensors

Strategy (recognition element)	Drug	Matrices	Linear range (nM)	LOD (nM)	Ref.
RNA aptamer/graphene oxide	Theophylline	Human serum	1000–100 × 10^3	155	[130]
RNA aptamer/fluorescently labeled DNA strand	Theophylline	Aqueous solution	–	2	[131]
Fluorescently labeled DNA duplex aptamer	Theophylline	Horse serum	5–20 × 10^3	320	[132]
RNA aptamer/carbon nanoparticle and cryonase	Theophylline	Fetal bovine serum	0–250	6.3	[133]
RNA ribozyme/DNase I/graphene oxide	Theophylline	Buffer solution	0.1–10 × 10^3	100	[134]
RNA aptamer/RNA enzyme	Theophylline	Human serum	0–500 × 10^3	92	[135]
DNA strand/antibody	Digoxin	Plasma sample	10–100	10	[136]
DNA aptamer/AuNPs	Digoxin	Rat serum	0–30	0.392	[58]
Polyclonal antibody/MIP	Digoxin	Human serum	Immunosensor 1.53-51.2 MIP sensor 0.021-5.12	1.53 0.02	[137]
MIP	Digoxin	Human serum	–	0.02	[138]
Antibody	Gentamicin	Animal-derived food	0.14 × 10^4–18.1 × 10^4	356	[139]
Antibody/liposomal nanovesicles	Gentamicin	Skim milk	29.6–20.9 × 10^4	29.65	[140]
Antibody/Colloidal gold	Gentamicin	Milk	20.9–12.3 × 10^2	10.47	[141]
Organic nanoparticles	Lithium	Aqueous media	0–104 × 10^3	122	[142]
Metallacrown complex	Lithium	Human serum	–	1000	[143]
Crowned spiropyran	Lithium	Acetonitrile	0–500 × 10^3	100	[144]
Quantum dots (CdTe)	Valproic acid	Tablet, urine, serum	2 × 10^3–52 × 10^3	1.66	[145]
Eosin Y	Clindamycin	Gel, solution, capsules, vaginal cream	433.4–43.3	281.7	[146]
Copper nanoclusters	Carbamazepine	Exhaled breath condensate	8.4 × 10^2—8.4 × 10^3	3.8 × 10^2	[147]
Monoclonal antibody	Cyclosporine	Whole blood, human serum	–	8.31	[148]
Warfarin–Eu^{3+}– 2-tenoyltrifluoroacetine (TTA)	Warfarin	Aqueous solution	1 × 10^3–1 × 10^5	5.1 × 10^2	[149]
Palladium complexes	Warfarin	Buffer solution	0–12 × 10^3	2 × 10^3	[150]
amino-functionalized graphene quantum dots	Aminophylline	Tablet sample	237.1–2371.1	95.1	[151]

this section, we have summarized CL-based assays for quantitative detection of NTIDs.

Detection and determination of vancomycin

The nanomaterials (NMs) as CL emitters have surface trap-control luminescence, high quantum yields, great molar extinction coefficients, chemical stability, and negligible photobleaching/photo-degradation [157]. The use of nanomaterials such as gold [158], silver [159], platinum [160], CdTe [161], TiO_2 [162], Se [163], and CuO nanoparticles [164] in CL systems can facilitate the fabrication of novel nano (bio)sensors with high sensitivity [165].

Recently, a nano sensor amplified flow-injection chemiluminescence (CL) system using CuO nanosheets (NSs) and luminol–H_2O_2–CuO nanosheets was fabricated for sensitive detection of the vancomycin [166]. In this approach, under alkaline conditions, CuO nanosheets act as a nano-catalyst on the luminol–H_2O_2 CL reaction which can be efficiently generating a remarkable increase in CL emission. By introducing vancomycin to this CL system, an efficient inhibition of the CL intensity of luminol–H_2O_2–CuO was observed. In the concentration ranges of 0.5–18.0 and 18.0–40.0 mgL^{-1}, the CL intensity of this system, under the optimized conditions, was proportional to the concentration of vancomycin with a detection limit of 0.1 mgL^{-1}. In CL systems, various QDs including semiconductor QDs, carbon nanodots (CDs), graphene quantum dots (GQD), graphitic carbon nitrides (g-CNQDs), black phosphorus quantum dots (BPQDs), nitrogen-rich QDs (N-dots), silicon carbide (SiC-dots), MoS_2 QDs, and so on were widely used as enhancers, catalysts, carriers, or quencher [167]. Mechanisms of QDs in chemiluminescence are as (i) direct chemiluminescence, QDs are emitter species after direct oxidation; (ii) chemiluminescence catalysts, QDs are catalysts of the reactions involving others luminophores; and (iii) chemiluminescent energy acceptor, QDs are emitter species after chemiluminescence resonance energy transfer (CRET) [168].

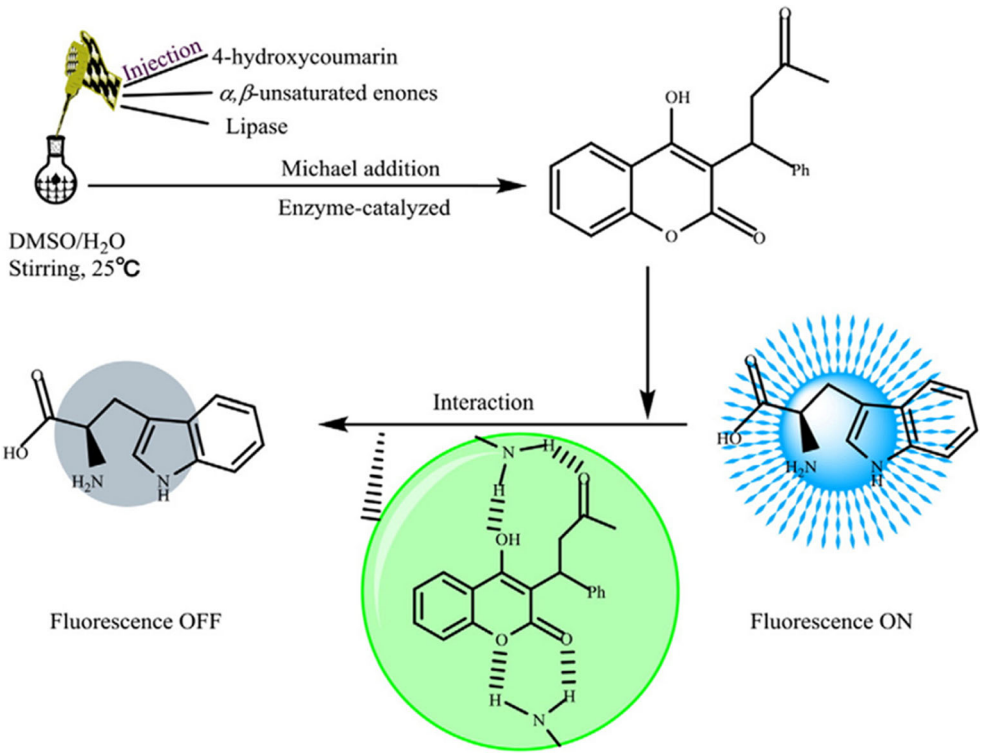

Fig. 11 Schematic presentation of warfarin detection and its interaction with tryptophan [129]

For sensitive detection of vancomycin, a CL nano sensor based on cadmium sulfide quantum dots (CdS QDs) which was decorated with L-cysteine as sensitizer in $KMnO_4$–morin CL system was developed [169]. In this study, CdS QDs as an acceptor part have a significant role in CL energy transfer from (morin)* as a donor. This process is accompanied by direct oxidation of CdS QDs. With the presence of vancomycin in the assay solution, the CL intensity of the $KMnO_4$–morin–CdS QDs system was remarkably enhanced. Enhancement CL intensity was proportional to vancomycin concentration in the linear range of 0.004 to 19 mg L^{-1}, with a detection limit (3σ) of 1.4 μg L^{-1}.

Detection and determination of aminophylline

One of the main disadvantages of the conventional CL systems is the low yield for transforming the chemical energy into light [170]. Recently, diverse catalysts including nanomaterials, such as noble metal nanoparticles [171, 172], and metal oxide nanostructures (TiO_2, ZnO_2) [173], usual peroxidase enzyme [174] and QDs [168], have been used for increasing the efficiency of CL. The selectivity of CL assay in direct CL systems remains a great challenge [170]. Magnetic iron oxide nanoparticles (MIONs) are one of the interesting approaches to overcome this challenge.

Owing to their particular physicochemical and magnetic properties, MIONs are widely used in human biomedical applications including magnetic separation of biological materials, diagnostic applications, labeling, and imaging [175]. Fe_3O_4 is one of these MIONs that can amplify the CL intensity of luminol by at least 20 times [170]. In the luminol−Fe_3O_4-based CL system, due to high peroxidase-like catalytic activity, Fe_3O_4 nanoparticles can act as a catalyzer for surface catalyzing of the disintegration of dissolved oxygen to superoxide anions [176]. In this CL system, it is concluded that Fe^{2+} ions, found in the Fe_3O_4 nanoparticles and dissolved oxygen, can act as light emitter factors. After generation of superoxide anions at the surface of Fe_3O_4 nanoparticles and under alkaline conditions, they oxidize luminol to produce the intense CL emission [170]. For detection of aminophylline (AMP) in human serum, Rezaei and coworkers used luminol–diperiodatoargentate(III) (DPA) system catalyzed by coated iron nanoparticles (CIN) to set up CL system. In this approach, FeNPs act as catalyzers for oxidation of luminol in the presence of oxygen. In the presence of FeNPs, due to their catalytic properties, the number of luminol free radicals increases and as a result the intensity of CL signal of luminol-DPA system can increased (amplified) and therefore the CL reaction response time is reduced (Fig. 12). In luminol–DPA–FeNPs system, the CL signal was proportional to the aminophylline (AMP) concentration in the range of 1.0×10^{-8}–2.0×10^{-6} $molL^{-1}$. Moreover, the LOD for this sensor was reported as 9.8×10^{-9} $molL^{-1}$ [177].

In the other study, a CL-based assay for the determination of AMP was developed which was based on the inhibition effect on the chemiluminescence emission of N-bromosuccinimide–luminol (NBS–luminol) system. NBS as brominating and oxidizing reagent was introduced into CL reaction. In luminol–NBS–AMP system, amino groups in

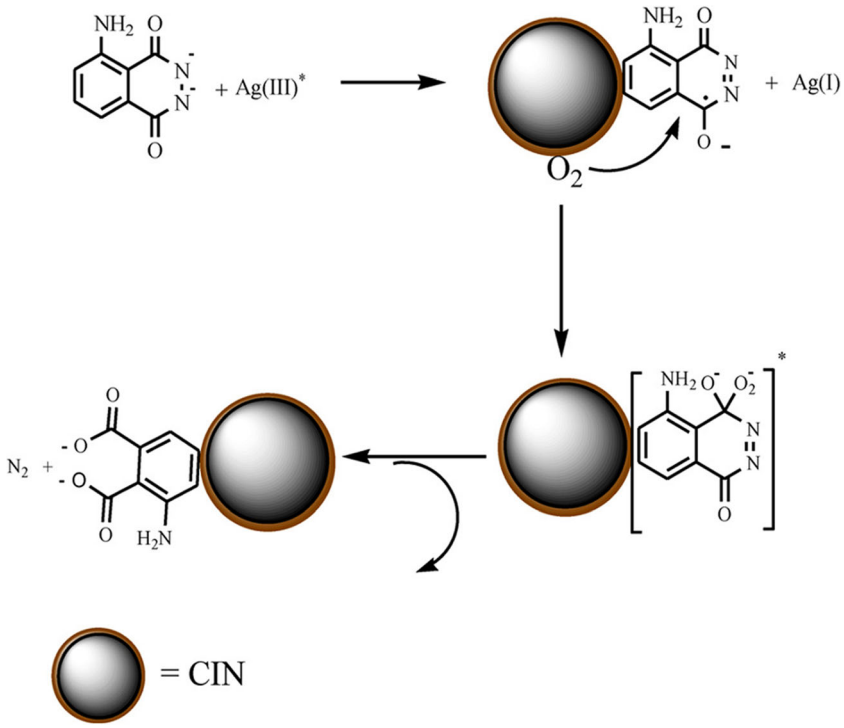

Fig. 12 Proposed CL reaction mechanism of luminol–DPA–AmP system in the presence of FeNPs [177]

the molecule structure of AMP make the redox with NBS. Therefore, consumption of NBS, the oxidant of luminol–NBS system, led to a decrease in CL intensity. The decreased CL intensity is proportional to the concentrations of AMP in a certain range. This CL assay was used successfully for the determination of AMP in pharmaceutical and spiked plasma samples. The detection limit was 3.4×10^{-8} gml^{-1} in the linear range of 1×10^{-7} to 7.0×10^{-6} gml^{-1} [178]. In summary, selected CL-based nano sensors and biosensors fabricated for NTIDs are presented in Table 4.

Electrochemical nano sensors and biosensors for detection of NTI drugs

The majority of NTI drugs pose a measurable electrical signal which can be used for quantitative analysis. Therefore, the measurement and determination of NTI drugs level can be provided via electrochemical approaches as a sensitive, simple, low cost, and selective method [189–193]. In between twenty-five NTI drugs reported by the FDA, theophylline, aminophylline, isoproterenol, and levoxyine are widely

Table 4 NTIDs nano CL-based sensors and biosensors

Strategy (recognition element)	Drug	Matrices	Linear range	LOD	Ref.
$Ru(bipy)_3^{3+}$	Carbamazepine	Tablet	4.0×10^{-3}–8.6×10^{7} mol/L	2.5×10^{-7} mol/L	[179]
Luminol/$K_3Fe(CN)_6$	Clindamycin	Capsule , human urine	0.7–1000 ng/mL	0.2 ng/mL	[180]
Luminol/hypochlorite	Gentamicin	Eye drops, injections	1.0–4.0 μgmL^{-1}	0.023 μgmL^{-1}	[181]
Peroxyoxalate CL/imidazole	Gentamicin	Injection ampoules, eye drops	3.93–30 μgmL^{-1}	1.18 μgmL^{-1}	[182]
Luminol/H_2O_2-Catalyzed by Cu(II)	Gentamicin	Pharmaceutical formulation/water samples	1.0–30.0 μgmL^{-1}	0.1 μgmL^{-1}	[183]
Monoclonal antibody	Theophylline	Human serum	0.51–40 mg/L	–	[184]
QDs–luminol–potassium periodate	Theophylline	Tablet	1.0×10^{-8}–1.0×10^{-5} g/mL	2.8×10^{-9} g/mL	[185]
Antibody-thermochemiluminescence/silica nanoparticles	Valproic acid	Blood, saliva	4–300 μgmL^{-1} 0.05–20 μgmL^{-1}	4 μgmL^{-1} 0.05 μgmL^{-1}	[186]
Luminol-$KMnO_4$	Levothyroxine	Tablet	5.0×10^{-8}–3.0×10^{-6} mol/L	8.9×10^{-9} mol/L	[187]
Magnetic nanoparticles labeled antibodies	Digoxin	Human serum	8.0×10^{-9}–800×10^{-9} mol/L	3.6 mol/L	[188]

studied by electrochemical methods. A wide spectrum of sensing platforms composed of carbon nano-materials, metal nanoparticles and, polymers in absence (sensors) or in presence (biosensors) of biological recognition elements such as DNA, aptamers, enzymes, and antibodies were designed for increasing the electrocatalytic activity of electrochemical sensors and biosensors [194–196]. It is noteworthy that the electrochemical techniques are commonly used for investigation, detection, and measurement of NTI drugs in serum and blood samples [197, 198]. In this part, some electrochemical sensor and biosensor approaches that were developed for measuring of NTI drugs are highlighted. To gain insight into the other reported progress, the fundamental cases of the electrochemical sensor and biosensors such as analytical parameters (linear range and detection limit), type of electrodes, and measurement methods are given in separate tables.

Electrochemical detection of theophylline

Based on electrochemical investigations, theophylline is oxidized with loss of two electrons and two protons via the irreversible mechanism [199, 200]. Ahn and coworkers [201] used a biological recognition element on the gold electrode to detect theophylline via differential pulse voltammetry system. A DNA duplex aptamer with an abasic (AP) site opposite of cytosine was coated on the gold surface via sulfur moiety. As the consequence of DNA damage or mutation (loss of nucleobase), apurinic/apyrimidinic or abasic (AP) sites which have high affinity for theophylline can be formed (Fig. 13I). Based on cyclic voltammetry data, the silver ions are captured into the AP site, and a strong electrochemical signal was observed in the absence of theophylline. The oxidation peak of Ag^+ was significantly reduced when the AP site was occupied via theophylline (Fig. 13II). This result is because of the non-electroactivity of theophylline in the AP site. The detection limit and linear range are achieved 3.2 and 0–50 μM, respectively.

In another approach, an electrochemical biosensor is fabricated and applied to detect the theophylline in serum samples with a remarkable detection limit (0.2 μM) by Ferapontova and coworkers [202]. The bio-recognition element is considered as an RNA aptamer which is accompanied with a probe (i.e., ferrocene (Fc)) and is attached to the gold electrode. In this approach, the electrochemical signal of Fc/Fc^+ is related to the conformation of RNA at the electrode surface. The gold modified electrode is prepared through an stepwise method including polishing of bare electrode, immobilization of RNA with sulfur moiety on gold electrode, synthesis of ferrocene-carboxylic acid N-succinimide ester (FcNHS) in dichloromethane (DCM)/EDC mixture solution, and finally, modification of aptamer with FcNHS (Fig. 14A, B). After the addition of theophylline, the conformational folding of the RNA can lead to increasing the electrical response of the Fc probe (Fig. 14C). The monitoring of theophylline and caffeine level in foodstuffs such as green tea is performed by Wang and coworkers [203]. The electronic and electrocatalytic features of the sensing platform (glassy carbon electrode) are increased with nitrogen-doped carbon nanotubes (N-CNT) and poly (L-cysteine). The constant applied potential (2.5 V) is used to electrodeposit N-CNT on the glassy carbon electrode. In the second step, repetitive cyclic voltammetry (10 cycles) was performed for electro-polymerization of L-cysteine in 0.1 M PBS (pH 6.0) solution (Fig. 15I). The highest current (maximum sensitivity) of oxidation peaks is

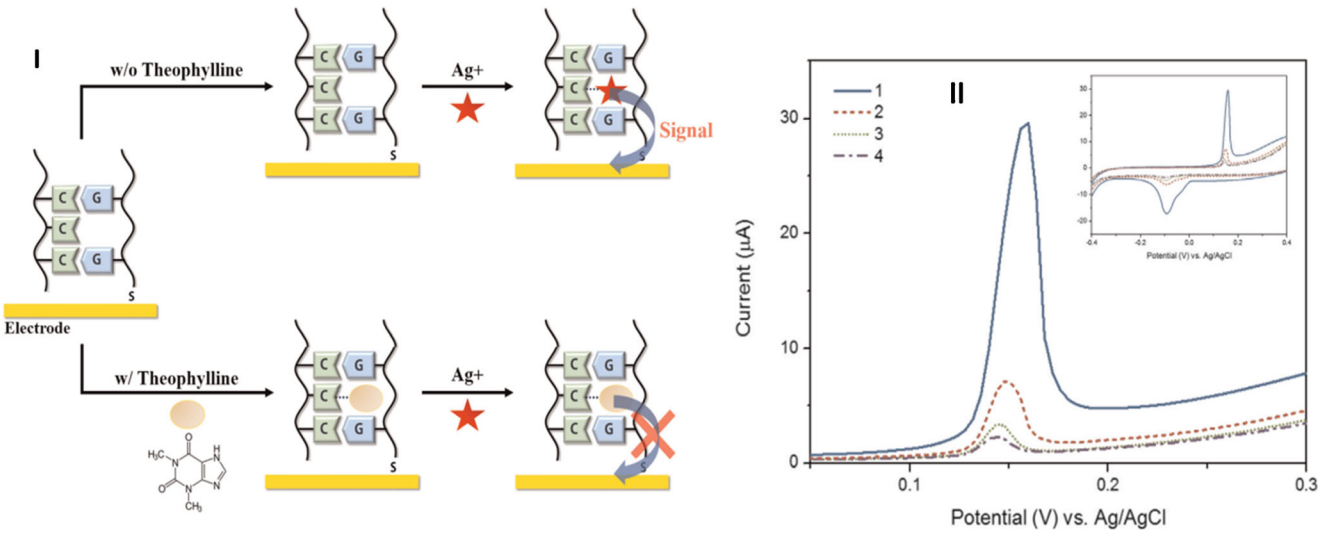

Fig. 13 (I) Schematic representation of electrochemical approach to detect theophylline based on the redox reaction of silver ions captured into AP site-incorporated duplex DNA. (II) Oxidation peak signal of cyclic voltammetry generated by silver ions within AP site-incorporated duplex DNA or full-matched duplex DNA in the absence and presence of theophylline (AP site-incorporated duplex DNA in the absence (1) and presence (2) of theophylline and full-matched duplex DNA in absence (3) and presence (4) of theophylline). Inset: cyclic voltammogram containing oxidation peak at + 0.15 V and reduction peak at − 0.09 V [201]

achieved on PLCY/N-CNT/GC electrode. The detection limit and linear range are achieved 0.033 and 0.1–70.0 μM, respectively (Fig. 15II). In summary, a variety of sensing platforms with related analytical parameters is given in Table 5.

Electrochemical detection of carbamazepine

Anodic oxidation of carbamazepine (CBZ) has been investigated at the various electrode surfaces with loss of one electron and formation of cation radical and CBZ dimer [233–236]. In 2011, Pruneanu [237] and coworkers successfully determined the concentrations of CBZ using the graphene-gold nanoparticle composites which were deposited on the gold electrode (Au-Gr-AuNPs) in acetonitrile and tetrabutyl ammonium perchlorate (TBAP) as supporting electrolyte. Two deposition steps were performed for preparing the sensing device. The stepwise preparation of the Au-Gr-AuNPs is illustrated in Fig. 16. In comparison to the bare gold

Table 5 A comparison of analytical parameters, sensing platforms, and electrochemical techniques of various theophylline nano sensors and biosensors

Electrode	Detection limit (μM)	Linear range (μM)	Method	Ref.
Nafion/MWNTs/GCE	0.02	0.08–60.0	DPV	[204]
MnO_2/MWNT/GCE	0.01	0.1–20.0	DPV	[205]
CdSe/GCE	0.4	0.1–700	DPV	[206]
ACNT/GCE	0.016	0.08–10.0	DPV	[207]
HMDE	0.6 $\mu g1^{-1}$	0.6–3.6 $\mu g1^{-1}$	DPCSV	[208]
AuNPs/MIP/GCE	0.1	0.4–3400	DPV	[209]
pPABSA/GCE	2.266	2.5–300	SWV	[210]
MWCNT-IL/GCE	0.16	0.5–98.0	DPV	[211]
SiO_2@TiO_2@MIP/CPE	0.0012	0.010–40	DPV	[212]
MB/RNA/Au	2.0	20 – 100	DPV	[213]
SPE	10	55–110	CV	[214]
GC/HDA/ERGO	0.0029	0.05–40.0	DPV	[215]
GQD/SPE	0.2	1.0–700.0	DPV	[216]
PFA/GR/GCE	0.03	0.2–100	DPV	[217]
MWNTs/Au/poly-L-lysine	2.0	10–200	SWV	[218]
graphene/Nafion/GCE	0.006	0.01–1.0	DPV	[219]
SPE	0.03	0.40–100	MPA	[220]
P (L-Asp)/fMWCNT/GCE	0.02	0.1–50	DPV	[221]
poly(CTAB)/GCE	0.11	0.5–1000	DPV	[222]
ssRNA/NPGs/GC	1.2	2.0–50.0	DPV	[223]
ThOx/SAM-modified Au	2000	2000–3000	AM	[224]
ThOx/DDAB on Gr	200	200–8000	AM	
ThOx in Os-polymer on Gr	20	20–600	AM	
MIP/GCE	0.32	0.4–17	AM	[225]
MWCNT-PE	0.0197	2.0–150	DPV	[226]
MIP/CNPs–SO_3H/GCE	0.0014	0.05–30	CV	[227]
GNP–CHIT/r-GO/GCE	0.000132	0.0025–2.1	DPV	[228]
MWCNT/GCE	0.05	0.3–10	CV	[199]
GNP/l-cys/Gr/Nafion/GCE	0.0004	0.004–60.0	DPV	[229]
Split RNA aptamers/AuNPs	0.07	0.1–80	SWV	[230]
MnO_x/NH_2-IL/Chit/GC	0.05	> 120.0	DPV	[231]
LMC/Nafion/GCE	0.37	0.8–180.0	DPV	[232]

*MWNTs*multi-walled carbon nanotubes, *GCE* glassy carbon electrode, *MnO_2* mangenesium oxide, *CdSe* cadmium selenide, *ACNT* aligned carbon nanotube, *HMDE* hanging mercury drop electrode, *AuNPs* gold nanoparticles, *MIP* molecular imprinting polymer, *pPABSA* poly para amino benzene sulfonic acid, *IL* ionic liquid, *SiO_2@TiO_2* silicon dioxide@titanium dioxide, *MB-, SPE*screen-printed electrode, *HAD* 1,6-hexadiamine, *ERGO* reduced graphene oxide, *GQD* graphene quantum dot, *PFA* poly(folic acid), *GR* graphene, *P (L-Asp)* poly(L-aspartic acid), *fMWCNT* functionalized multi-walled carbon nanotube, *CTAB* cetyltrimethylammonium bromide, *ssRNA*single-stranded RNA, *ThOx* theophylline oxidase, *SAM*self-assembled monolayer, *DDAB* didodecyldimethylammonium bromide, *Os* osmium, *PE* paste electrode, *CHIT* chitosan, *LMC* large mesoporous carbon

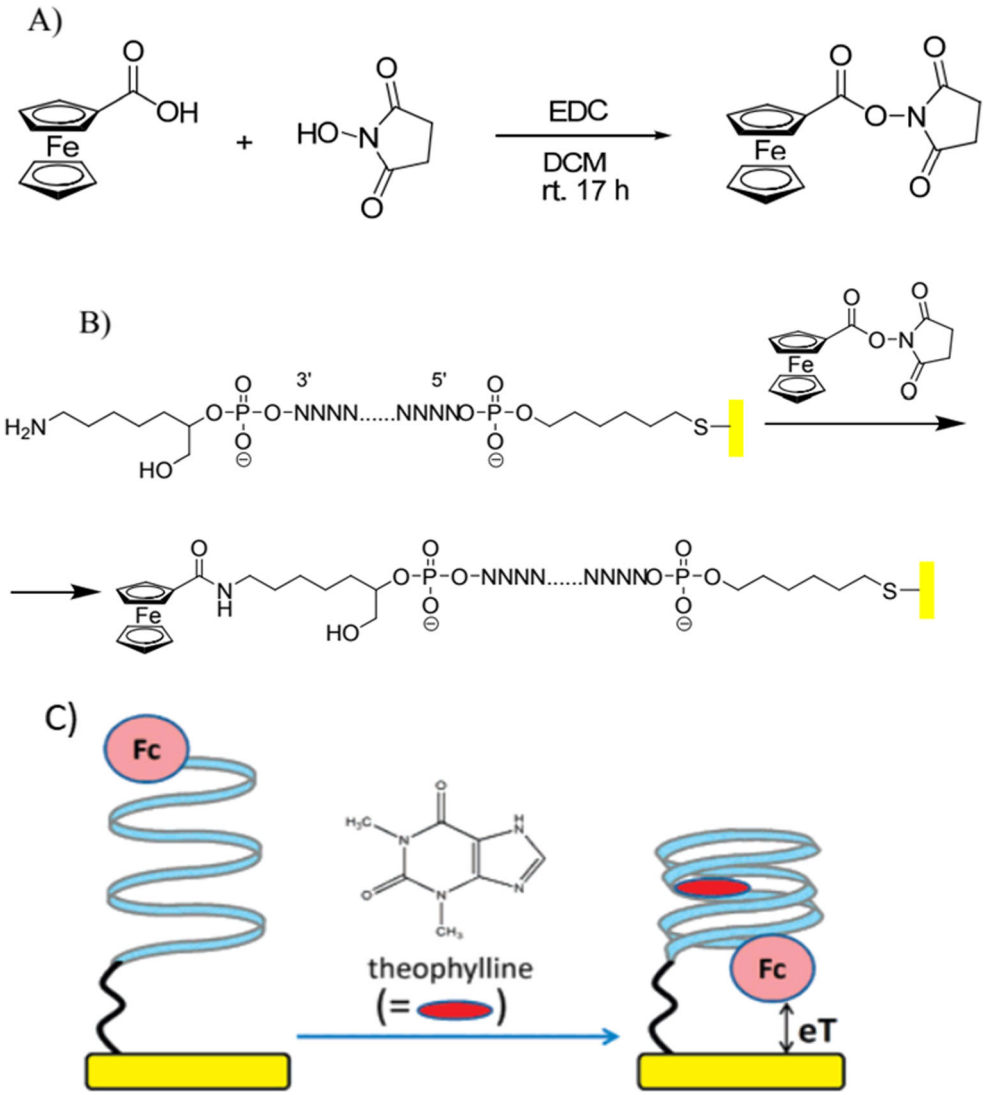

Fig. 14 (A) Synthesis of ferrocene-carboxylic acid N-hydroxysuccinimide ester and (B) surface modification of the RNA aptamer, immobilized at the electrode, with a Fc probe. (C) Schematic representation of the electrochemical RNA aptamer-based sensor for theophylline [202]

electrodes, the electrical signal of the modified electrode exhibited significant sensitivity (up to 2 times). This positive effect is shown at two concentrations (0.01 and 0.001 M) in Fig. 17. The analytical parameters are achieved as 3.03 and 5.0–20000 μM for detection limit and linear range, respectively. In another electrochemical approach, Lavanya and coworkers [238] detected CBZ on the screen printed carbon electrode modified by iron doped tin dioxide nanoparticles (SPE/Fe/SnO_2) with a detection limit of 92 nM in pharmaceutical products. The immobilization of Fe/SnO_2 was carried out using the dropwise addition of its homogeneous suspension on SPE. As depicted in Fig. 18 I, II, during the modification of the electrode surface, the current of oxidation peak at 0.6 V vs. Ag pseudo-reference electrode was increased. The maximum anodic current was observed using 5 wt% of Fe–SnO_2/SPCEs. The various designed electrochemical sensors accompanied with analytical parameters and type of electrodes as well as the application methods are presented in Table 6.

Electrochemical detection of isoproterenol

To the best of our knowledge, 1, 2-dihydroxybenzenes, or catechol derivatives can be oxidized (-$2H^+$, -$2e^-$) at the surface of electrodes and converted to *o*-benzoquinones compounds [250–252]. Therefore, the measurement of IP level as NTI drug is achieved via electrochemical method. Mazloum-Ardakani applied electrocatalytic approaches (EC' mechanism) for electrochemical sensors. In EC' mechanism, the electrode device has catalytic activity for isoproterenol (IP) detection and the presence of IP cause significant increase in the oxidation peak current [253, 254]. In one of these attitudes in 2015, the glassy carbon electrode (GCE) was modified with gold nanoparticle (AuNP) and then immersed in 3,4-dihydroxyphenyl-azo-2-thiophenol (DAT) solution [254]. The DAT was covalently connected to AuNP via the sulfur functional group (Fig. 19I). The results indicated that the IP (0.05 mmol/L) is oxidized at 0.35 V vs SCE on the bare GCE

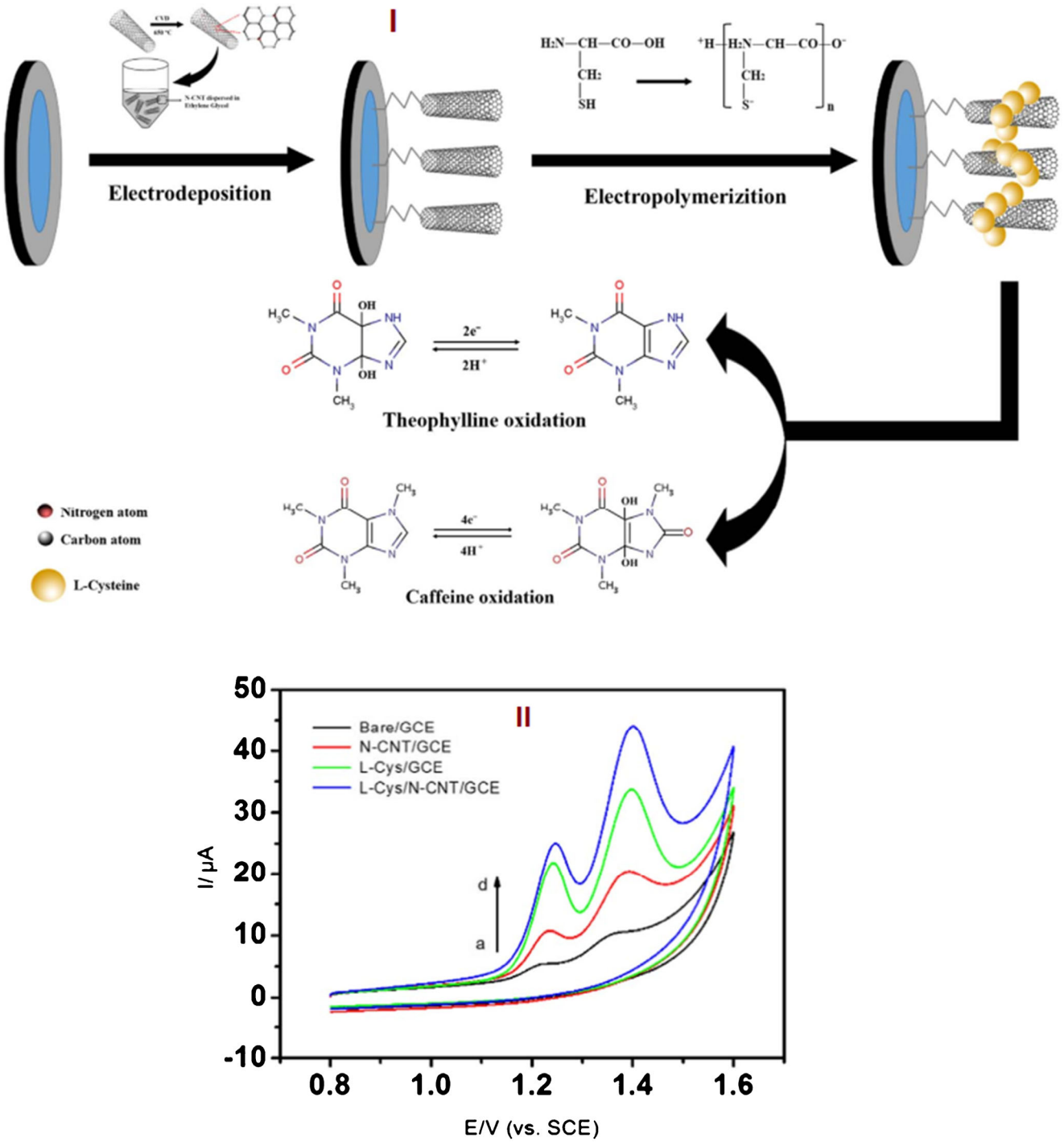

Fig. 15 (I) The stepwise of the synthesis of PLCY/N-CNT/GCE and the electrochemical oxidization of THEO and CAF. (II) Cyclic voltammograms for 10 μM theophylline and 20 μM caffeine in 0.01 M H_2SO_4-Na_2SO_4 (pH 1.70) at bare GCE (a, the blank curve), N-CNT/GCE (b, the red curve), PLCY/GCE (c, the green curve), and PLCY/N-CNT/GCE (d, the blue curve) [203]

surface and the catalytic mechanism was observed for the oxidation of IP at GCE/AuNP-DAT(Fig. 19II). In the absence of IP, a weak oxidation peak was observed at 0.21 V vs SCE. Based on DPV diagrams in different IP concentrations, 1–1500 and 0.46 μmol/L was obtained for linear range and detection limit, respectively. Conductive polymers accompanied with nano-carbon materials can enhance the sensitivity of IP detection. Palakollu and coworkers [255] fabricated the modified GCE with poly-(acid yellow 9) (PAY), β-cyclodextrin (β-CD), and graphene oxide (GO). After polishing and cleaning of GCE, repetitive cyclic voltammetry (10 cycles) of 0.25 M AY was performed in the range of − 0.5 to 2.0 V

Table 6 The comparison of different reported nano electrochemical sensors for the determination of CBZ

Electrode	Detection limit (μM)	Linear range (μM)	Method	Ref.
TiO_2NPs/Nafion/GCE	0.054	0.4–12	DPV	[239]
GCE	Water: 4.65 Ethanol: 38.1	Water: 3–500 μg/mL Ethanol: 11–600 μg/mL	DPV DPV	[240]
MWCNTs/GCE	0.04	0.13–1.60	CV	[241]
fullerene-C_{60}/GCE	0.0162	0.09–10	DPV	[242]
GR/MWCNT/CILPE	0.233	1–60	DPV	[243]
GCE/ERGO–SWCNT	0.029	0.05–3	Amperometry	[244]
[BnMIM]PF_6/CPE	0.98	7.0–700	DPV	[245]
GCE	DMF: 0.76 μg mL^{-1} ACN: 0.92 μg mL^{-1}	DMF: 20–200 μg mL^{-1} ACN: 20–200 μg mL^{-1}	DPV DPV	[246]
Au@AgPdNPs-β-CD-IL/GCE	0.089	0.5–90	SWV	[247]
Au	0.01 mol dm^{-3}	0.1–100 mol dm^{-3}	CV	[248]
BSA/GCE	1 μg/mL	2.0–23.6 μg/mL	DPV	[249]

CILPE carbon ionic liquid paste electrode, *ERGO* electrochemically reduced graphene oxide, *SWCNT* single walled carbon nanotube, *[BnMIM]PF_6-1*benzyl-3-methylimidazole hexafluorophosphate, *β-CD* β-cyclodextrin, *BSA* bovine serum albumin

in 0.1 M PBS (pH = 7.0) solution. The PAY was successfully coated on GCE, and the β-CD/GO composite was immobilized via drop casting method (Fig. 20). Electrochemical impedance spectroscopy (EIS) and cyclic voltammetry (CV) have been performed for characterization of GC modified electrode. For redox probe $[Fe(CN)_6]^{3-/4-}$ at β-CDGO/PAY/GCE, the diameter of the semicircle in the Nyquist (charge transfer resistance (R_{ct})) diagram was reached to the minimum value (Fig. 21A, curve f). This was attributed to the excellent conductivity and high electron transfer rate of the PAY and β-CDGO, respectively. Also, this phenomenon was confirmed via voltammetry and electrical current reduction (Fig. 21B, curve f). This collection (β-CDGO+ PAY) has the synergistic effect for determination of IP in urine samples. For simplification, electrochemical approaches with analytical details are presented in Table 7.

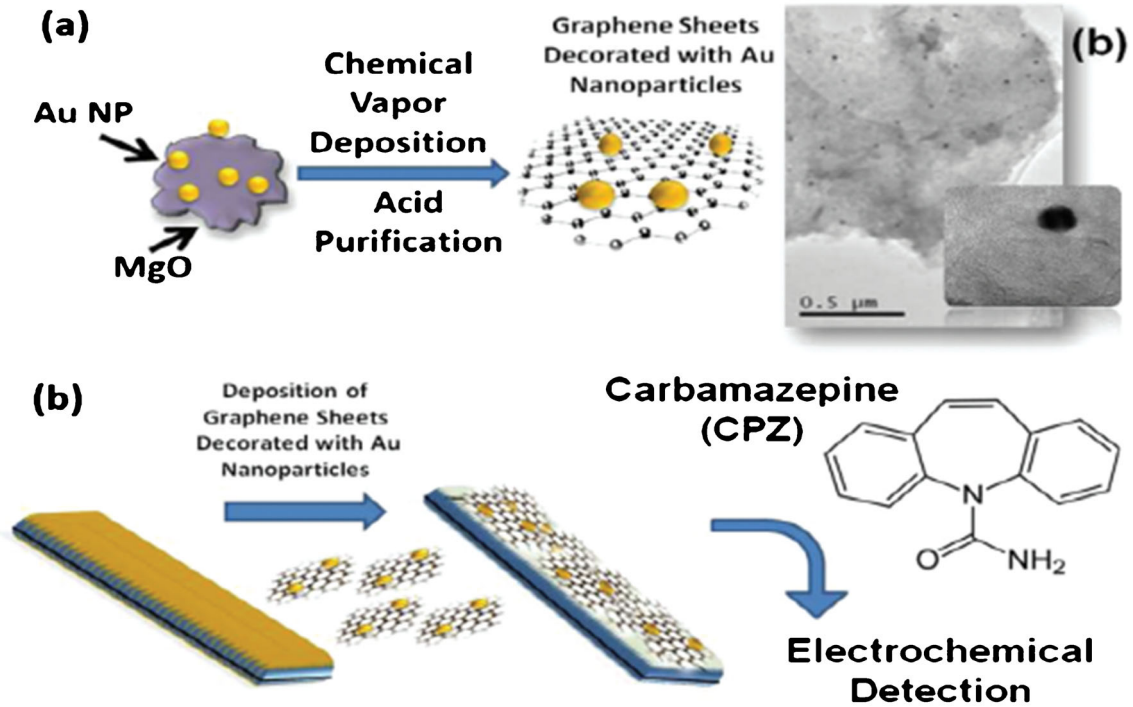

Fig. 16 (a) Schematic representation of the synthesis of graphene decorated with Au nanoparticles by over an Au/MgO catalyst; (b) the process used to deposit graphene-AuNPs composite over the top surface of a gold electrode to be further used in an electrochemical setup for the detection of carbamazepine [237]

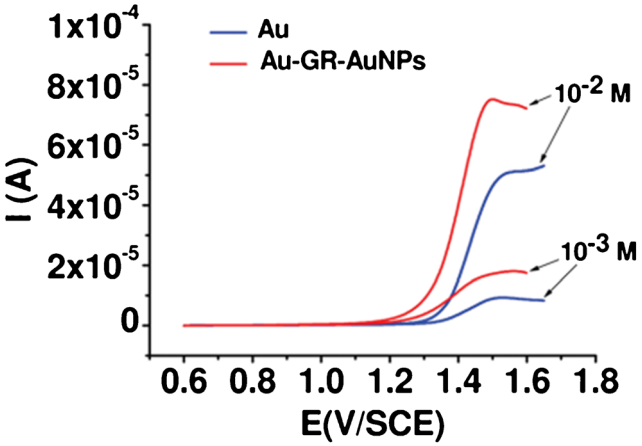

Fig. 17 LSVs recorded with Au (blue line) and Au-GR-AuNPs electrode (red line), respectively, in electrolyte containing various concentrations of carbamazepine (10^{-2} and 10^{-3} M), with scan rate 25 mV s^{-1} [237]

Electrochemical detection of levothyroxine

The electrochemical response (i.e., oxidation and reduction) of levothyroxine can be investigated using cyclic votammetry and differential pulse voltammetry techniques. It can be accomplished thorough variety of sensing platforms such as surfactant modified carbon paste and silver electrodes [278–280]. Lotfi and coworkers applied HPLC and electrochemical (DPV) approaches for the detection of levothyroxine (T_4) in real samples [281]. The homogeneous suspension of multi-walled carbon nanotubes (MWCNT) modified with gold nanoparticles/ mercaptoethanol/ melamine was cast onto a cleaned glassy carbon electrode. For electrochemical measurement, the relative recovery and relative standard deviation (RSD) values are comparable with HPLC results. By combination of electrochemical procedures with either liquid chromatography, high-performance frontal analysis (HPFA), electrospray ionization-mass spectrometry, capillary electrophoresis or luminescence attitudes, some reliable, fast, and high precision methods for medical or clinical diagnostic can be achieved [282–286]. Li and coworkers obtained a low detection limit (1.0 ng/mL) via immunoassay-electrochemical approach, and their results were more satisfactory than spectrophotometric enzyme-linked immunosorbent immunoassay (ELISA) method [287]. He and coworkers indicated that the oxidation peak current of thyroxine at the carbon paste electrode significantly increased in the presence of cetyltrimethyl ammonium bromide (CTAB) [288]. In addition to CTAB, two surfactants such as TritonX-100(TX-100) and Sodium Dodecyl Sulfate (SDS) were used to reinforce electrochemical responses (cathodic and anodic current) [278]. The remarkable features of multi-walled carbon nanotube (MWNT) films, such as high activity and improved conductivity, can present a high sensitive platform for detection of T_4 in blood and urine samples. In a study performed by Prasad and coworkers, detection of T_4 enantiomers (D- and L-thyroxine) have been carried out via modification of silver electrode with a multilayer of molecularly imprinted polymer (MIP) [289]. In this study, layer-by-layer strategy was used in fabrication procedure. In the first step, a mixture composed of monomer (1,3-diacryl urea), template (D- and L-thyroxine), cross linker (ethylene glycol dimethacrylate (EGDMA)), reducing agent (triethylamine (TEA)), catalyst ($CuCl_2$- 2,2'bipyridyl (bpy)-complex), and initiator (chloroform ($CHCl_3$)) was prepared and then stirred in presence of carbon powder in dimethyl sulfoxide (Fig. 22). By performing this step in triplicate, three layers were coated, and D- and L-thyroxine has been extracted by submerging the modified electrode into ethanol–ammonium hydroxide (1:2, v/v) mixture. To ensure complete

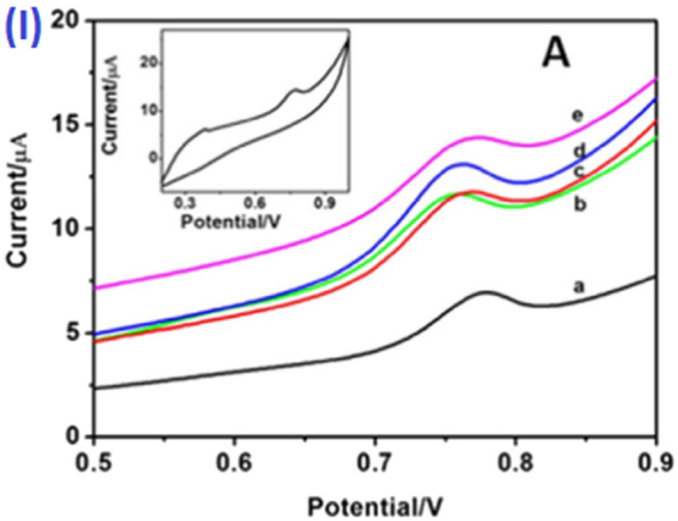

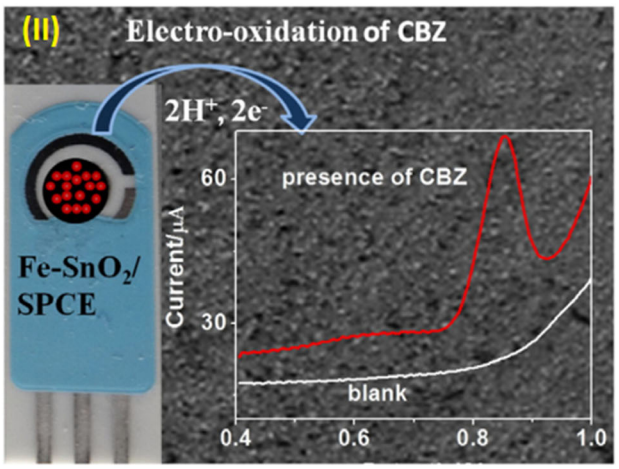

Fig. 18 (I) Anodic scan of CVs of 50 μM CBZ at (a) bare SPCE, (b) SnO_2, (c) 1 wt.%, (d) 3 wt.%, and (e) 5 wt.% Fe–SnO2/SPCEs in 1 M PBS (pH 7.0) at a scan rate of 50 mV s^{-1}. Inset shows the entire CV cycle of 5 wt.% Fe–SnO^2/SPCE. (II) Schematic representation of Fe–SnO_2/SPCE for the detection of CBZ [238]

Table 7 The comparison of different nano modified electrodes with its analytical parameters for the determination of IP

Electrode	Detection limit (μM)	Linear range (μM)	Method	Ref.
HGGCE	0.5 μM	1.0–800 μM	SWV	[256]
ZnO/NP/IL/CPE	0.09 μM	0.3–320 μM	SWV	[257]
DHB/CNT/CPE	1.24 μM	10–6000 μM	DPV	[258]
CD-TMCPE	0.47 μM	0.5–1000 μM	DPV	[259]
EFTAG-CPE	0.034 μM	0.1–400 μM	SWV	[260]
NYB/CNP/RGO/CPE	0.065 μM	0.5–1000.0 μM	DPV	[253]
1,4-BBFT/IL/GPE	12.0 nM	0.06–700 μM	SWV	[261]
CuNPs- GO-CB-PEDOT:PSS/GCE	1.9 μM	8.0–50 μM	SWV	[262]
GQDs/SPE	0.6 μM	1.0–900.0 μM	DPV	[263]
2,7-BFCNPE	26.0 ± 2 nM	0.08–700 μM	DPV	[264]
PGRMMWCNTPE	0.47 μM	0.8–570 μM	SWV	[16]
MWCNTPE	0.09 μM	0.3–450.0 μM	LSV	[265]
Lac-SiSG/MWCNT/GCE	0.18 μM	50.0–250.0 μM	DPV	[266]
MWCNTILE	0.85 μM	1.0 to 520 μM	DPV	[267]
GME	0.064 μM	0.21–100 μM	CV	[268]
3,4'-AAGCPE	0.012 μM	0.025–20 μM	SWV	[269]
5ADMBCNPE	39.0 nM	20–400 μM	SWV	[270]
MC-CNPE	35.0 nM	0.7–600.0 μM	DPV	[271]
FCMWCNTPE	0.07 μM	–	DPV	[272]
MCSILCPE	0.63 μM	1.0–700 μM	DPV	[273]
poly(1-methylpyrrole)-DNA/GCE	0.16 μM	2.0–60 μM	CV	[274]
CuHCF/CPE	80.0 μM	196–1070 μM	CV	[275]
DDF-CNT-TiO_2/IL/GC	28 ± 2 nM	0.1–1300 μM	DPV	[276]
5ADBCNPE	0.2 μM	0.4–900 μM	SWV	[277]

ZnO zinc oxide, *ILCPE* carbon paste electrode modified, *HGGCE*hematoxylin/graphene modified glassy carbon electrode with ionic liquid, *NP* nanoparticle, *DHB* 2-((7-(2,5-dihydrobenzylideneamino)heptylimino)methyl) benzene-1,4-diol, *CD-TMCPE* (E)-2-((2-chlorophenylimino)methyl)benzene-1,4-diol TiO_2 nanoparticles modified carbon paste electrode, *EFTAG* graphene and ethyl 2-(4-ferrocenyl-[1,2,3]triazol-1-yl) acetate, *NYB* (Z)-4-(naphthalen-1- ylimino methyl) benzene-1, 2-dio, *1,4-BBFT* 1-(4-bromobenzyl)-4-ferrocenyl-1H-[1,2,3]-triazole, *CB* carbon black, *PEDOT:PSS* poly(3,4- ethylenedioxythiophene)-poly(styrenesulfonate), *2,7-BFCNPE* 2,7-bis(ferrocenyl ethyl)fluoren-9-one modified carbon nanotube paste electrode, *PGRMMWCNTPE* pyrogallol red modified-multiwalled carbon nanotube paste electrode, *MWCNTPE* modified multiwall carbon nanotube paste electrode, *Lac-SiSG* laccase silica sol–gel, *MWCNTILE* multiwall carbon nanotubes ionic liquid electrode, *GME*graphene-modified glassy carbon electrode, *3,4'-AAGCPE* 3-(4'-amino-3'-hydroxy-biphenyl-4-yl)-acrylic acid modified graphene oxide nano sheets paste electrode, *5ADMBCNPE* 5-amino-20,40-dimethoxybiphenyl-2-ol, *MC-CNPE* modified carbon nanotube paste electrode, *FCMWCNTPE* ferrocene multi wall carbon nanotubes paste electrode, *MCSILCPE* carbon paste electrode modified with ionic liquid (n-hexyl-3-methylimidazolium hexafluoro phosphate) and magnetic core-shell nanoparticles, *2CBFCPE-2* chlorobenzoyl ferrocene modified carbon nanotube paste electrode, *CuHCF* copper(II) GU(III), *DDF* 9-(1,3-dithiolan-2-yl)-6,7-dihydroxy-3,3-dimethyl-3,4-dihydrodibenzo[b,d]furan-1(2H)-one, *5ADBCNPE* carbon paste electrode modified with 5-amino-3,4-dimethylbiphenyl-2-ol and carbon nanotube

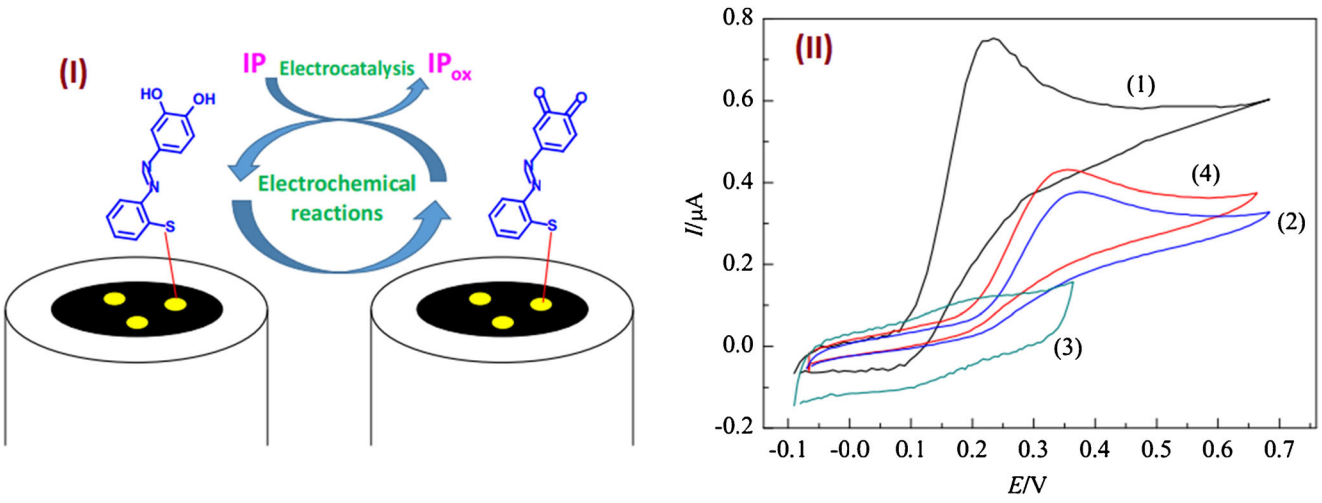

Fig. 19 (I) The schematic representation of electrochemical reactions of DAT, and the electrocatalytic oxidation of IP at the GCE/AuNP-DAT. (II) Cyclic voltammograms obtained in the presence of IP (0.05 mmol/L) at (1) the GCE/AuNP-DAT, (2) the bare GCE, and (4) the GCE/AuNPs;(3) Cyclic voltammogram measured for GCE/AuNP-DAT in the absence of IP. In all cases the supporting solution was PBS (0.1 mol/L, pH = 7.0), and the scan rate was 20 mV/s [254]

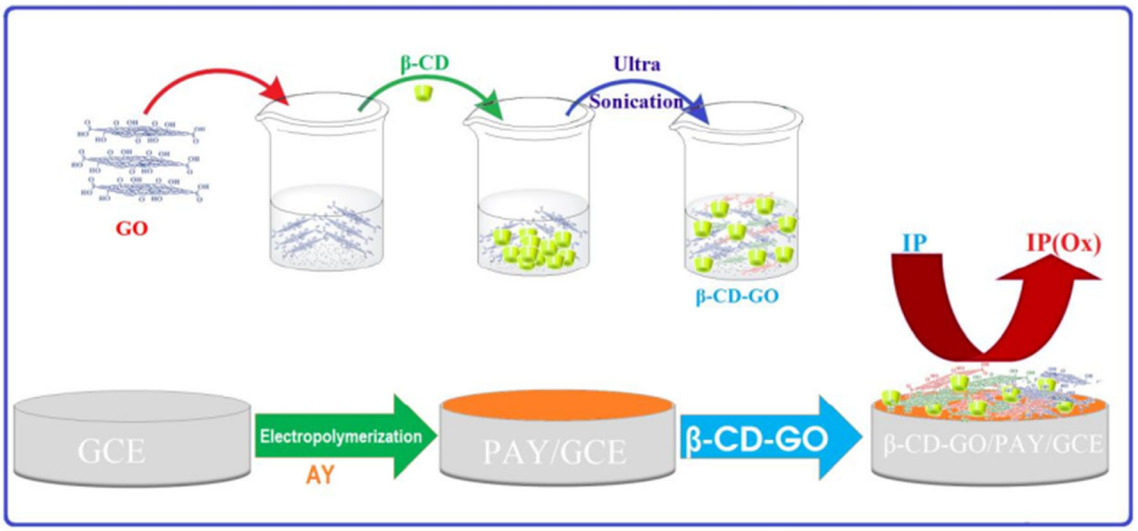

Fig. 20 Schematic representation of stepwise preparation of β-CD-GO/PAY/GCE [255]

removal of the D- and L-T_4 molecules and formation of MIP cavities, the sensing platform must have no electrical signal of the D- and L-T_4 in the absence of D- and L-T_4(Fig. 23). This attitude indicated low detection limits (0.0060 ng mL^{-1} for L- and 0.0062 for D- T_4 by differential pulse anodic stripping voltammetric method.

Electrochemical detection of warfarin sodium

The electrochemical oxidation process of warfarin has been performed at different electrode surfaces by Gholivand and coworkers [290, 291]. The number of electrons and protons at the surface of magnetic Fe_3O_4 nanoparticles modified carbon paste electrode (Fe_3O_4/CPE) was $2e^-$ and $1H^+$. However, these values were different at the carbon paste electrode which was modified by β-cyclodextrin/ multi-walled carbon nanotubes/cobalt oxide nanoparticles (β-CD/MWCNTs/Co_3O_4NPs/CPE) and it was reported as $2e^-/2H^+$. For detection and determination of warfarin in real, biological, and pharmaceutical samples, there are many electrochemical sensors which can be modified with multi-walled carbon nanotubes and metal oxide nanoparticles [290], magnetic nanoparticles [292, 293], molecularly imprinted polymers [294, 295], ionic liquids [296], chitosan, and quantum dots [297]. For example, Gholivand and coworkers [297] constructed a warfarin sensor in which CdS-QDs were covalently bonded to the amino group (-NH_2) of CS and carboxylic acid (-COOH) moiety of functionalized MWCNT. In addition, the surface of CdS-QDs was covered by cysteine (Fig. 24). Electrochemical

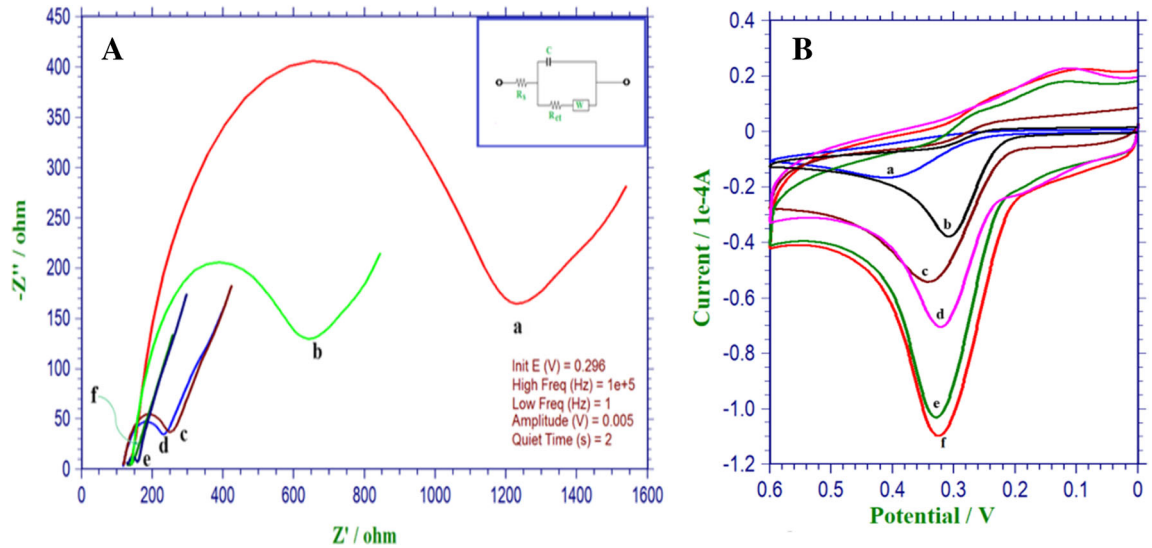

Fig. 21 (A) EIS spectra of 0.1 M KCl containing 2.5 mM $[Fe(CN)_6]^{3-/4-}$ at (a) GCE, (b) PAY/GCE, (c) GO/PAY/GCE, (d) GO/GCE, (e) β-CD-GO/GCE and (f) β-CDGO/PAY/GCE. Inset- Randles equivalent circuit model. (B) Cyclic voltammograms at (a) GCE, (b) PAY/GCE, (c)GO/GCE and (d) β-CDGO/GCE (e) GO/PAY/GCE and (f) β-CD-GO/PAY/GCE in 0.1 M PBS (pH 7.0) containing 0.2 mM IP [255]

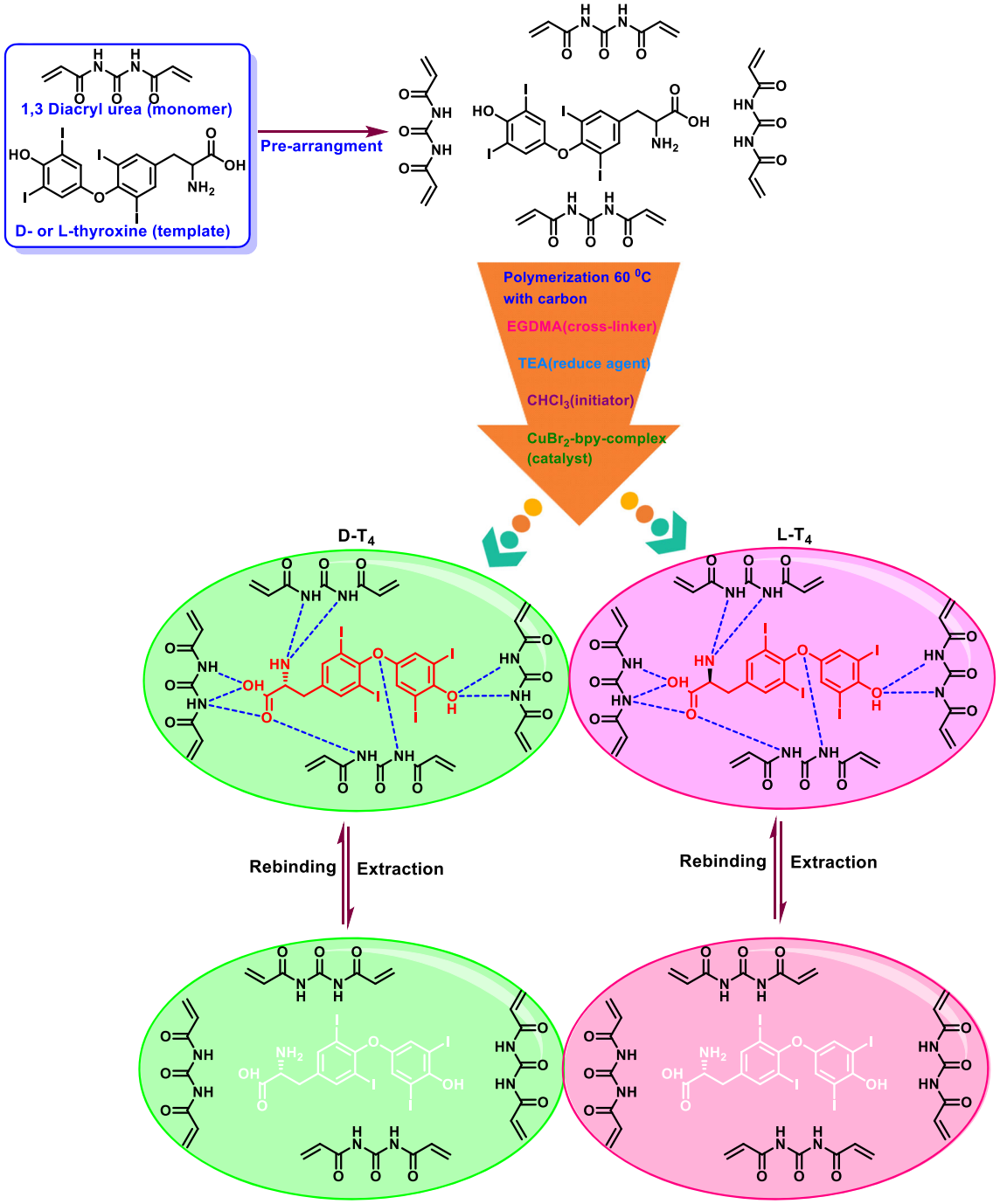

Fig. 22 Suggested enantioselective binding mechanism of D- and L -T_4 in their respective MIP cavities [289]

investigations of the modification steps have been performed by cyclic voltammetry technique. The maximum oxidation peak current of warfarin is achieved at the QDs/CS/MWCNTs/GCE (Fig. 24 curve d). The detection limit and linear range are obtained as 0.0085 μM and 0.050–80 μM, respectively. In Table 8, a comparison of the major characteristics such as detection limit, linear range, sensing platforms, and determination methods of some electrochemical warfarin sensors have been reported.

Electrochemical detection of digoxin

Digoxin can produce an electrical signal when the potential is scanned between two ranges, and the height of peak current is depended on the digoxin concentration ($I_{Digoxin} \propto C_{Digoxin}$) [302]. The modified electrode can act as a sensor for detection of low levels of digoxin in biological and pharmaceutical samples. Aptasensors and immunosensors are attractive electrochemical approaches for the determination of digoxin in

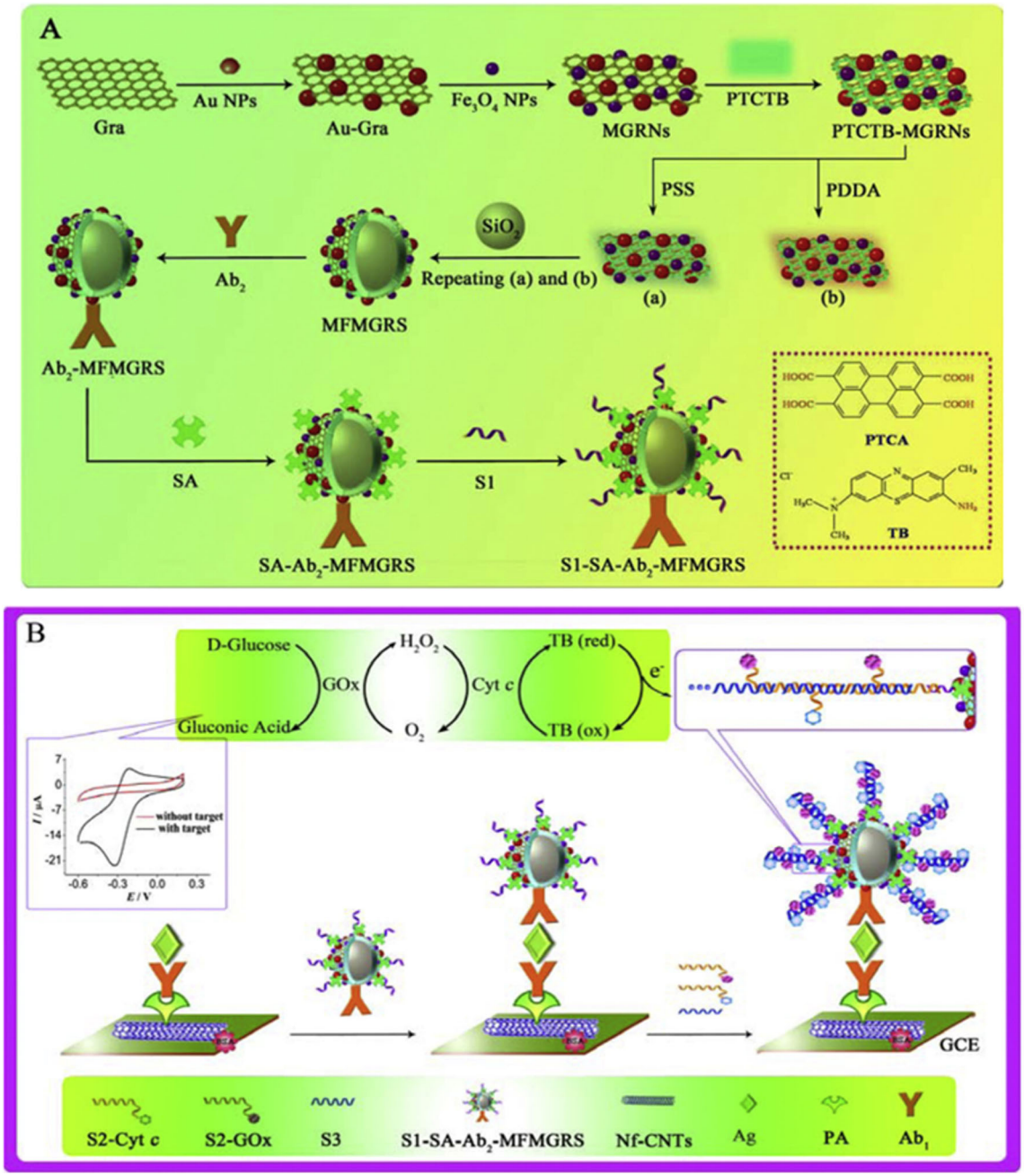

Fig. 23 Suggested enantioselective binding mechanism of D- and L -T_4 in their respective MIP cavities [289]

blood plasma samples. Ahmadi and coworkers [303] presented a competitive electrochemical immunosensor. In this study, the two paths for stepwise fabrication of sensing platform were reported (Fig .25). In the first strategy (Fig. 25 steps a and b), immobilization of poly-vinyl aniline (PVA), secondary antibody on screen-printed electrode, and surface blocking via 0.5 % BSA was performed. In the second assay (Fig. 25 step c), synthesis of nanospheres with magnetic cores (Fe_3O_4-NPs) via co-precipitation procedure, and fabrication of Fe_3O_4-Au-NPs was carried out. Then, (Fig. 25 step d), the immobilization of antibody (digoxin-bovine serum albumin (BSA)) onto the Fe_3O_4-Au-NPs had been performed in Tris–HCl buffer (pH 7.4, 0.05 M) solution and the peroxidation of Au-NPs was carried out at the constant potential of + 1.30 V in 1 mol/l hydrochloric acid. Finally, the reduction of $Au^{3+}(AuCl_4^-)$ to Au(0) as electrical signal was detected (Fig. 25 step e). Owing to non-electroactivity of PVA and secondary antibody-PVA, no cathodic current was observed (Fig. 26 curve b) but, the electrical signal is reinforced at the surface of secondary antibody-PVA-Fe_3O_4-Au-NPs/SPE and it is reached the highest value for digoxin-Fe_3O_4-Au-NPs/SPE (Fig. 26 curve e). At optimized condition of designed

Table 8 The comparison of different nano modified electrodes with its analytical parameters for the determination of warfarin

Electrode	Detection limit (μM)	Linear range (μM)	Method	Ref.
β-CD/MWCNTs/Co_3O_4NPs/CPE	0.02	0.05–150	DPV	[290]
PVC Ferroin-based membrane sensors	2.59	19.4–9729.8	Potentiometry	[298]
MWCNT/$ZnCrFeO_4$/CPEs	0.003	0.02–920.0	DPV	[293]
AuNP/MIP/f-MWCNT/GCE	0.024 ng mL^{-1}	0.031–0.616 ng mL^{-1}	SWV	[294]
MIP/NPAMW	5.0	5.0–400.0	DPV	[299]
MIP/NPGL/GE	4.1×10^{-5}	1×10^{-4}–8×10^{-2}	CV	[295]
MWCNTs/CoHCF/IL/CPE	0.3	1.0–100.0	DPV	[296]
BDDE	0.16	4.0–400.0	FIA-MPA	[300]
BDDE	0.10	2.0–200.0	BIA-MPA	
HMDE	6.5×10^{-4}	5×10^{-3}–4×10^{-1}	SWAdCS	[301]
Fe_3O_4/CPE	0.21	0.5–1000	SWAS	[291]
CdS-QDs/CS/MWCNTs/GCE	0.0085	0.05–80	DPSV	[297]
MWCNTs/$MnFe_2O_4$/CPE	0.08	0.10–447.0	DPV	[292]

β-CD β –cyclodextrin, *MWCNTs*multi-walled carbon nanotubes, *Co_3O_4NPs* cobalt oxide nanoparticles, *CPE* carbon paste electrode, *$ZnCrFeO_4$* zinc chromium ferrite, *MIP* molecularly imprinted polymer, *GCE* glassy carbon electrode, *DPV* differential pulse voltammetry, *SWV* square wave voltammetry, *NPAMW*Au–Ag alloy microwire, *NPGL* nanoporous gold leaf, *IL* ionic liquid, *CoHCF* cobalt hexacyanoferrate, *CV* cyclic voltammetry, *FIA and BIA* flow and batch injection analysis, *BDDE*boron-doped diamond electrode, *MPA*multiple-pulse amperometric, *SWAdCS*square-wave adsorptive cathodic stripping voltammetry, *HMDE* hanging mercury drop electrode, *SWAS* square wave anodic stripping, *CdS-QDs*CdS-quantum dots, *CS* chitosan, *DPSV* differential pulse stripping voltammetry

immunosensor, 0.5–5 ng mL^{-1} and 0.05 ng mL^{-1} were obtained for linear range and detection limit, respectively.

Signal on/off electrochemical aptamer-based(EAB) sensors are another approach for detection of digoxin in urine and blood plasma samples. Bagheri and co-workers used a sensing platform in which the thiolated digoxin aptamer was coated onto the gold nanoparticles deposited fluorine-doped tin oxide (GNPs/FTO) surface [304]. They accumulated methylene blue (MB) as a redox label and in the presence of digoxin, the MB current was decreased (signal off). This effect was observed because binding of the aptamer to digoxin can desorb some of the MB molecules which were previously

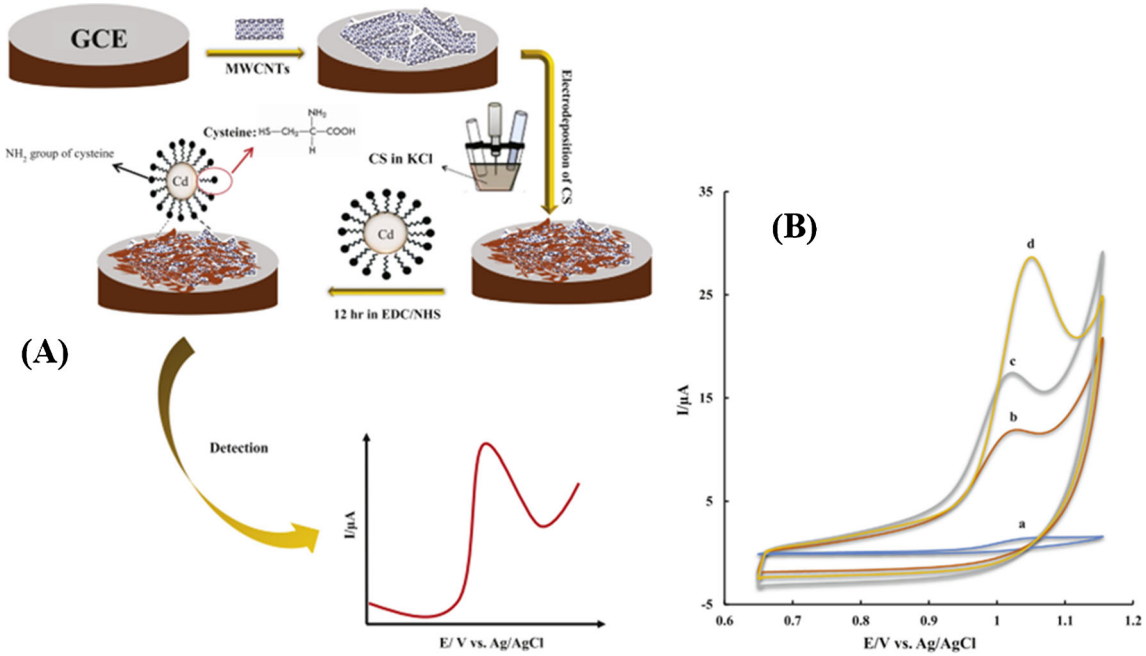

Fig. 24 (A) Schematic representation of the stepwise fabrication process of Cd QD/CS/MWCNT/GC electrode. (B) The CVs response of 5 μM warfarin solution at the (a) bare GCE, (b) MWCNTs/GCE, (c) CS/MWCNTs/GCE and (d) QDs/CS/MWCNTs/GCE (curve d) in PBS (0.1 M, pH = 2.0) at scan rate = 100 mV s^{-1} [291]

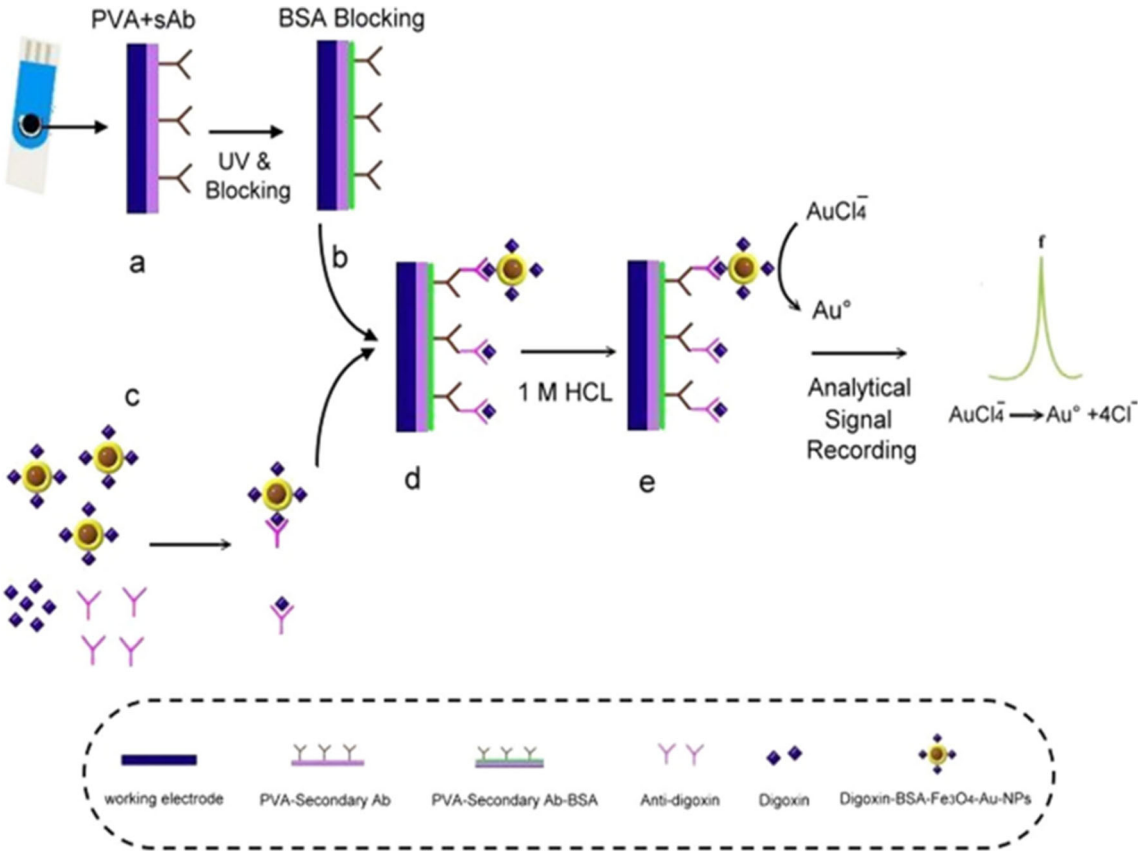

Fig. 25 Schematic representation of a direct competitive electrochemical immunosensor fabrication process [303]

adsorbed on the surface of the aptamer. Recently, Wijesinghe and coworkers designed a signal on aptasensor for detection of digoxin [305]. As shown in Fig. 27, the reduction current of the MB was increased in the presence of digoxin. The conformation of the aptamer was changed and the methylene blue was brought closer to the electrode surface.

Other electrochemical nano sensor and biosensors of NTI drugs

The usability of electrochemical approaches for detection of narrow therapeutic index drugs has been proven and comprehensive information from the designed

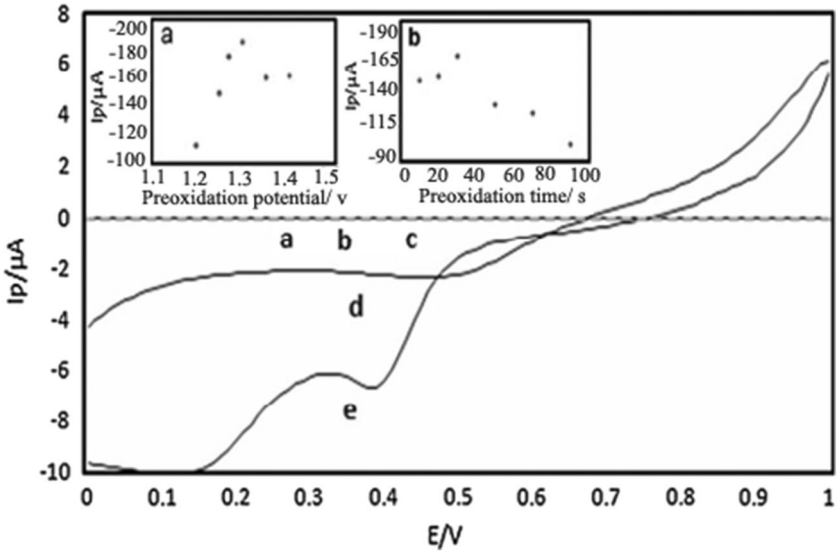

Fig. 26 Cyclic voltammograms of the different modified electrode measured in 1 M HCl at the potential range of 0.0 to +1 V and the scan rate of 50 mV s-1: (a) bare electrode, (b) PVA, (c) secondary antibody-PVA, (d) secondary antibody-PVA-Fe3O4-Au-NPs, and (e) digoxin-Fe_3O_4-Au-NPs and anti-digoxin antibody on secondary antibody-PVA [303]

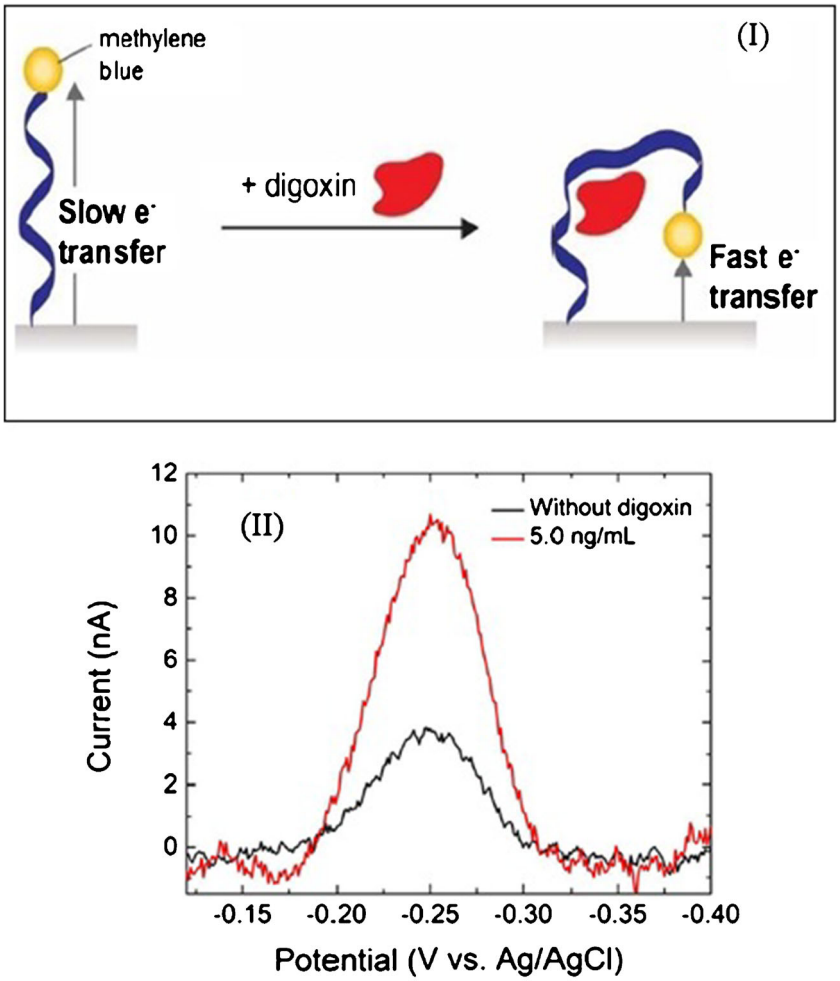

Fig. 27 (I) Schematic illustration of signal-on digoxin sensor, and (II) square wave voltammetry (SWV) responses for MB before and after exposure of aptamer electrode to 5.0 ng/mL digoxin for 480 min [305]

sensors and biosensors has been reported. In addition to the mentioned NTI drugs, disopyramide, gentamicin, gluconate, guanethidine, metaporterenol, minoxidil, phenytoin, prazosin, theophyllinate, valproic acid, vancomycin, and warfarin sodium have been extensively and partially measured by different electrochemical techniques and sensing platforms. In Table 9, the studied electrodes, their targets, and their relevant analytical parameters such as detection limit and linear range are reported.

Conclusion and future prospects

In this review, a comprehensive overview for detection of NTIDs using nano-optical and electrochemical sensors and biosensors was provided. The aim of this review is to create a comprehensive basis for further development of novel nano sensors and biosensors for detection of NTIDs, especially those that have received less attention. Both optical and electrochemical sensors/biosensors have their own advantages and disadvantages. But considering all aspects, electrochemical technology seems to be a better candidate for fabrication of (bio)sensors to detect NTIDs because of its high potential for portability, miniaturization, and commercial capability. Nano-(bio)sensing technology as a powerful point-of-care diagnostic tool has opened a new approach to monitoring the concentrations of these NTIDs. Considering the clinical demands, the application of nano(bio)sensing technology in detection of NTIDs can be commercially available as pregnancy tests and glucose monitoring (bio)sensors that have been used for decades. However, before the coming of this future, several challenges need to be addressed including lack of one outstanding technique in (bio)sensing approach that is set to become the gold standard for monitoring of NTIDs and providing a high level of standardization,

Table 9 The overall results of some nano sensors and biosensors for NTIs drugs detection with analytical parameters

Electrodes	Target	LR (μM)	Method	LOD (μM)	Reference
Ion-selective electrode	Disopyramide	0.5–25	PM	0.8	[306]
HMDE	Disopyramide	0.0715–1.43	SWCAdSV	0.0565	[307]
GCE	Disopyramide	> 120	DPV	1.27	[308]
TTF-GADH-MPA-AuE	Gluconic acid	0.6–20	AM	0.19	[309]
GK+CK+CRE+SAOX+ HRP/MWCNT nanocomposite electrode	Gluconic acid	4.0–620	AM	2.6	[310]
PEDGE/PANIPAAMPSA/SPCE	Gluconic acid	0.005–0.10 mM	AM	0.003 mM	[311]
MQO-TTF-AuNPs-SPCEs	Gluconic acid	0.79–437.06	AM	0.79	[312]
Epoxy-graphite-Ps	Gluconic acid	7.0-250	AM	–	[313]
SPCE/GADH	Gluconic acid	9.0–131.4	CHA	9.0	[314]
SPCE	Gluconic acid	7.46–71.43	CHA	7.46	[315]
MDWE	Guanethididne	–	SV	0.992 ng/cm^3	[316]
AuNPs/GCE	Metaproterenol	0.001–10	DPV	0.00003	[317]
ITONPs/MWCNTs/GCE	Metaproterenol	0.03–22	DPV	0.0012	[318]
–	Minoxidil	500 pg–10 ng/ml	HPLC-EC	500pg/ml	[319]
MIP–CPE	Minoxidil	0.001–0.4	DPV	0.0003	[320]
AgNPs/MIP/GCE	Minoxidil	0.03–500	ASSWV	0.01	[321]
GCE	Minoxidil	0.1–100	FIA-AM	2.2	[322]
CdSe QDs-IL-GPE	Minoxidil	0.01–8.0	DPV	0.0055	[323]
HMDA	Minoxidil	0.005–2.5	AdsCSV	0.002	[324]
GCE	Minoxidil	0.3–100 ng/ml	HPLC-AM	0.3ng/ml	[325]
Au/GCE	Phenytoin	0.5–200	DPV	0.302	[326]
Nafion-loaded CPE	Phenytoin	0.2–5	SWV	0.2	[327]
BDD	Prazosin	2.0–200	MPA	0.5	[328]
PVC membrane	Prazosin	10–10000	PM	6.3	[329]
NMCPE	Prazosin	0.00004–0.04	AdS-DPV	0.00003	[330]
(PVC) membrane	Prazosin	2.7–10000	PM	–	[331]
APTES-MNPs/PGE	Valproic Acid	1.0–100 ppm	DPV	0.4ppm	[332]
HMDE	Valproic Acid	146–1000	SqWV	109	[333]
–	Valproic Acid	0.36–14.4 μ g/mL	HPLC-ECD	0.11 μg/mL	[334]
–	Vancomycin	5.0–100 μ g/mL	HPLC-ECD	0.5 μ g/mL	[335]
AuNS–G–SPE	Vancomycin	1–100	DPV	0.29	[336]
GR-GC	Vancomycin	0.70–50	SWV	0.20	[337]
DME	Vancomycin	15−60 M	DPP	1.8	[338]
NIP/sol–gel/MWNT/Au	Clindamycin	0.5–80	Amperometric	0.0244	[339]
AuNPs-GO-CTS-ECH/GCE	Clindamycin	0.95–140	SWV	0.29	[340]
Ion selective electrode	Clindamycin	316-316000	Potentiometric	–	[341]
Au microelectrode	Clindamycin	4–42 pg/ml	FFTCV	1.3 pg/ml	[342]
CPE	Clindamycin	DP: 86–430 ng/ml SW: 90–813 ng/ml	DP and SW	DP: 32.60 ng/ml SW: 90.73 ng/ml	[343]
GCE	Clindamycin	0.045–0.900 μg	HPLC-DPV	100 pg	[344]

PM potentiometry, *SWCAdSV*square-wave cathodic adsorptive stripping voltammetric, *HMDE* hanging mercury drop electrode, *TTF* tetrathiafulvalene, *GADH* gluconate dehydrogenase, *MPA*3-mercaptopropionic acid, *AuE* gold electrode, *GK* gluconate kinase, *CK* creatine kinase, *CRE* creatinase, *SAOX* sarcosine oxidase, *HRP* peroxidase, *PEDGE* diglycidyl ether, *PANI* polyaniline, *PAAMPSA* poly(2-acrylamido-2-methyl-1-propane sulfonic acid), *SPCE*screen-printed carbon electrode, *AM* amperometric, *MQO* malate quinone oxido-reductase enzyme, *TTF* tetrathiafulvalene, *GADH* gluconate dehydrogenase, *MDWE* mercury drop working electrode, *CHA* chronoamperometric, *SV* stripping voltammetry, *DPV* differential pulse voltammetry, *ITONPs* indium tin oxide nanoparticles, *HPLC*high-performance liquid chromatography, *EC* electrochemical detection, *ASSWV* anodic stripping square wave voltammogram, *FIA* flow injection analysis, *AdsCSV* adsorptive cathodic stripping voltammetry, *CP* chronopotentiometry, *ISME*ion-selective membrane electrodes, *BDD*boron-doped diamond, *MPA*multiple-pulse amperometric, *PM* potentiometric, *AdS-DPV* adsorptive stripping-differential pulse voltammetry, *PVC* polyvinylchloride, *APTES* 3 aminopropyletriethoxy silane coated, *MNPs* magnetic nanoparticles, *DME* dropping mercury electrode, *DPP* differential pulse polarography, *NPAMW* 3D nanoporous Au–Ag alloy microwire, *NPGL* nanoporous gold leaf, *CS* chitosan, *DPSV* differential pulse stripping voltammetry, *BDDE*boron-doped diamond electrode, *MPA*multiple-pulse amperometric, *SWAdCS*square-wave adsorptive cathodic stripping, *SWASV* square wave anodic stripping voltammetry, *FFTCV* fast Fourier transformation with cyclic voltammetry, *DP* differential pulse, *SW* square wave

quality control, and validation which are considered as the main requirements which should be met in the medical industry, particularly therapeutic drug monitoring.

Funding Financial support of this study was provided by deputy of research and technology, Hamadan University of Medical Sciences.

Declarations

Conflict of interest The authors declare no competing interests.

References

1. Ernst FR, Grizzle AJ (1996)Drug-related morbidity and mortality: updating the cost-of-illness model. Journal of the American Pharmaceutical Association 41(2001):192–199
2. Winterstein AG, Sauer BC, Hepler CD, Poole C (2002) Preventable drug-related hospital admissions. Annals of Pharmacotherapy 36:1238–1248
3. Patel P, Zed PJ (2002)Drug-related visits to the emergency department: how big is the problem? Pharmacotherapy: The Journal of Human Pharmacology and Drug Therapy 22:915–923
4. Tamargo J, Le Heuzey J-Y, Mabo P (2015) Narrow therapeutic index drugs: a clinical pharmacological consideration to flecainide. European journal of clinical pharmacology 71:549–567
5. Burns M (1999) Management of narrow therapeutic index drugs. Journal of Thrombosis and Thrombolysis 7:137–143
6. A.Z. Gondal, H. Zulfiqar, Aminophylline, StatPearls [Internet], StatPearls Publishing 2019.
7. Greenberg RG, Melloni C, Wu H, Gonzalez D, Ku L, Hill KD, Hornik CP, Zheng N, Jiang W, Cohen-Wolkowiez M (2016) Therapeutic index estimation of antiepileptic drugs: a systematic literature review approach. Clinical Neuropharmacology 39:232
8. Bonnaire A, Vernet-Garnier V, Lebrun D, Bajolet O, Bonnet M, Hentzien M, Xavier O, Diallo S, Firouzé B-S(2020) Clindamycin combination treatment for the treatment of bone and joint infections caused by clindamycin-susceptible, erythromycin-resistant Staphylococcus spp. Diagnostic Microbiology and Infectious Disease 115225
9. Cairns R, Brown JA, Buckley NA (2019) Clonidine exposures in children under 6 (2004–2017): a retrospective study. Archives of disease in childhood 104:287–291
10. Kahan BD, Keown P, Levy GA, Johnston A (2002) Therapeutic drug monitoring of immunosuppressant drugs in clinical practice. Clinical Therapeutics 24:330–350
11. Cheng M-C, Chi K-M, Chang SY (2013) Detection of digoxin in urine samples by surface-assisted laser desorption/ionization mass spectrometry with dispersive liquid–liquid microextraction. Talanta 115:123–128
12. Walter E, McKinlay J, Corbett J, Kirk-Bayley J (2018) Review of management in cardiotoxic overdose and efficacy of delayed intralipid use. Journal of the Intensive Care Society 19:50–55
13. Saleh P, Abbasalizadeh S, Rezaeian S, Naghavi-Behzad M, Piri R, Pourfeizi HH (2016)Gentamicin-mediated ototoxicity and nephrotoxicity: a clinical trial study. Nigerian Medical Journal 57:347
14. Desai C (2016) Meyler's side effects of drugs: the international encyclopedia of adverse drug reactions and interactions. Indian Journal of Pharmacology 48:224
15. Williams DM, Rubin BK (2018) Clinical Pharmacology of Bronchodilator Medications. Respiratory Care 63:641–654
16. Keyvanfard M, Alizad K (2016) Determination of isoproterenol in pharmaceutical and biological samples using a pyrogallol red multiwalled carbon nanotube paste electrode as a sensor. Chinese Journal of Catalysis 37:579–583
17. Jonklaas J, Bianco AC, Bauer AJ, Burman KD, Cappola AR, Celi FS, Cooper DS, Kim BW, Peeters RP, Rosenthal MS (2014) Guidelines for the treatment of hypothyroidism: prepared by the american thyroid association task force on thyroid hormone replacement. Thyroid 24:1670–1751
18. Gelenberg AJ, Kane JM, Keller MB, Lavori P, Rosenbaum JF, Cole K, Lavelle J (1989) Comparison of standard and low serum levels of lithium for maintenance treatment of bipolar disorder. New England Journal of Medicine 321:1489–1493
19. MaGuire GP, Emirgil C (1986) Bronchodilator and side effects of different modes of administration of metaproterenol: inhaled, oral, and in combination. The American journal of the medical sciences 291:168–174
20. Suchonwanit P, Thammarucha S, Leerunyakul K (2019) Minoxidil and its use in hair disorders: a review, Drug Design. Development and Therapy 13:2777
21. Kuo H-F, Lai Y-J, Wu J-C, Lee K-T, Chu C-S, Chen J, Wu J-R, Wu B-N(2014) A xanthine-derivative K+-channel opener protects against serotonin-induced cardiomyocyte hypertrophy via the modulation of protein kinases. International journal of biological sciences 10:64
22. Koola MM, Varghese SP, Fawcett JA (2014)High-dose prazosin for the treatment of post-traumatic stress disorder. Therapeutic advances in psychopharmacology 4:43–47
23. Bentue-Ferrer D, Verdier M-C, Tribut O (2012) Therapeutic drug monitoring of primidone and phenobarbital. Therapie 67:381
24. Fukuoka M, Kuki I, Kawawaki H, Okazaki S, Kim K, Hattori Y, Tsuji H, Nukui M, Inoue T, Yoshida Y (2017) Quinidine therapy for West syndrome with KCNTI mutation: a case report. Brain and Development 39:80–83
25. Zeidman A, Gardyn J, Fradin Z, Fink G, Mittelman M (1997) Therapeutic and toxic theophylline levels in asthma attacks—is there a need for additional theophylline? Harefuah 133:3–5 80
26. Martin JH, Norris R, Barras M, Roberts J, Morris R, Doogue M, Jones GR (2010) Therapeutic monitoring of vancomycin in adult patients: a consensus review of the American Society of Health-System Pharmacists, the Infectious Diseases Society of America, and the Society Of Infectious Diseases Pharmacists. The Clinical biochemist Reviews 31:21
27. Kwon M-J, Kim H-J, Kim J-W, Lee K-H, Sohn K-H, Cho H-J, On Y-K, Kim J-S, Lee S-Y(2009) Determination of plasma warfarin concentrations in Korean patients and its potential for clinical application. The Korean journal of laboratory medicine 29:515–523
28. Rheinstein P (1993) The generic drug approval process. American family physician 48:1357–1360
29. Berg M, Gross R, Tomaszewski K, Zingaro W, Haskins L (2008) Generic substitution in the treatment of epilepsy: case evidence of breakthrough seizures. Neurology 71:525–530
30. Crawford P, Feely M, Guberman A, Kramer G (2006) Are there potential problems with generic substitution of antiepileptic drugs?: a review of issues. Seizure 15:165–176
31. Holbrook A, Schulman S, Witt DM, Vandvik PO, Fish J, Kovacs MJ, Svensson PJ, Veenstra DL, Crowther M, Guyatt GH (2012)Evidence-based management of anticoagulant therapy: antithrombotic therapy and prevention of thrombosis: American College of Chest Physicians evidence-based clinical practice guidelines. Chest 141:e152S–e184S
32. Caraballo PJ, Heit JA, Atkinson EJ, Silverstein MD, O'Fallon WM, Castro MR, Melton LJ (1999)Long-term use of oral anticoagulants and the risk of fracture. Archives of Internal Medicine 159:1750–1756

33. Rybak M, Lomaestro B, Rotschafer JC, Moellering R, Craig W, Billeter M, Dalovisio JR, Levine DP (2009) Therapeutic monitoring of vancomycin in adult patients: a consensus review of the American Society of Health-System Pharmacists, the Infectious Diseases Society of America, and the Society of Infectious Diseases Pharmacists. American Journal of Health-System Pharmacy 66:82–98
34. R. Walls, R. Hockberger, M. Gausche-Hill, Rosen's emergency medicine-concepts and clinical practice e-book, Elsevier Health Sciences 2017.
35. Seneff M, Scott J, Friedman B, Smith M (1990) Acute theophylline toxicity and the use of esmolol to reverse cardiovascular instability. Annals of emergency medicine 19:671–673
36. De Marco FA, Ghizoni E, Kobayashi E, Li LM, Cendes F (2003) Cerebellar volume and long-term use of phenytoin. Seizure 12: 312–315
37. Koliqi R, Polidori C, Islami H (2015) Prevalence of side effects treatment with carbamazepine and other antiepileptics in patients with epilepsy. Materia socio-medica 27:167
38. Yaylacı S, Demir MV, Acar B, Sipahi S, Tamer A (2012) Successful treatment of excessive dose of carbamazepine. Indian Journal of Pharmacology 44:417
39. Al-Jenoobi FI, Ahad A, Mahrous GM, Raish M, Alam MA, Al-Mohizea AM (2015) A simple HPLC–UV method for the quantification of theophylline in rabbit plasma and its pharmacokinetic application. Journal of Chromatographic Science 53:1765–1770
40. Charehsaz M, Gürbay A, Aydin A, Şahin G (2014) Simple, fast and reliable liquid chromatographic and spectrophotometric methods for the determination of theophylline in urine, saliva and plasma samples. Iranian journal of Pharmaceutical Research: IJPR 13:431
41. Gu X, Yu S, Peng Q, Ma M, Hu Y, Zhou B (2020) Determination of unbound valproic acid in plasma using centrifugal ultrafiltration and gas chromatography: application in TDM. Analytical biochemistry 588:113475
42. Bartella L, Di Donna L, Napoli A, Siciliano C, Sindona G, Mazzotti F (2019) A rapid method for the assay of methylxanthines alkaloids: theobromine, theophylline and caffeine, in cocoa products and drugs by paper spray tandem mass spectrometry. Food chemistry 278:261–266
43. Babu AS, Thippeswamy B, Vinod A, Ramakishore E, Anand S, Senthil D (2011) Determination of theophylline in rabbit plasma by triple quadrupole LC/MS. Pharmaceutical methods 2:211–217
44. Di Corcia D, Morra V, Pazzi M, Vincenti M (2010) Simultaneous determination of β2-agonists in human urine by fast-gaschromatography/mass spectrometry: method validation and clinical application. Biomedical Chromatography 24:358–366
45. Mei S, Wang J, Chen D, Zhu L, Zhao M, Tian X, Hu X, Zhao Z (2018) Simultaneous determination of cyclosporine and tacrolimus in human whole blood by ultra-high performance liquid chromatography tandem mass spectrometry and comparison with a chemiluminescence microparticle immunoassay. Journal of Chromatography B 1087:36–42
46. Weerathunge P, Ramanathan R, Shukla R, Sharma TK, Bansal V (2014)Aptamer-controlled reversible inhibition of gold nanozyme activity for pesticide sensing. Analytical chemistry 86:11937–11941
47. Lin Z, Ma Q, Fei X, Zhang H, Su X (2014) A novel aptamer functionalized CuInS2 quantum dots probe for daunorubicin sensing and near infrared imaging of prostate cancer cells. Analytica chimica acta 818:54–60
48. Shayesteh OH, Khosroshahi AG (2020) A polyA aptamer-based label-free colorimetric biosensor for the detection of kanamycin in human serum. Analytical Methods 12:1858–1867
49. Hassanpour S, Behnam B, Baradaran B, Hashemzaei M, Oroojalian F, Mokhtarzadeh A, Guardia M (2021) Carbon based nanomaterials for the detection of narrow therapeutic index pharmaceuticals. Talanta 221:121610
50. Feng C, Dai S, Wang L (2014) Optical aptasensors for quantitative detection of small biomolecules: a review. Biosensors and Bioelectronics 59:64–74
51. Shayesteh OH, Ghavami R (2019) Two colorimetric ampicillin sensing schemes based on the interaction of aptamers with gold nanoparticles. Microchimica Acta 186:485
52. Rhouati A, Bulbul G, Latif U, Hayat A, Li Z-H, Marty JL (2017)Nano-aptasensing in mycotoxin analysis: recent updates and progress. Toxins 9:349
53. Song Y, Wei W, Qu X (2011) Colorimetric biosensing using smart materials. Advanced Materials 23:4215–4236
54. Shayesteh OH, Ghavami R (2020) A novel label-free colorimetric aptasensor for sensitive determination of PSA biomarker using gold nanoparticles and a cationic polymer in human serum. Spectrochimica Acta Part A: Molecular and Biomolecular Spectroscopy 226:117644
55. Shi H, He X, Cui W, Wang K, Deng K, Li D, Xu F (2014) Locked nucleic acid/DNA chimeric aptamer probe for tumor diagnosis with improved serum stability and extended imaging window in vivo. Analytica Chimica Acta 812:138–144
56. Katiyar N, Selvakumar LS, Patra S, Thakur MS (2013) Gold nanoparticles based colorimetric aptasensor for theophylline. Analytical Methods 5:653–659
57. Ma X, Guo Z, Mao Z, Tang Y, Miao P (2018) Colorimetric theophylline aggregation assay using an RNA aptamer and non-crosslinking gold nanoparticles. Microchimica Acta 185:33
58. Emrani AS, Danesh NM, Lavaee P, Jalalian SH, Ramezani M, Abnous K, Taghdisi SM (2015) Sensitive and selective detection of digoxin based on fluorescence quenching and colorimetric aptasensors. Analytical Methods 7:3419–3424
59. Nikfarjam A, Rezayan AH, Mohammadkhani G, Mohammadnejad J (2017)Label-free detection of digoxin using localized surface plasmon resonance-based nanobiosensor. Plasmonics 12:157–164
60. Yan S, Lai X, Du G, Xiang Y (2018) Identification of aminoglycoside antibiotics in milk matrix with a colorimetric sensor array and pattern recognition methods. Analytica Chimica Acta 1034: 153–160
61. Miranda-Andrades JR, Pérez-Gramatges A, Pandoli O, Romani EC, Aucélio RQ, da Silva AR (2017) Spherical gold nanoparticles and gold nanorods for the determination of gentamicin. Spectrochimica Acta Part A: Molecular and Biomolecular Spectroscopy 172:126–134
62. Jahed FS, Hamidi S, Nemati M (2018)Dopamine-capped silver nanoparticles as a colorimetric probe for on-site detection of cyclosporine. ChemistrySelect 3:13323–13328
63. Zhan L, Yang T, Zhen SJ, Huang CZ (2017) Cytosine triphosphate-capped silver nanoparticles as a platform for visual and colorimetric determination of mercury (II) and chromium (III). Microchimica Acta 184:3171–3178
64. Khoubnasabjafari M, Salari R, Samadi A, Jouyban-Gharamaleki V, Jouyban A (2019) Colorimetric determination of phenytoin using indoxyl sulfate capped silver nanoparticles. Analytical Methods 11:3324–3330
65. Jing L, Zhang Q, Wang Y, Liu X, Wei T (2016) Surface plasmon resonance sensor for theophylline using a water-compatible molecularly imprinted film. Analytical Methods 8:2349–2356
66. Feng S, Chen C, Wang W, Que L (2018) An aptamer nanopore-enabled microsensor for detection of theophylline. Biosensors and Bioelectronics 105:36–41
67. Ikram F, Qayoom A, Shah MR (2018) Synthesis of epicatechin coated silver nanoparticles for selective recognition of gentamicin. Sensors and Actuators B: Chemical 257:897–905

68. Gukowsky JC, Tan C, Han Z, He L (2018)Cysteamine-modified gold nanoparticles as a colorimetric sensor for the rapid detection of gentamicin. Journal of food science 83:1631–1638
69. Obare SO, Hollowell RE, Murphy CJ (2002) Sensing strategy for lithium ion based on gold nanoparticles. Langmuir 18:10407–10410
70. Grabchev I, Dumas S, Chovelon J-M(2009) A polyamidoamine dendrimer as a selective colorimetric and ratiometric fluorescent sensor for Li+ cations in alkali media. Dyes and Pigments 82:336–340
71. May J, Hickey M, Triantis I, Palazidou E, Kyriacou PA (2015) Spectrophotometric analysis of lithium carbonate used for bipolar disorder. Biomedical optics express 6:1067–1073
72. Khoubnasabjafari M, Samadi A, Jouyban A (2019)In-situ microscale spectrophotometric determination of phenytoin by using branched gold nanoparticles. Microchimica Acta 186:422
73. Akhtar S, Shahzad K, Mushtaq S, Safi F, Ali I, Bhatti KA (2019) Synthesis and characterization of amphotericin B stabilized gold nanoparticles sensor for detection of clindamycin drug. Materials Research Express 6:075068
74. Omidfar K, Kia S, Kashanian S, Paknejad M, Besharatie A, Kashanian S, Larijani B (2010) Colloidal nanogold-based immunochromatographic strip test for the detection of digoxin toxicity. Applied biochemistry and biotechnology 160:843–855
75. Ruppert C, Phogat N, Laufer S, Kohl M, Deigner H-P(2019) A smartphone readout system for gold nanoparticle-based lateral flow assays: application to monitoring of digoxigenin. Microchimica Acta 186:119
76. Fitzpatrick B, O'Kennedy R (2004) The development and application of a surface plasmon resonance-based inhibition immunoassay for the determination of warfarin in plasma ultrafiltrate. Journal of immunological methods 291:11–25
77. Belal TS, El-Kafrawy DS, Mahrous MS, Abdel-Khalek MM, Abo-Gharam AH (2016) Validated spectrophotometric methods for determination of sodium valproate based on charge transfer complexation reactions. Spectrochimica Acta Part A: Molecular and Biomolecular Spectroscopy 155:47–53
78. Altintas Z (2018) Surface plasmon resonance based sensor for the detection of glycopeptide antibiotics in milk using rationally designed nanoMIPs. Scientific reports 8:1–12
79. Korposh S, Chianella I, Guerreiro A, Caygill S, Piletsky S, James SW, Tatam RP (2014) Selective vancomycin detection using optical fibre long period gratings functionalised with molecularly imprinted polymer nanoparticles. Analyst 139:2229–2236
80. Wang G, Zhu Y, Chen L, Zhang X (2015) Photoinduced electron transfer (PET) based label-free aptasensor for platelet-derived growth factor-BB and its logic gate application. Biosensors and Bioelectronics 63:552–557
81. Sharma A, Khan R, Catanante G, Sherazi TA, Bhand S, Hayat A, Marty JL (2018) Designed strategies for fluorescence-based biosensors for the detection of mycotoxins. Toxins 10:197
82. Zhou D-M, Xi Q, Liang M-F, Chen C-H, Tang L-J, Jiang J-H(2013) Graphene oxide-hairpin probe nanocomposite as a homogeneous assay platform for DNA base excision repair screening. Biosensors and Bioelectronics 41:359–365
83. Chou C-C, Huang Y-H(2012) Nucleic acid sandwich hybridization assay with quantum dot-induced fluorescence resonance energy transfer for pathogen detection. Sensors 12:16660–16672
84. Dong Y, Li G, Zhou N, Wang R, Chi Y, Chen G (2012) Graphene quantum dot as a green and facile sensor for free chlorine in drinking water. Analytical Chemistry 84:8378–8382
85. Adhikari B, Banerjee A (2010) Facile synthesis of water-soluble fluorescent silver nanoclusters and HgII sensing. Chemistry of Materials 22:4364–4371
86. L. Chen, Y. Wang, X. Fu, L. Chen, Novel optical nanoprobes for chemical and biological analysis, Springer 2014.
87. Song S, Wang L, Li J, Fan C, Zhao J (2008)Aptamer-based biosensors. TrAC Trends in Analytical Chemistry 27:108–117
88. de-los Santos-Álvarez N, Lobo-Castañón MJ, Miranda-Ordieres AJ, Tuñón-Blanco P (2007)Modified-RNA aptamer-based sensor for competitive impedimetric assay of neomycin B. Journal of the American Chemical Society 129:3808–3809
89. Brumbt A, Ravelet C, Grosset C, Ravel A, Villet A, Peyrin E (2005) Chiral stationary phase based on a biostable L-RNA aptamer. Analytical chemistry 77:1993–1998
90. Ni S, Yao H, Wang L, Lu J, Jiang F, Lu A, Zhang G (2017) Chemical modifications of nucleic acid aptamers for therapeutic purposes. International journal of molecular sciences 18:1683
91. Kuwahara M, Sugimoto N (2010) Molecular evolution of functional nucleic acids with chemical modifications. Molecules 15:5423–5444
92. Li N, Nguyen HH, Byrom M, Ellington AD (2011) Inhibition of cell proliferation by an anti-EGFR aptamer. PloS one 6:e20299
93. Hernandez FJ, Stockdale KR, Huang L, Horswill AR, Behlke MA, McNamara JO (2012) Degradation of nuclease-stabilized RNA oligonucleotides in Mycoplasma-contaminated cell culture media. Nucleic Acid Therapeutics 22:58–68
94. Jiang H, Ling K, Tao X, Zhang Q (2015) Theophylline detection in serum using a self-assembling RNA aptamer-based gold nanoparticle sensor. Biosensors and Bioelectronics 70:299–303
95. S. Bi, Y. Yan, Nucleic acid amplification strategies-based chemiluminescence biosensors, Nucleic Acid Amplification Strategies for Biosensing, Bioimaging and Biomedicine, Springer 2019, pp. 45-66.
96. Huang J, Wu Y, Chen Y, Zhu Z, Yang X, Yang CJ, Wang K, Tan W (2011)Pyrene-excimer probes based on the hybridization chain reaction for the detection of nucleic acids in complex biological fluids. Angewandte Chemie International Edition 50:401–404
97. Luo J, Shen X, Li B, Li X, Zhou X (2018) Signal amplification by strand displacement in a carbon dot based fluorometric assay for ATP. Microchimica Acta 185:392
98. Zhou F, Meng R, Liu Q, Jin Y, Li B (2016) Photoinduced electron transfer-based fluorescence quenching combined with rolling circle amplification for sensitive detection of MicroRNA. ChemistrySelect 1:6422–6428
99. Xu X, Zhang B, Gan P, Wu J, Dai W, Zhang L, Wang J (2017)On-nylon membrane detection of nucleic acid molecules by rolling circle amplification. Analytical Biochemistry 533:26–33
100. Ma F, Liu M, Tang B, Zhang C-y(2017) Sensitive quantification of microRNAs by isothermal helicase-dependent amplification. Analytical Chemistry 89:6182–6187
101. Demuth C, Spindler K-LG, Johansen JS, Pallisgaard N, Nielsen D, Hogdall E, Vittrup B, Sorensen BS (2018) Measuring KRAS mutations in circulating tumor DNA by droplet digital PCR and next-generation sequencing. Translational Oncology 11:1220–1224
102. Schuler F, Trotter M, Zengerle R, von Stetten F (2016) Monochrome multiplexing in polymerase chain reaction by photobleaching of fluorogenic hydrolysis probes. Analytical chemistry 88:2590–2595
103. Zhang W, Li N, Koga D, Zhang Y, Zeng H, Nakajima H, Lin J-M, Uchiyama K (2018) Inkjet printing based droplet generation for integrated online digital polymerase chain reaction. Analytical chemistry 90:5329–5334
104. Zhao Y, Chen F, Li Q, Wang L, Fan C (2015) Isothermal amplification of nucleic acids. Chemical reviews 115:12491–12545
105. Lou Y-F, Peng Y-B, Luo X, Yang Z, Wang R, Sun D, Li L, Tan Y, Huang J, Cui L (2019) A universal aptasensing platform based on cryonase-assisted signal amplification and graphene oxide induced quenching of the fluorescence of labeled nucleic acid probes: application to the detection of theophylline and ATP. Microchimica Acta 186:494

106. Ji X, Wang H, Song B, Chu B, He Y (2018) Silicon nanomaterials for biosensing and bioimaging analysis. Frontiers in chemistry 6: 38
107. Jafari S, Derakhshankhah H, Alaei L, Fattahi A, Varnamkhasti BS, Saboury AA (2019) Mesoporous silica nanoparticles for therapeutic/diagnostic applications. Biomedicine & Pharmacotherapy 109:1100–1111
108. Peng J, Li J, Xu W, Wang L, Su D, Teoh CL, Chang Y-T(2018) Silica nanoparticle-enhanced fluorescent sensor array for heavy metal ions detection in colloid solution. Analytical Chemistry 90:1628–1634
109. Emrani AS, Taghdisi SM, Danesh NM, Jalalian SH, Ramezani M, Abnous K (2015) A novel fluorescent aptasensor for selective and sensitive detection of digoxin based on silica nanoparticles. Analytical Methods 7:3814–3818
110. Y. Dong, Aptamers for analytical applications: affinity acquisition and method design, John Wiley & Sons 2019.
111. Elmizadeh H, Faridbod F, Soleimani M, Ganjali MR, Bardajee GR (2020) Fluorescent apta-nanobiosensors for fast and sensitive detection of digoxin in biological fluids using rGQDs: comparison of two approaches for immobilization of aptamer. Sensors and Actuators B: Chemical 302:127133
112. N. Chaniotakis, R. Buiculescu, Semiconductor quantum dots in chemical sensors and biosensors, Nanosensors for Chemical and Biological Applications, Elsevier 2014, pp. 267-294.
113. Bala R, Swami A, Tabujew I, Peneva K, Wangoo N, Sharma RK (2018)Ultra-sensitive detection of malathion using quantum dots-polymer based fluorescence aptasensor. Biosensors and Bioelectronics 104:45–49
114. Pourghobadi Z, Mirahmadpour P, Zare H (2018) Fluorescent biosensor for the selective determination of dopamine by TGA-capped CdTe quantum dots in human plasma samples. Optical Materials 84:757–762
115. Chen J, Huang Z, Meng H, Zhang L, Ji D, Liu J, Yu F, Qu L, Li Z (2018) A facile fluorescence lateral flow biosensor for glutathione detection based on quantum dots-MnO2 nanocomposites. Sensors and Actuators B: Chemical 260:770–777
116. Borghei YS, Hosseini M (2018) Ratiometric fluorescence biosensor based on DNA/miRNA duplex@ CdTe QDs and oxidized luminol as a fluorophore for miRNA detection. Journal of Luminescence 204:16–23
117. Liang W, Liu S, Liu Z, Li D, Wang L, Hao C, He Y (2015) Electron transfer and fluorescence "turn-off" based CdTe quantum dots for vancomycin detection at nanogram level in aqueous serum media. New Journal of Chemistry 39:4774–4782
118. Bigdeli A, Ghasemi F, Abbasi-Moayed S, Shahrajabian M, Fahimi-Kashani N, Jafarinejad S, Nejad MAF, Hormozi-Nezhad MR (2019) Ratiometric fluorescent nanoprobes for visual detection: design principles and recent advances—a review. Analytica chimica acta 1079:30–58
119. Liu H, Jia L, Wang Y, Wang M, Gao Z, Ren X (2019) Ratiometric fluorescent sensor for visual determination of copper ions and alkaline phosphatase based on carbon quantum dots and gold nanoclusters. Analytical and bioanalytical chemistry 411:2531–2543
120. Liu J, Zhang S, Zhao B, Shen C, Zhang X, Yang G (2019) A novel triarylboron based ratiometric fluorescent probe for in vivo targeting and specific imaging of cancer cells expressing abnormal concentration of GGT. Biosensors and Bioelectronics 142:111497
121. Li X, Hu Y, Li X, Ma H (2019)Mitochondria-immobilized near-infrared ratiometric fluorescent pH probe to evaluate cellular mitophagy. Analytical chemistry 91:11409–11416
122. Deng T, Hu S, Zhao L, Wu S, Liu W, Chen T, Fu T, Wang H, Shi H, Huang X-a(2019) A ratiometric fluorescent probe for sensitive determination of the important glycopeptide antibiotic vancomycin. Analytical and Bioanalytical Chemistry 411:8103–8111
123. Panigrahi SK, Mishra AK (2019) Inner filter effect in fluorescence spectroscopy: as a problem and as a solution. Journal of Photochemistry and Photobiology C: Photochemistry Reviews 41:100318
124. Wang J, Wu Y, Zhou P, Yang W, Tao H, Qiu S, Feng C (2018) A novel fluorescent aptasensor for ultrasensitive and selective detection of acetamiprid pesticide based on the inner filter effect between gold nanoparticles and carbon dots. Analyst 143:5151–5160
125. Wei J, Yang Y, Dong J, Wang S, Li P (2019) Fluorometric determination of pesticides and organophosphates using nanoceria as a phosphatase mimic and an inner filter effect on carbon nanodots. Microchimica Acta 186:1–9
126. Li C, Liu W, Sun X, Pan W, Yu G, Wang J (2018) Excitation dependent emission combined with different quenching manners supports carbon dots to achieve multi-mode sensing. Sensors and Actuators B: Chemical 263:1–9
127. Hu Y, Gao Z (2019)Hot-injection strategy for 1-min synthesis of carbon dots from oxygen-containing organic solvents: toward fluorescence sensing of hemoglobin. Dyes and Pigments 165: 429–435
128. Ma Y, Song Y, Ma Y, Wei F, Xu G, Cen Y, Shi M, Xu X, Hu Q (2018)N-doped carbon dots as a fluorescent probe for the sensitive and facile detection of carbamazepine based on the inner filter effect. New Journal of Chemistry 42:8992–8997
129. Yuan Y, Yang L, Liu S, Yang J, Zhang H, Yan J, Hu X (2017)Enzyme-catalyzed Michael addition for the synthesis of warfarin and its determination via fluorescence quenching of L-tryptophan. Spectrochimica Acta Part A: Molecular and Biomolecular Spectroscopy 176:183–188
130. Ling K, Jiang H, Li Y, Tao X, Qiu C, Li F-R(2016) A self-assembling RNA aptamer-based graphene oxide sensor for the turn-on detection of theophylline in serum. Biosensors and Bioelectronics 86:8–13
131. Rankin C, Fuller E, Hamor K, Gabarra S, Shields T (2006) A simple fluorescent biosensor for theophylline based on its RNA aptamer. Nucleosides, Nucleotides, and Nucleic Acids 25:1407–1424
132. Li M, Sato Y, Nishizawa S, Seino T, Nakamura K, Teramae N (2009)2-Aminopurine-modified abasic-site-containing duplex DNA for highly selective detection of theophylline. Journal of the American Chemical Society 131:2448–2449
133. Gong X, Yu C, Zhang Y, Sun Y, Ye L, Li J (2019) Carbon nanoparticle-protected RNA aptasensor for amplified fluorescent determination of theophylline in serum based on nuclease-aided signal amplification. RSC advances 9:33898–33902
134. Li X, Song J, Wang Y, Cheng T (2013) Cyclically amplified fluorescent detection of theophylline and thiamine pyrophosphate by coupling self-cleaving RNA ribozyme with endonuclease. Analytica Chimica Acta 797:95–101
135. Lam BJ, Joyce GF (2011) An isothermal system that couples ligand-dependent catalysis to ligand-independent exponential amplification. Journal of the American Chemical Society 133:3191–3197
136. Kjelstrup MV, Nielsen LD, Hansen-Bruhn M, Gothelf KV (2018) A DNA-based assay for digoxin detection. Biosensors 8:19
137. González GP, Hernando PF, Alegría JSD (2009) A MIP-based flow-through fluoroimmunosensor as an alternative to immunosensors for the determination of digoxin in serum samples. Analytical and bioanalytical chemistry 394:963–970
138. González GP, Hernando PF, Alegría JD (2008) Determination of digoxin in serum samples using a flow-through fluorosensor based on a molecularly imprinted polymer. Biosensors and Bioelectronics 23:1754–1758
139. Li C, Zhang Y, Eremin SA, Yakup O, Yao G, Zhang X (2017) Detection of kanamycin and gentamicin residues in animal-

derived food using IgY antibody based ic-ELISA and FPIA. Food chemistry 227:48–54
140. Ho TYJ, Chan C-C, Chan K, Wang YC, Lin J-T, Chang C-M, Chen C-S(2013) Development of a novel bead-based 96-well filtration plate competitive immunoassay for the detection of Gentamycin. Biosensors and Bioelectronics 49:126–132
141. Beloglazova N, Shmelin P, Eremin S (2016) Sensitive immunochemical approaches for quantitative (FPIA) and qualitative (lateral flow tests) determination of gentamicin in milk. Talanta 149: 217–224
142. Kaur G, Singh A, Venugopalan P, Kaur N, Singh N (2016) Selective recognition of lithium (i) ions using Biginelli based fluorescent organic nanoparticles in an aqueous medium. RSC advances 6:1792–1799
143. Rochat S, Grote Z, Severin K (2009)Ruthenium-based metallacrown complexes for the selective detection of lithium ions in water and in serum by fluorescence spectroscopy. Organic & Biomolecular Chemistry 7:1147–1153
144. Stubing D, Heng S, Abell A (2016) Crowned spiropyran fluoroionophores with a carboxyl moiety for the selective detection of lithium ions. Organic & biomolecular chemistry 14:3752–3757
145. Sorouraddin M-H, Imani-Nabiyyi A, Najibi-Gehraz SA, Rashidi M-R(2014) A new fluorimetric method for determination of valproic acid using TGA-capped CdTe quantum dots as proton sensor. Journal of luminescence 145:253–258
146. Wahba M, El-Enany N, Belal F (2015) Application of the Stern–Volmer equation for studying the spectrofluorimetric quenching reaction of eosin with clindamycin hydrochloride in its pure form and pharmaceutical preparations. Analytical Methods 7:10445–10451
147. Hatefi A, Rahimpour E, Khoubnasabjafari M, Edalat M, Jouyban-Gharamaleki V, Alvani-Alamdari S, Nokhodchi A, Pournaghi-Azar MH, Jouyban A (2019) A single-shot diagnostic platform based on copper nanoclusters coated with cetyl trimethylammonium bromide for determination of carbamazepine in exhaled breath condensate. Microchimica Acta 186:1–8
148. Wang PP, Simpson E, Meucci V, Morrison M, Lunetta S, Zajac M, Boeckx R (1991) Cyclosporine monitoring by fluorescence polarization immunoassay. Clinical biochemistry 24:55–58
149. Smirnova T, Nevryueva N, Shtykov S, Kochubei V, Zhemerichkin D (2009) Determination of warfarin by sensitized fluorescence using organized media. Journal of Analytical Chemistry 64:1114
150. Kumar P, Kumar V, Gupta R (2017) Detection of the anticoagulant drug warfarin by palladium complexes. Dalton Transactions 46:10205–10209
151. Wang M, Tian B, Xue Y, Li R, Zhai T, Tan L (2020) Determination of aminophylline based on fluorescence quenching of amino-functionalized graphene quantum dots induced by photoilluminated riboflavin-aminophylline system. Spectrochimica Acta Part A: Molecular and Biomolecular Spectroscopy 118306
152. Duan H, Li L, Wang X, Wang Y, Li J, Luo C (2015) A sensitive and selective chemiluminescence sensor for the determination of dopamine based on silanized magnetic graphene oxide-molecularly imprinted polymer. Spectrochimica Acta Part A: Molecular and Biomolecular Spectroscopy 139:374–379
153. Nirala NR, Harel Y, Lellouche J-P, Shtenberg G (2020) Ultrasensitive haptoglobin biomarker detection based on amplified chemiluminescence of magnetite nanoparticles. Journal of nanobiotechnology 18:1–10
154. He Y, Xu B, Li W, Yu H (2015) Silver nanoparticle-based chemiluminescent sensor array for pesticide discrimination. Journal of agricultural and food chemistry 63:2930–2934
155. Qi Y, Xiu F-R, Yu G, Huang L, Li B (2017) Simple and rapid chemiluminescence aptasensor for Hg2+ in contaminated samples: a new signal amplification mechanism. Biosensors and Bioelectronics 87:439–446
156. Zhang Z, Zhang S, Zhang X (2005) Recent developments and applications of chemiluminescence sensors. Analytica Chimica Acta 541:37–46
157. Tiwari A, Dhoble S (2018) Recent advances and developments on integrating nanotechnology with chemiluminescence assays. Talanta 180:1–11
158. Qi Y, Li B (2013) Enhanced effect of aggregated gold nanoparticles on luminol chemiluminescence system and its analytical application. Spectrochimica Acta Part A: Molecular and Biomolecular Spectroscopy 111:1–6
159. Haghighi B, Bozorgzadeh S (2010) Flow injection chemiluminescence determination of isoniazid using luminol and silver nanoparticles. Microchemical journal 95:192–197
160. Liu B, He Y, Duan C, Li N, Cui H (2011) Platinum nanoparticle-catalyzedlucigenin–hydrazine chemiluminescence. Journal of Photochemistry and Photobiology A: Chemistry 217:62–67
161. Zhang H, Zhang L, Lu C, Zhao L, Zheng Z (2012) CdTe nanocrystals-enhanced chemiluminescence from peroxynitrous acid–carbonate and its application to the direct determination of nitrite. Spectrochimica Acta Part A: Molecular and Biomolecular Spectroscopy 85:217–222
162. Wu J, Fu X, Xie C, Yang M, Fang W, Gao S (2011) TiO2 nanoparticles-enhanced luminol chemiluminescence and its analytical applications in organophosphate pesticide imprinting. Sensors and Actuators B: Chemical 160:511–516
163. Iranifam M, Fathinia M, Rad TS, Hanifehpour Y, Khataee A, Joo S (2013) A novel selenium nanoparticles-enhanced chemiluminescence system for determination of dinitrobutylphenol. Talanta 107:263–269
164. Chen W, Hong L, Liu A-L, Liu J-Q, Lin X-H, Xia X-H(2012) Enhanced chemiluminescence of the luminol-hydrogen peroxide system by colloidal cupric oxide nanoparticles as peroxidase mimic. Talanta 99:643–648
165. Li Q, Zhang L, Li J, Lu C (2011)Nanomaterial-amplified chemiluminescence systems and their applications in bioassays. TrAC Trends in Analytical Chemistry 30:401–413
166. Khataee A, Hasanzadeh A, Iranifam M, Fathinia M, Hanifehpour Y, Joo S (2014) CuO nanosheets-enhanced flow-injection chemiluminescence system for determination of vancomycin in water, pharmaceutical and human serum. Spectrochimica Acta Part A: Molecular and Biomolecular Spectroscopy 122:737–743
167. Song H, Su Y, Zhang L, Lv Y (2019) Quantum dots-based chemiluminescence probes: an overview. Luminescence 34:530–543
168. Chen H, Lin L, Li H, Lin J-M(2014) Quantum dots-enhanced chemiluminescence: mechanism and application. Coordination Chemistry Reviews 263:86–100
169. Khataee A, Lotfi R, Hasanzadeh A (2015) A novel permanganate–morin–CdS quantum dots flow injection chemiluminescence system for sensitive determination of vancomycin. RSC advances 5: 82645–82653
170. Guan G, Yang L, Mei Q, Zhang K, Zhang Z, Han M-Y(2012) Chemiluminescence switching on peroxidase-like Fe3O4 nanoparticles for selective detection and simultaneous determination of various pesticides. Analytical chemistry 84:9492–9497
171. Zhang Z-F, Cui H, Lai C-Z, Liu L-J(2005) Gold nanoparticle-catalyzed luminol chemiluminescence and its analytical applications. Analytical chemistry 77:3324–3329
172. Duan C-F, Cui H (2009)Time-tunable autocatalytic lucigenin chemiluminescence initiated by platinum nanoparticles and ethanol. Chemical communications:2574–2576

173. Yang L, Guan G, Wang S, Zhang Z (2012)Nano-anatase-enhanced peroxyoxalate chemiluminescence and its sensing application. The Journal of Physical Chemistry C 116:3356–3362
174. Marquette CA, Blum LJ (2006) Applications of the luminol chemiluminescent reaction in analytical chemistry. Analytical and bioanalytical chemistry 385:546–554
175. Apopa PL, Qian Y, Shao R, Guo NL, Schwegler-Berry D, Pacurari M, Porter D, Shi X, Vallyathan V, Castranova V (2009) Iron oxide nanoparticles induce human microvascular endothelial cell permeability through reactive oxygen species production and microtubule remodeling. Particle and fibre toxicology 6:1–14
176. Gao L, Zhuang J, Nie L, Zhang J, Zhang Y, Gu N, Wang T, Feng J, Yang D, Perrett S (2007) Intrinsic peroxidase-like activity of ferromagnetic nanoparticles. Nature nanotechnology 2:577–583
177. Rezaei B, Ensafi AA, Zarei L (2012) Fast and sensitive chemiluminescence assay of aminophylline in human serum using luminol–diperiodatoargentate(III) system catalyzed by coated iron nanoparticles. Spectrochimica Acta Part A: Molecular and Biomolecular Spectroscopy 90:223–229
178. Wang Z, Zhang Z, Fu Z, Luo W, Zhang X (2004)Flow-injection chemiluminescence determination of aminomethylbenzoic acid and aminophylline based on N-bromosuccinimide–luminol reaction. Talanta 62:611–617
179. Lee SH, Li M, Suh JK (2003) Determination of carbamazepine by chemiluminescence detection using chemically prepared tris (2, 2′-bipyridine) ruthenium (III) as oxidant. Analytical sciences 19: 903–906
180. Wei G, Dang G, Li H (2007) Ultrasensitive assay of clindamycin in medicine and bio-fluids with chemiluminescence detection. Luminescence: The journal of biological and chemical luminescence 22:534–539
181. L.H. Santos, A. Araújo, B. Reis, M. Montenegro, Development of a multicommutated flow system with chemiluminometric detection for quantification of gentamicin in pharmaceuticals, Journal of Automated Methods and Management in Chemistry, 2010 (2010).
182. Fernández-Ramos JM, García-Campaña AM, Alés-Barrero F, Bosque-Sendra JM (2006) Determination of gentamicin in pharmaceutical formulations using peroxyoxalate chemiluminescent detection in flow-injection analysis. Talanta 69:763–768
183. Iranifam M, Hasanzadeh A, Fathinia M, Khataee A, Mousavi S (2014)Flow-injection chemiluminescence determination of gentamicin: optimization by central composite design. Luminescence 29:230–238
184. Zhou M-x, Guan C-y, Chen G, Xie X-y, Wu S-h(2005) Determination of theophylline concentration in serum by chemiluminescent immunoassay. Journal of Zhejiang University SCIENCE B 6:1148–1152
185. Zhou M, Chen Q, Wang A, Li J, Ma Y (2019)Flow-injection chemiluminescence of the luminol–potassium periodate system enhanced by TGA–capped CdTe quantum dots for the determination of theophylline. Luminescence 34:673–679
186. Roda A, Zangheri M, Calabria D, Mirasoli M, Caliceti C, Quintavalla A, Lombardo M, Trombini C, Simoni P (2019) A simple smartphone-based thermochemiluminescent immunosensor for valproic acid detection using 1, 2-dioxetane analogue-doped nanoparticles as a label. Sensors and Actuators B: Chemical 279:327–333
187. Cao J, Wang H, Liu Y (2015) Determination of l-thyroxine in pharmaceutical preparations by flow injection analysis with chemiluminescence detection based on the enhancement of the luminol–KMnO4 reaction in a micellar medium. Spectrochimica Acta Part A: Molecular and Biomolecular Spectroscopy 140:162–165
188. Huang Y, Zhao S, Shi M, Liu J, Liang H (2012) Microchip electrophoresis coupled with on-line magnetic separation and chemiluminescence detection for multiplexed immunoassay. Electrophoresis 33:1198–1204
189. Lima HRS, da Silva JS, de Oliveira Farias EA, Teixeira PRS, Eiras C, Nunes LCC (2018) Electrochemical sensors and biosensors for the analysis of antineoplastic drugs. Biosens. Bioelectron. 108:27–37
190. Cesewski E, Johnson BN (2020) Electrochemical biosensors for pathogen detection. Biosens. Bioelectron. 112214
191. E.O. Blair, D.K. Corrigan, A review of microfabricated electrochemical biosensors for DNA detection, Biosens. Bioelectron., (2019).
192. Vidal JC, Bonel L, Ezquerra A, Hernández S, Bertolín JR, Cubel C, Castillo JR (2013) Electrochemical affinity biosensors for detection of mycotoxins: a review. Biosens. Bioelectron. 49:146–158
193. El Harrad L, Bourais I, Mohammadi H, Amine A (2018) Recent advances in electrochemical biosensors based on enzyme inhibition for clinical and pharmaceutical applications. Sensors 18:164
194. Arduini F, Cinti S, Scognamiglio V, Moscone D (2016) Nanomaterials in electrochemical biosensors for pesticide detection: advances and challenges in food analysis. Microchim. Acta 183:2063–2083
195. Rasheed PA, Sandhyarani N (2017) Carbon nanostructures as immobilization platform for DNA: a review on current progress in electrochemical DNA sensors. Biosens. Bioelectron. 97:226–237
196. Zhu C, Yang G, Li H, Du D, Lin Y (2015) Electrochemical sensors and biosensors based on nanomaterials and nanostructures. Anal. Chem. 87:230–249
197. Sadik OA, Aluoch AO, Zhou A (2009) Status of biomolecular recognition using electrochemical techniques. Biosens. Bioelectron. 24:2749–2765
198. Farghaly OA, Hameed RA, Abu-Nawwas A-AH (2014) Analytical application using modern electrochemical techniques. Int. J. Electrochem. Sci 9:3287–3318
199. Zhu Y-H, Zhang Z-L, Pang D-W(2005) Electrochemical oxidation of theophylline at multi-wall carbon nanotube modified glassy carbon electrodes. J. Electroanal. Chem. 581:303–309
200. Chiarotto I, Mattiello L, Pandolfi F, Rocco D, Feroci M, Petrucci R (2019) Electrochemical oxidation of theophylline in organic solvents: HPLC-PDA-ESI-MS/MS analysis of the oxidation products. ChemElectroChem 6:4511–4521
201. Ahn JK, Park KS, Won BY, Park HG (2015) A novel electrochemical method to detect theophylline utilizing silver ions captured within abasic site-incorporated duplex DNA. Biosens. Bioelectron. 67:590–594
202. Ferapontova EE, Olsen EM, Gothelf KV (2008) An RNA aptamer-based electrochemical biosensor for detection of theophylline in serum. J. Am. Chem. Soc. 130:4256–4258
203. Wang Y, Ding Y, Li L, Hu P (2018)Nitrogen-doped carbon nanotubes decorated poly (L-Cysteine) as a novel, ultrasensitive electrochemical sensor for simultaneous determination of theophylline and caffeine. Talanta 178:449–457
204. Yang S, Yang R, Li G, Li J, Qu L (2010) Voltammetric determination of theophylline at a Nafion/multi-wall carbon nanotubes composite film-modified glassy carbon electrode. Journal of chemical sciences 122:919–926
205. Yang YJ, Li W (2015) High sensitive determination of theophylline based on manganese oxide nanoparticles/multiwalled carbon nanotube nanocomposite modified electrode. Ionics 21:1121–1128
206. Yin H, Meng X, Su H, Xu M, Ai S (2012) Electrochemical determination of theophylline in foodstuff, tea and soft drinks based on urchin-like CdSe microparticles modified glassy carbon electrode. Food Chem. 134:1225–1230

207. Sun W, Hu J (2013) Voltammetric determination of theophylline in pharmaceutical formulations using aligned carbon nanotubes (ACNTs) film modified electrode. J. Anal. Chem. 68:694–699
208. AbuáZuhri AZ (1994) Adsorptive cathodic stripping voltammetric determination of theophylline at a hanging mercury drop electrode. Analyst 119:1967–1970
209. Kan X, Liu T, Zhou H, Li C, Fang B (2010) Molecular imprinting polymer electrosensor based on gold nanoparticles for theophylline recognition and determination. Microchim. Acta 171:423–429
210. Jesny S, Girish Kumar K (2017)Non-enzymatic electrochemical sensor for the simultaneous determination of xanthine, its methyl derivatives theophylline and caffeine as well as its metabolite uric acid. Electroanalysis 29:1828–1837
211. Gholivand MB, Khodadadian M (2014) Simultaneous voltammetric determination of theophylline and guaifenesin using a multiwalled carbon nanotube-ionic liquid modified glassy carbon electrode. Electroanalysis 26:1975–1983
212. Gan T, Zhao A, Wang Z, Liu P, Sun J, Liu Y (2017) An electrochemical sensor based on SiO 2@ TiO 2-embedded molecularly imprinted polymers for selective and sensitive determination of theophylline. J. Solid State Electrochem. 21:3683–3691
213. Ferapontova EE, Gothelf KV (2009) Optimization of the electrochemical RNA-aptamer based biosensor for theophylline by using a methylene blue redox label. Electroanalysis: An International Journal Devoted to Fundamental and Practical Aspects of Electroanalysis 21:1261–1266
214. Wang T, Randviir EP, Banks CE (2014) Detection of theophylline utilising portable electrochemical sensors. Analyst 139:2000–2003
215. Raj MA, John SA (2014) Graphene layer modified glassy carbon electrode for the determination of norepinephrine and theophylline in pharmaceutical formulations. Analytical Methods 6:2181–2188
216. Ganjali MR, Dourandish Z, Beitollahi H, Tajik S, Hajiaghababaei L, Larijani B (2018) Highly sensitive determination of theophylline based on graphene quantum dots modified electrode. Int. J. Electrochem. Sci 13:2448–2461
217. Shu X, Bian F, Wang Q, Qin X, Wang Y (2017) Electrochemical sensor for simultaneous determination of theophylline and caffeine based on a novel poly (folic acid)/graphene composite film modified electrode. Int. J. Electrochem. Sci 12:4251–4264
218. Peng A, Yan H, Luo C, Wang G, Ye X, Ding H (2017) Electrochemical determination of theophylline pharmacokinetic under the effect of roxithromycin in rats by the MWNTs/Au/poly-L-lysine modified sensor. Int. J. Electrochem. Sci 12:330–346
219. Li Y, Wu S, Luo P, Liu J, Song G, Zhang K, Ye B (2012) Electrochemical behavior and voltammetric determination of theophylline at a glassy carbon electrode modified with graphene/nafion. Anal. Sci. 28:497–502
220. de Jesus Guedes T, Pio dos Santos WT (2018) Fast and simple electrochemical analysis kit for quality control of narrow therapeutic index drugs. Electroanalysis 30:1740–1749
221. Mekassa B, Tessema M, Chandravanshi BS (2017) Simultaneous determination of caffeine and theophylline using square wave voltammetry at poly (l-aspartic acid)/functionalized multi-walled carbon nanotubes composite modified electrode. Sensing and biosensing research 16:46–54
222. Yang YJ, Guo L, Zhang W (2016) The electropolymerization of CTAB on glassy carbon electrode for simultaneous determination of dopamine, uric acid, tryptophan and theophylline. J. Electroanal. Chem. 768:102–109
223. Zhao G-C, Yang X (2010) A label-free electrochemical RNA aptamer for selective detection of theophylline. Electrochem. Commun. 12:300–302
224. Ferapontova EE, Shipovskov S, Gorton L (2007) Bioelectrocatalytic detection of theophylline at theophylline oxidase electrodes. Biosens. Bioelectron. 22:2508–2515
225. Aswini K, Mohan AV, Biju V (2016) Molecularly imprinted poly (4-amino-5-hydroxy-2, 7-naphthalenedisulfonic acid) modified glassy carbon electrode as an electrochemical theophylline sensor. Materials Science and Engineering: C 65:116–125
226. Malode SJ, Shetti NP, Nandibewoor ST (2012) Voltammetric behavior of theophylline and its determination at multi-wall carbon nanotube paste electrode. Colloids and Surfaces B: Biointerfaces 97:1–6
227. Güney S, Cebeci FC (2015) Selective electrochemical sensor for theophylline based on an electrode modified with imprinted sol–gel film immobilized on carbon nanoparticle layer. Sensors and Actuators B: Chemical 208:307–314
228. Yang G, Zhao F, Zeng B (2014) Facile fabrication of a novel anisotropic gold nanoparticle–chitosan–ionic liquid/graphene modified electrode for the determination of theophylline and caffeine. Talanta 127:116–122
229. Zi L, Li J, Mao Y, Yang R, Qu L (2012) High sensitive determination of theophylline based on gold nanoparticles/l-cysteine/Graphene/Nafion modified electrode. Electrochim. Acta 78:434–439
230. Chen X, Guo Z, Tang Y, Shen Y, Miao P (2018) A highly sensitive gold nanoparticle-based electrochemical aptasensor for theophylline detection. Anal. Chim. Acta 999:54–59
231. MansouriMajd S, Teymourian H, Salimi A, Hallaj R (2013) Fabrication of electrochemical theophylline sensor based on manganese oxide nanoparticles/ionic liquid/chitosan nanocomposite modified glassy carbon electrode. Electrochim. Acta 108:707–716
232. Gao Y, Wang H, Guo L (2013) Simultaneous determination of theophylline and caffeine by large mesoporous carbon/Nafion modified electrode. J. Electroanal. Chem. 706:7–12
233. Teixeira JG, Veiga A, Carvalho AJP, Teixeira DM (2013)Electrooxidation of carbamazepine metabolites: characterization and influence in the voltammetric determination of the parent drug. Electrochim. Acta 108:51–65
234. Kalanur SS, Seetharamappa J (2010) Electrochemical oxidation of bioactive carbamazepine and its interaction with DNA. Anal. Lett. 43:618–630
235. Domínguez JNR, González T, Palo P, Sánchez-Martín J (2010) Electrochemical advanced oxidation of carbamazepine on boron-doped diamond anodes. Influence of operating variables. Industrial & Engineering Chemistry Research 49:8353–8359
236. García-Gómez C, Drogui P, Zaviska F, Seyhi B, Gortáres-Moroyoqui P, Buelna G, Neira-Sáenz C, Estrada-Alvarado M, Ulloa-Mercado R (2014) Experimental design methodology applied to electrochemical oxidation of carbamazepine using Ti/PbO2 and Ti/BDD electrodes. Journal of Electroanalytical Chemistry 732:1–10
237. Pruneanu S, Pogacean F, Biris AR, Ardelean S, Canpean V, Blanita G, Dervishi E, Biris AS (2011) Novel graphene-gold nanoparticle modified electrodes for the high sensitivity electrochemical spectroscopy detection and analysis of carbamazepine. The Journal of Physical Chemistry C 115:23387–23394
238. Lavanya N, Sekar C, Ficarra S, Tellone E, Bonavita A, Leonardi S, Neri G (2016) A novel disposable electrochemical sensor for determination of carbamazepine based on Fe doped SnO2 nanoparticles modified screen-printed carbon electrode. Materials Science and Engineering: C 62:53–60
239. Tarahomi S, Rounaghi GH, Zavar MHA, Daneshvar L (2018) Electrochemical sensor based on TiO2 nanoparticles/nafion biocompatible film modified glassy carbon electrode for carbamazepine determination in pharmaceutical and urine samples. J. Electrochem. Soc. 165:B946

240. Atkins S, Gonzalez-Rodriguez J, Sevilla J, Blazquez M, Pineda T, Jimenez-Perez R (2013) Electrochemical reduction of carbamazepine in ethanol and water solutions using a glassy carbon electrode. International Journal of Electrochemical Science 8:2056–2068
241. Veiga A, Dordio A, Carvalho AP, Teixeira DM, Teixeira JG (2010)Ultra-sensitive voltammetric sensor for trace analysis of carbamazepine. Anal. Chim. Acta 674:182–189
242. Kalanur SS, Jaldappagari S, Balakrishnan S (2011) Enhanced electrochemical response of carbamazepine at a nano-structured sensing film of fullerene-C60 and its analytical applications. Electrochim. Acta 56:5295–5301
243. Daneshvar L, Rounaghi G, E'shaghi Z, Chamsaz M, Tarahomi S (2016) Electrochemical determination of carbamazepin in the presence of paracetamol using a carbon ionic liquid paste electrode modified with a three-dimensionalgraphene/MWCNT hybrid composite film. J. Mol. Liq. 215:316–322
244. Unnikrishnan B, Mani V, Chen S-M(2012) Highly sensitive amperometric sensor for carbamazepine determination based on electrochemically reduced graphene oxide–single-walled carbon nanotube composite film. Sensors and Actuators B: Chemical 173:274–280
245. Liu L-H, Duan C-Q, Gao Z-N(2012) Electrochemical behaviors and electrochemical determination of carbamazepine at ionic liquid modified carbon paste electrode in the presence of sodium dodecyl sulfate. J. Serb. Chem. Soc. 77:483–496
246. Atkins S, Sevilla J, Blazquez M, Pineda T, Gonzalez-Rodriguez J (2010) Electrochemical behaviour of carbamazepine in acetonitrile and dimethylformamide using glassy carbon electrodes and microelectrodes. Electroanalysis 22:2961–2966
247. Daneshvar L, Rounaghi GH (2017) An electrochemical sensing platform for carbamazepine determination based on trimetallic Au-Ag-Pd dendritic nanopatricles, supramolecular β-cyclodextrin and [bmim] NTF2 ionic liquids. J. Electrochem. Soc. 164:B177
248. Trišović NP, Božić B, Petrović SD, Tadić SJ, Avramov Ivić M (2014) Electrochemical characterization and determination of carbamazepine as pharmaceutical standard and tablet content on gold electrode. Hemijska industrija 68:207–212
249. Wang H, Pan M, Su YO, Tsai S, Kao C, Sun S, Lin W (2011) Comparison of Differential Pulse Voltammetry (DPV)—a new method of carbamazepine analysis—with Fluorescence Polarization Immunoassay (FPIA). J. Anal. Chem. 66:415–420
250. Jamshidi M, Nematollahi D (2017) Green electrochemical synthesis of N-phenylquinoneimine derivatives: dual action of 4-morpholinoaniline and N-(4-aminophenyl) acetamide. ACS Sustainable Chemistry & Engineering 5:9423–9430
251. Wahedi K, Amooshahi P, Jamshidi M, Khazalpour S (2020) Electrochemical assessment of EC and ECE mechanisms for caffeic acid in the presence of aromatic amines. Analytical and Bioanalytical Chemistry Research 7:345–353
252. Nematollahi D, Ghasemi F, Khazalpour S, Varmaghani F (2016) Kinetic study on electrochemical oxidation of catechols in the presence of cycloheptylamine and aniline: experiments and digital simulation. Journal of Chemical Sciences 128:1887–1894
253. Mazloum-Ardakani M, Rajabzadeh N, Dehghani-Firouzabadi A, Benvidi A, Mirjalili B, Zamani L (2016) Development of an electrode modified on the basis of carbon nanoparticles and reduced graphene oxide for simultaneous determination of isoproterenol, uric acid and tryptophan in real samples. J. Electroanal. Chem. 760:151–157
254. Mazloum-Ardakani M, Sheikh-Mohseni MA, Mirjalili B-F, Ahmadi R, Mirhoseini MA (2015) A nanocomposite electrocatalyst for the electro-oxidation of isoproterenol and its application as a sensor. Chinese Journal of Catalysis 36:1273–1279
255. Palakollu VN, Chiwunze TE, Gill AA, Thapliyal N, Maru SM, Karpoormath R (2017) Electrochemical sensitive determination of isoprenaline at β-cyclodextrin functionalized graphene oxide and electrochemically generated acid yellow 9 polymer modified electrode. J. Mol. Liq. 248:953–962
256. Beitollahi H, Salimi H (2016) A triple electrochemical platform for simultaneous determination of isoproterenol, acetaminophen and tyrosine based on a glassy carbon electrode modified with hematoxylin and graphene. J. Electrochem. Soc. 163:H1157
257. Karimi-Maleh H, Rostami S, Gupta VK, Fouladgar M (2015) Evaluation of ZnO nanoparticle ionic liquid composite as a voltammetric sensing of isoprenaline in the presence of aspirin for liquid phase determination. J. Mol. Liq. 201:102–107
258. Mazloum-Ardakani M, Sabaghian F, Khoshroo A, Naeimi H (2014) Simultaneous determination of the concentrations of isoproterenol, uric acid, and folic acid in solution using a novel nanostructure-based electrochemical sensor. Chinese Journal of Catalysis 35:565–572
259. Mazloum-Ardakani M, Hosseinzadeh L, Khoshroo A, Naeimi H, Moradian M (2014) Simultaneous determination of isoproterenol, acetaminophen and folic acid using a novel nanostructure-based electrochemical sensor. Electroanalysis 26:275–284
260. Beitollahi H, Movlaee K, Ganjali MR, Norouzi P (2017) A sensitive graphene and ethyl 2-(4-ferrocenyl-[1, 2, 3] triazol-1-yl) acetate modified carbon paste electrode for the concurrent determination of isoproterenol, acetaminophen, tryptophan and theophylline in human biological fluids. J. Electroanal. Chem. 799:576–582
261. Tajik S, Taher MA, Beitollahi H (2014) Application of a new ferrocene-derivative modified-graphene paste electrode for simultaneous determination of isoproterenol, acetaminophen and theophylline. Sensors and Actuators B: Chemical 197:228–236
262. Wong A, Santos AM, Silva TA, Fatibello-Filho O (2018) Simultaneous determination of isoproterenol, acetaminophen, folic acid, propranolol and caffeine using a sensor platform based on carbon black, graphene oxide, copper nanoparticles and PEDOT: PSS. Talanta 183:329–338
263. Dourandish Z, Beitollahi H (2018) Electrochemical sensing of isoproterenol using graphite screen-printed electrode modified with graphene quantum dots. Anal. Bioanal. Chem 10:192–202
264. Beitollahi H, Raoof J-B, Karimi-Maleh H, Hosseinzadeh R (2012) Electrochemical behavior of isoproterenol in the presence of uric acid and folic acid at a carbon paste electrode modified with 2, 7-bis (ferrocenyl ethyl) fluoren-9-one and carbon nanotubes. J. Solid State Electrochem. 16:1701–1707
265. Keyvanfard M, Ahmadi M, Karimi F, Alizad K (2014) Voltammetric determination of cysteamine at multiwalled carbon nanotubes paste electrode in the presence of isoproterenol as a mediator. Chin. Chem. Lett. 25:1244–1246
266. Gopal P, Reddy TM, Nagaraju C, Narasimha G (2014) Preparation, characterization and analytical application of an electrochemical laccase biosensor towards low level determination of isoprenaline in human serum samples. RSC Advances 4:57591–57599
267. Ensafi AA, Karimi-Maleh H (2011) Voltammetric determination of isoproterenol using multiwall carbon nanotubes-ionic liquid paste electrode. Drug testing and analysis 3:325–330
268. Chen M, Ma X, Li X (2012) Electrochemical determination of isoprenaline using a graphene-modified glassy carbon electrode. J. Solid State Electrochem. 16:3261–3266
269. Mohammadi SZ, Beitollahi H, Fadaeian H (2018) Voltammetric determination of isoproterenol using a graphene oxide nano sheets paste electrode. J. Anal. Chem. 73:705–712
270. Beitollahi H, Khabazzadeh H, Karimi-Maleh H, Akbari A (2012) Voltammetric determination of isoproterenol using a 5-amino-2′, 4′-dimethoxybiphenyl-2-ol modified carbon nanotube paste electrode. Chin. Chem. Lett. 23:719–722

271. Beitollahi H, Sheikhshoaie I (2011) Electrocatalytic and simultaneous determination of isoproterenol, uric acid and folic acid at molybdenum (VI)complex-carbon nanotube paste electrode. Electrochim. Acta 56:10259–10263
272. Ensafi AA, Khoddami E, Karimi-Maleh H (2011) Electrocatalytic detection of isoproterenol at a ferrocene-multiwall carbon nanotubes paste electrode. Int. J. Electrochem. Sci 6:2596–2608
273. Mohammadi SZ, Beitollahi H, Afzali H (2016) A novel electrochemical nanosensor for voltammetric determination of isoproterenol. ANALYTICAL & BIOANALYTICAL ELECTROCHEMISTRY 8:977–987
274. Kutluay A, Aslanoglu M (2010) Electrocatalytic oxidation of isoproterenol and its voltammetric determination in pharmaceuticals and urine samples using a poly (1-methylpyrrole)-DNA modified electrode. J. Acta Chim. Slovenica 57:157–162
275. Bonifácio VG, Marcolino LH Jr, Teixeira MF, Fatibello-Filho O (2004) Voltammetric determination of isoprenaline in pharmaceutical preparations using a copper (II) hexacyanoferrate (III) modified carbon paste electrode. Microchem. J. 78:55–59
276. Mazloum-Ardakani M, Khoshroo A (2014) Electrocatalytic properties of functionalized carbon nanotubes with titanium dioxide and benzofuran derivative/ionic liquid for simultaneous determination of isoproterenol and serotonin. Electrochim. Acta 130:634–641
277. Beitollahi H, Mohadesi A, Mohammadi S, Akbari A (2012) Electrochemical behavior of a carbon paste electrode modified with 5-amino-3′, 4′-dimethyl-biphenyl-2-ol/carbon nanotube and its application for simultaneous determination of isoproterenol, acetaminophen and N-acetylcysteine. Electrochim. Acta 68:220–226
278. Chitravathi S, Kumaraswamy B, Niranjana E, Chandra U, Mamatha G, Sherigara B (2009) Electrochemical studies of sodium levothyroxine at surfactant modified carbon paste electrode. Int. J. Electrochem. Sci 4:223–237
279. Chitravathi S, Swamy BK, Chandra U, Mamatha G, Sherigara B (2010) Electrocatalytic oxidation of sodium levothyroxine with phenyl hydrazine as a mediator at carbon paste electrode: a cyclic voltammetric study. J. Electroanal. Chem. 645:10–15
280. Iwamoto M, Webber A, Osteryoung RA (1984) Cathodic reduction of thyroxine and related compounds on silver. Anal. Chem. 56:1202–1206
281. Lotfi S, Veisi H (2019) Synthesis and characterization of novel nanocomposite (MWCNTs/CC-SH/Au) and its use as a modifier for construction of a sensitive sensor for determination of low concentration of levothyroxine in real samples. Chem. Phys. Lett. 716:177–185
282. He Z, Jin W (2003) Capillary electrophoretic enzyme immunoassay with electrochemical detection for thyroxine. Anal. Biochem. 313:34–40
283. Mak CK, Wehe CA, Sperling M, Karst U (2015) Identification and quantification of electrochemically generated metabolites of thyroxine by means of liquid chromatography/electrospray-mass spectrometry and countergradient liquid chromatography/inductively coupled plasma-mass spectrometry. J. Chromatogr. A 1419:81–88
284. Hay ID, Annesley TM, Jiang NS, Gorman CA (1981) Simultaneous determination of D-and L-thyroxine in human serum by liquid chromatography with electrochemical detection. Journal of Chromatography B: Biomedical Sciences and Applications 226:383–390
285. Kazemifard AG, Moore DE, Aghazadeh A (2001) Identification and quantitation of sodium-thyroxine and its degradation products by LC using electrochemical and MS detection. J. Pharm. Biomed. Anal. 25:697–711
286. Kimura T, Nakanishi K, Nakagawa T, Shibukawa A, Matsuzaki K (2005) Simultaneous determination of unbound thyroid hormones in human plasma using high performance frontal analysis with electrochemical detection. J. Pharm. Biomed. Anal. 38:204–209
287. Li XM, Zhang F, Zhang SS (2008) Capillary electrophoresis enzyme immunoassay for alpha-fetoprotein and thyroxine in human serum with electrochemical detection. J. Sep. Sci. 31:336–340
288. He Q, Dang X, Hu C, Hu S (2004) The effect of cetyltrimethyl ammonium bromide on the electrochemical determination of thyroxine. Colloids and Surfaces B: Biointerfaces 35:93–98
289. Prasad BB, Madhuri R, Tiwari MP, Sharma PS (2010)Layer-by-layer assembled molecularly imprinted polymer modified silver electrode for enantioselective detection of d-and l-thyroxine. Anal. Chim. Acta 681:16–26
290. Gholivand M-B, Solgi M (2018) Simultaneous electrochemical sensing of warfarin and maycophenolic acid in biological samples. Analytica chimica acta 1034:46–55
291. Gholivand MB, Torkashvand M (2015) Electrooxidation behavior of warfarin in Fe3O4 nanoparticles modified carbon paste electrode and its determination in real samples. Materials Science and Engineering: C 48:235–242
292. Taei M, Hasanpour F, Basiri F, Tavakkoli N, Rasouli N (2016) Highly selective differential pulse voltammetric determination of warfarin in pharmaceutical and biological samples using MnFe2O4/MWCNT modified carbon paste electrode. Microchemical Journal 129:166–172
293. Taei M, Abedi F (2016) New modified multiwalled carbon nanotubes paste electrode for electrocatalytic oxidation and determination of warfarin in biological and pharmaceutical samples. Chinese Journal of Catalysis 37:436–445
294. Rezaei B, Rahmanian O, Ensafi AA (2014) An electrochemical sensor based on multiwall carbon nanotubes and molecular imprinting strategy for warfarin recognition and determination. Sensors and Actuators B: Chemical 196:539–545
295. Li Y, Zhang L, Liu J, Zhou S-F, Al-Ghanim KA, Mahboob S, Ye B-C, Zhang X (2016) A novel sensitive and selective electrochemical sensor based on molecularly imprinted polymer on a nanoporous gold leaf modified electrode for warfarin sodium determination. RSC advances 6:43724–43731
296. Damiri S, Oskoei YM, Fouladgar M (2016) Highly sensitive voltammetric and impedimetric sensor based on an ionic liquid/cobalt hexacyanoferrate nanoparticle modified multi-walled carbon nanotubes electrode for diclofenac analysis. Journal of Experimental Nanoscience 11:1384–1401
297. Gholivand MB, Mohammadi-Behzad L (2015) An electrochemical sensor for warfarin determination based on covalent immobilization of quantum dots onto carboxylated multiwalled carbon nanotubes and chitosan composite film modified electrode. Materials Science and Engineering: C 57:77–87
298. Hassan SS, Mahmoud WH, Abdel-Samad MS (1998) Direct potentiometry and potentiotitrimetry of warfarin and ibuprofen in pharmaceutical preparations using PVC ferroin-based membrane sensors. Microchimica Acta 129:251–257
299. Liu J, Zhang Y, Jiang M, Tian L, Sun S, Zhao N, Zhao F, Li Y (2017) Electrochemical microfluidic chip based on molecular imprinting technique applied for therapeutic drug monitoring. Biosensors and Bioelectronics 91:714–720
300. de Jesus Guedes T, Andrade GAR, Lima AB, da Silva RAB, dos Santos WTP (2017) Simple and fast determination of warfarin in pharmaceutical samples using boron-doped diamond electrode in BIA and FIA systems with multiple pulse amperometric detection. Electroanalysis 29:2340–2347
301. Ghoneim M, Tawfik A (2004) Assay of anti-coagulant drug warfarin sodium in pharmaceutical formulation and human biological fluids by square-wave adsorptive cathodic stripping voltammetry. Analytica chimica acta 511:63–69
302. Gonzalez-Rodriguez J, Bellia G, Corrall H, Baron M, Croxton R (2017) An investigation of digoxin by cyclic voltammetry using

gold and silver solid electrodes and chemometric analysis. International Journal of Electrochemical Science 12:3050–3062
303. Ahmadi A, Shirazi H, Pourbagher N, Akbarzadeh A, Omidfar K (2014) An electrochemical immunosensor for digoxin using core–shell gold coated magnetic nanoparticles as labels. Molecular biology reports 41:1659–1668
304. Bagheri H, Talemi R, Afkhami A (2015) Gold nanoparticles deposited on fluorine-doped tin oxide surface as an effective platform for fabricating a highly sensitive and specific digoxin aptasensor. RSC Advances 5:58491–58498
305. Wijesinghe MS, Ngwa W, Chow KF (2020) Direct electrochemical aptamer-based detection of digoxin. ChemistrySelect 5:2408–2411
306. Katsu T, Mori Y (1997) Determination of free disopyramide in blood serum in situ using a disopyramide-sensitive membrane electrode. Anal. Chim. Acta 343:79–83
307. Öztürk F, Taşdemir IH, Durmuş Z, Kiliç E (2010) Electrochemical behavior of disopyramide and its adsorptive stripping determination in pharmaceutical dosage forms and biological fluids. Collect. Czech. Chem. Commun. 75:685–702
308. Diculescu VC, Enache TA, Oliveira-Brett AM (2007) Electrochemical oxidation at a glassy carbon electrode of the anti-arrhythmia drug disopyramide. Anal. Lett. 40:2860–2871
309. Campuzano S, Gamella M, Serra B, Reviejo A, Pingarron J (2007) Integrated electrochemical gluconic acid biosensor based on self-assembled monolayer-modified gold electrodes. Application to the analysis of gluconic acid in musts and wines. J. Agric. Food. Chem 55:2109–2114
310. Stredansky M, Martínez JMO, Stredansky M, Labuda J (2017) Multienzyme amperometric gluconic acid biosensor based on nanocomposite planar electrodes for analysis in musts and wines. International Journal of Electrochemical Science:1183–1192
311. Albanese D, Malvano F, Sannini A, Pilloton R, Di Matteo M (2014) A doped polyaniline modified electrode amperometric biosensor for gluconic acid determination in grapes. Sensors 14: 11097–11109
312. Molinero-Abad B, Alonso-Lomillo MA, Domínguez-Renedo O, Arcos-Martínez MJ (2015) Simultaneous amperometric determination of malic and gluconic acids in wine using screen-printed carbon electrodes. Sensors and Actuators B: Chemical 211:250–254
313. Cetó X, Céspedes F, Capdevila J, Del Valle M (2011) A new amperometric bienzymatic biosensor based on biocomposites for the determination of gluconic acid in wines. Talanta 85:1207–1212
314. del Torno-de Román L, Alonso-Lomillo MA, Domínguez-Renedo O, Jaureguibeitia A, Arcos-Martínez MJ (2014) GADH screen-printed biosensor for gluconic acid determination in wine samples. Sensors and Actuators B: Chemical 192:56–59
315. Del Torno-de Román L, Alonso-Lomillo M, Domínguez-Renedo O, Arcos-Martínez M (2013) Gluconic acid determination in wine by electrochemical biosensing. Sensors and Actuators B: Chemical 176:858–862
316. Kasim EA, Ghandour MA, El-Haty MT, Ahmed MM (2002) Application of stripping voltammetry to the determination of guanethidine. Monatshefte für Chemie/Chemical Monthly 133:1397–1404
317. Duan J, He D, Wang W, Liu Y, Wu H, Wang Y, Fu M (2013) Glassy carbon electrode modified with gold nanoparticles for ractopamine and metaproterenol sensing. Chem. Phys. Lett. 574: 83–88
318. Baytak AK, Aslanoglu M (2015) Decorating carbon nanotubes with nanoparticles of indium tin oxide for the voltammetric determination of metaproterenol. J. Electroanal. Chem. 757:210–215
319. Carrum G, Abernethy DR, Sadhukhan M, Wright CE III (1986) Minoxidil analysis in human plasma using high-performance liquid chromatography with electrochemical detection: application to pharmacokinetic studies. Journal of Chromatography B: Biomedical Sciences and Applications 381:127–135
320. Dehdashtian S, Hashemi B (2020) Voltammetric sensing of minoxidil using a molecularly imprinted polymer (MIP)-modified carbon paste electrode. Chemical Papers 74:157–165
321. Karimian N, Gholivand M, Taherkhani F (2015) Computational design and development of a novel voltammetric sensor for minoxidil detection based on electropolymerized molecularly imprinted polymer. J. Electroanal. Chem. 740:45–52
322. Pfaffen V, Ortiz PI (2006) Electrochemical determination of minoxidil in different pharmaceutical formulations by flow injection analysis. Anal. Sci. 22:91–94
323. Shamsipur M, Pashabadi A, Taherpour AA, Hemmateenejad B, Khosousi T, Parvin MH (2016) Synthesis and characterization of glucose-capped CdSe quantum dots. Electrochemical and computational studies of corresponding carbon-ionic liquid electrode for quantitative determination of minoxidil. J. Electroanal. Chem. 778:116–125
324. Ahmadi F, Ghasemi S, Rahimi-Nasrabadi M (2011) Adsorptive cathodic stripping determination of minoxidil in pharmaceutical, cream and shampoo products. Collect. Czech. Chem. Commun. 76:371–382
325. Golden MH, Zoutendam PH (1987) The determination of minoxidil in human serum by high-performance liquid chromatography with amperometric detection. J. Pharm. Biomed. Anal. 5:543–551
326. Doğan T, Anik Ü, Dursun Z (2019) Development of practical electrochemical system for phenytoin detection. ChemistrySelect 4:7704–7708
327. Bordes A-L, Limoges BT, Brossier P, Degrand C (1997) Simultaneous homogeneous immunoassay of phenytoin and phenobarbital using a Nafion-loaded carbon paste electrode and two redox cationic labels. Anal. Chim. Acta 356:195–203
328. de Jesus Guedes T, Alecrim MF, Oliveira FM, Lima AB, Barbosa SL, dos Santos WT (2016) Determination of prazosin in pharmaceutical samples by flow injection analysis with multiple-pulse amperometric detection using boron-doped diamond electrode. J. Solid State Electrochem. 20:2445–2451
329. Faridbod F, Ganjali MR, Larijani B, Nasli-Esfahani E, Riahi S, Norouzi P (2010) Quantitative analysis of prazosin hydrochloride in pharmaceutical formulation by prazosin potentiometric sensor based on computational investigation. Int J Electrochem Sci 5: 653–667
330. Arranz A, de Betoño SF, Echevarria C, Moreda JMA, Cid A, Valentín JFA (1999) Voltammetric and spectrophotometric techniques for the determination of the antihypertensive drug Prazosin in urine and formulations. J. Pharm. Biomed. Anal. 21:797–807
331. Khalil S, Kelzieh A, Ibrahim S (2003)Ion-selective electrode for the determination of prazosin in tablets. J. Pharm. Biomed. Anal. 33:825–829
332. Zabardasti A, Afrouzi H, Talemi RP (2017) A simple and sensitive methodology for voltammetric determination of valproic acid in human blood plasma samples using 3-aminopropyletriethoxy silane coated magnetic nanoparticles modified pencil graphite electrode. Materials Science and Engineering: C 76:425–430
333. ACAR ET, Onar AN (2016) Square wave voltammetric determination of valproic acid in pharmaceutical Preparations. Turkish Journal of Chemistry 40:106–116
334. Kotani A, Kotani T, Ishii N, Hakamata H, Kusu F (2014) The effect of hyperglycemia on the pharmacokinetics of valproic acid studied by high-performance liquid chromatography with electrochemical detection. J. Pharm. Biomed. Anal. 97:47–53
335. Favetta P, Guitton J, Bleyzac N, Dufresne C, Bureau J (2001) New sensitive assay of vancomycin in human plasma using high-performance liquid chromatography and electrochemical

detection. Journal of Chromatography B: Biomedical Sciences and Applications 751:377–382
336. Blidar A, Feier B, Pusta A, Drăgan A-M, Cristea C (2019)Graphene–gold nanostructures hybrid composites screen-printed electrode for the sensitive electrochemical detection of vancomycin. Coatings 9:652
337. Hadi M, Mollaei T (2019) Electroanalytical determination of vancomycin at a graphene-modified electrode: comparison of electrochemical property between graphene, carbon nanotube, and carbon black. Electroanalysis 31:1224–1228
338. Belal F, El-Ashry SM, El-Kerdawy MM, El-Wasseef DR (2001) Voltametric determination of vancomycin in dosage forms through treatment with nitrous acid. Arzneimittelforschung 51: 763–768
339. Zhang Z, Hu Y, Zhang H, Yao S (2010) Novel layer-by-layer assembly molecularly imprinted sol–gel sensor for selective recognition of clindamycin based on Au electrode decorated by multi-wall carbon nanotube. J. Colloid Interface Sci. 344:158–164
340. Wong A, Razzino CA, Silva TA, Fatibello-Filho O (2016)Square-wave voltammetric determination of clindamycin using a glassy carbon electrode modified with graphene oxide and gold nanoparticles within a crosslinked chitosan film. Sensors and Actuators B: Chemical 231:183–193
341. M.S. Rizk, H.A. Merey, S.M. Tawakkol, M.N. Sweilam, New potentiometric determination of clindamycin hydrochloride in pharmaceuticals, (2013).
342. Norouzi P, Larijani B, Ezoddin M, Ganjali M (2008)Sub-second adsorption for the fast sub-nanomolar monitoring of Clindamycin in its pure and pharmaceutical samples by fast Fourier transformation with the use of continuous cyclic voltammetry at an Au microelectrode in a flowing system. Materials Science and Engineering: C 28:87–93
343. Habib I, Rizk M, El-Aryan TR (2011) Determination of clindamycin in dosage forms and biological samples by adsorption stripping voltammetry with carbon paste electrode. Pharm. Chem. J. 44:705
344. Hornedo-Nunez A, Getek T, Korfmacher W, Simenthal F (1990)High-performance liquid chromatography of clindamycin and clindamycin phosphate with electrochemical detection. J. Chromatogr. A 503:217–225